

**INFLUENCE OF WALL DIMENSION AND
GEOCOMPOSITE TRANSMISSIVITY ON
GROUNDWATER CONDITIONS IN MECHANICAL
STABILIZED EARTH WALL**



**A Thesis Submitted in Partial Fulfillment of the Requirements for the
Degree of Doctor of Philosophy in Civil, Transportation
and Geo-resources Engineering
Suranaree University of Technology
Academic Year 2020**

อิทธิพลของขนาดกำแพงและค่าความสามารถในการระบายน้ำของวัสดุโดย
สังเคราะห์ต่อสภาพน้ำในดินของกำแพงกันดินเสริมกำลัง

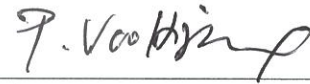


วิทยานิพนธ์นี้เป็นส่วนหนึ่งของการศึกษาตามหลักสูตรปริญญาวิศวกรรมศาสตรดุษฎีบัณฑิต
สาขาวิชาวิศวกรรมโยธา ขนส่ง และทรัพยากรธรณี
มหาวิทยาลัยเทคโนโลยีสุรนารี
ปีการศึกษา 2563

**INFLUENCE OF WALL DIMENSION AND GEOCOMPOSITE
TRANSMISSIVITY ON GROUNDWATER CONDITIONS IN
MECHANICAL STABILIZED EARTH WALL**

Suranaree University of Technology has approved this thesis submitted in partial fulfillment of the requirements for the Degree of Doctor of Philosophy.

Thesis Examining Committee



(Prof. Dr. Panich Voottri-pruex)

Chairperson



(Prof. Dr. Avirut Chinkulkijniwat)

Member (Thesis Advisor)



(Prof. Dr. Suksum Horpibulsuk)

Member



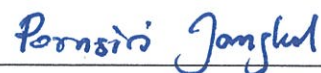
(Asst. Dr. Pornpot Tanseng)

Member

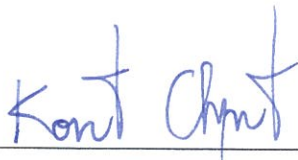


(Asst. Dr. Cherdsak Suksiripattanapong)

Member



(Assoc. Prof. Dr. Pornsiri Jongkol)



(Assoc. Prof. Flt. Lt. Dr. Kontorn Chamniprasart)

Vice Rector for Academic Affairs

Dean of Institute of Engineering

and Internationalization

ลา คอง ไช้ : อิทธิพลของขนาดกำแพงและค่าความสามารถในการระบายน้ำของวัสดุไส้
สังเคราะห์ต่อสภาพน้ำในดินของกำแพงกันดินเสริมกำลัง (INFLUENCE OF WALL
DIMENSION AND GEOCOMPOSITE TRANSMISSIVITY ON GROUNDWATER
CONDITIONS IN MECHANICAL STABILIZED EARTH WALL) อาจารย์ที่ปรึกษา :
ศาสตราจารย์ ดร.อวิรุทธิ์ ชินกุลกิจนิวัฒน์, 158 หน้า.

วัตถุประสงค์ของวิทยานิพนธ์นี้มีจุดมุ่งหมายเพื่อตรวจสอบผลกระทบของขนาดกำแพงกัน
ดินเสริมกำลังแต่ละขนาด คุณสมบัติการระบายน้ำของวัสดุสังเคราะห์ทางธรณีเทคนิค (T_{net})
เปรียบเทียบกับความหนาของแกน (tmet) การซึมผ่านของตาข่ายวัสดุสังเคราะห์ (knet) คุณสมบัติ
ของดินต่อระดับความอิ่มตัวประสิทธิภาพ (Seff) และระดับน้ำสูงสุดภายในบริเวณเสริมกำลัง (h_o)
วิทยานิพนธ์นี้ยังได้เสนอสมการเพื่อประมาณค่าระดับน้ำสูงสุดภายในบริเวณเสริมกำลังในกำแพง
ดินเสริมกำลัง ผลการศึกษาแสดงให้เห็นถึงผลกระทบต่อระดับน้ำสูงสุดในบริเวณเสริมกำลัง (h_o)
เนื่องจากจากต้นน้ำจนถึงรอบประบายน้ำ (L) ความสามารถในการซึมผ่านของดินที่ระยะ (k) และ
วัสดุระบายน้ำ (T_{net}) ผลการตรวจสอบความถูกต้องของสมการเชิงเส้นที่เสนอสำหรับการประมาณ
ค่าระดับน้ำสูงสุดในบริเวณเสริมกำลัง ระบุว่ามีความแม่นยำสูงและใกล้เคียงกับการจำลองด้วย
โปรแกรม Plaxis

เนื้อหาหลักในบทที่ 1 และบทที่ 2 นำเสนอคำชี้แจง ที่มาของปัญหา และวัตถุประสงค์ของ
การวิจัยวิทยานิพนธ์นี้ ความแตกต่างทางความรู้ของวรรณกรรมก่อนหน้าจำนวนมากได้ถูกเชื่อมโยง
จนกระทั่งเป็นหัวข้อการศึกษาของวิทยานิพนธ์นี้ ในบทที่ 2 อธิบายภาพรวมความสำคัญของขนาด
กำแพงกันดินเสริมกำลัง คุณสมบัติการระบายน้ำของวัสดุสังเคราะห์ทางธรณีเทคนิค และคุณสมบัติ
ของดินซึ่งได้ถูกนำเสนอไว้ในวรรณกรรมก่อนหน้าหลายฉบับ บทที่ 3 เสนองานวิจัยเกี่ยวกับ
น้ำใต้ดินกรณีสถานะคงที่ในกำแพงดินเสริมกำลังในขนาดต่าง ๆ พร้อมกับการติดตั้งท่อระบายน้ำ
ด้านหลังแผ่นใยสังเคราะห์แบบผสม การศึกษาอิทธิพลของพารามิเตอร์รูปร่างที่มีผลต่อการซึมผ่าน
น้ำ ระดับน้ำสูงสุดและความอิ่มตัวของน้ำในเขตป้องกันของกำแพงดินเสริมกำลัง ที่มีระบบระบาย
น้ำด้านหลังแผ่นใยสังเคราะห์แบบผสม นอกเหนือจากพารามิเตอร์รูปร่างที่เกี่ยวข้องแล้ว ยังมีการ
ตรวจสอบอิทธิพลของการซึมผ่านน้ำของแผ่นใยสังเคราะห์แบบตาข่าย ซึ่งเป็นองค์ประกอบหลัก
ของระบบการระบายน้ำที่ใช้แผ่นใยสังเคราะห์แบบผสม บทที่ 4 นำเสนอการประมาณระดับน้ำใต้
ดินในกำแพงดินเสริมกำลังที่มีระบบการระบายน้ำด้านหลังแผ่นใยสังเคราะห์แบบผสม การ
วิเคราะห์ความสัมพันธ์เชิงเส้น เช่น พารามิเตอร์รูปร่าง (L) การซึมผ่านของดิน (k) และลึอกาลิทิ้ม
ของตาข่ายวัสดุสังเคราะห์ (T_{net}) มีบทบาทสำคัญต่อระดับน้ำสูงสุดในเขตป้องกัน การใช้

แบบจำลองเชิงเส้นช่วยให้ง่ายต่อการปฏิบัติ ดังนั้น การประมาณค่าเชิงเส้นของระดับน้ำสูงสุดภายในเขตป้องกันที่ติดตามความสัมพันธ์ที่เกิดขึ้น จึงมีความสำคัญต่อการออกแบบกำแพงดินเสริมกำลังเพื่อต่อต้านการวิบัติของกำแพงดิน บทที่ 5 นำเสนอข้อสรุปและข้อเสนอแนะทั้งหมดสำหรับวิทยานิพนธ์นี้ ข้อเสนอแนะเชิงปฏิบัติและเชิงทฤษฎีเพิ่มเติมเกี่ยวกับการต่อยอดการวิจัยในแบบจำลองกำแพงดินเสริมกำลังได้รับการกล่าวถึงเพื่อผลงานที่จะเกิดขึ้นอนาคต



สาขาวิชา วิศวกรรมโยธา
ปีการศึกษา 2563

ลายมือชื่อนักศึกษา

ลายมือชื่ออาจารย์ที่ปรึกษา

LA DUONG HAI : INFLUENCE OF WALL DIMENSION AND
GEOCOMPOSITE TRANSMISSIVITY ON GROUNDWATER
CONDITIONS IN MECHANICAL STABILIZED EARTH WALL.
THESIS ADVISOR : PROF. AVIRUT CHINKULKIJNIWAT,
Ph.D., 158 PP.

MSE WALL/GEOCOMPOSITE/STEADY STATE FLOW/SHAPE PARAMETER /
PHREATIC LEVEL/GEOCOMPOSITE TRANSMISSIVITY/LINEAR
ASSOCIATION

This thesis aims to investigate influence of individual MSE wall dimensions and geocomposite back drainage properties to steady state effective saturation degree (S_{eff}) and the highest water level inside protected zone (h_o). The geonet transmissivity (T_{net}) is main parameter which reflects geocomposite drainage capacity and be expressed from geonet thickness (t_{net}) and geonet permeability (k_{net}). In addition, a linear model was conducted by Plaxis simulation to estimate value of h_o . This h_o estimation is in relationship among influences of length from upstream water to the drainage face (L); soil permeabilities (k); and geonet transmissivity (T_{net}). Linear equation establishing utilized wide range of different native and backfill soil hydrological properties as permeability. Verification results of proposed linear equation for estimation of h_o value indicate high accuracy and identical in comparing with Plaxis simulation.

According to the main contents in Chapter I presents the statement of the problems and the objectives of this research thesis. The gap of knowledge of previous literatures link to thesis topic. In Chapter II, the importance of MSE wall dimensions, geocomposite back drainage properties with geonet transmissivity, have been presented

in several previous literatures. Chapter III presents steady state groundwater in mechanical stabilized earth walls of various dimensions with geocomposite back drain installation. This chapter content indicates influences of MSE wall shape parameters on the h_o and S_{eff} in MSE protected zone with a geocomposite back drain. Other than the relevant shape parameters, the influence of geonet transmissivity, which is a main component of geocomposite drainage systems, was also investigated. Chapter IV presents h_o estimation in MSE wall with geocomposite back drain by linear association analysis. The linear equation is established in relevant relationship with MSE wall shape parameter (L), soil permeability (k) and logarithm geonet transmissivity ($\log T_{net}$). Good verification result of linear equation for h_o estimation in relevant relationships is, therefore, vital for the design of MSE wall against failure. Chapter V presents all conclusions and recommendations for this thesis. More practical and theoretical suggestions about expansion of research in MSE wall model are shown for the future works.

มหาวิทยาลัยเทคโนโลยีสุรนารี

School of Civil Engineering

Academic Year 2020

Student's Signature



Advisor's Signature



ACKNOWLEDGEMENTS

In last three year ago in 2017, I was successful passed the full Doctoral scholarship in geotechnical topic from School of Civil Engineering, Suranaree University of Technology, Thailand. Last several times marked a mile stone in my life as great and wonderful memory. I deeply thanks and appreciate so much to my advisor Professor Avirut Chinkulkijniwat. My fortunately for being under his supervision and guidance not only great and benefit for my expertise knowledge and skills improve comprehensively, but also encourage students with kindness and enthusiasm especially when I met the trouble in search works or normal life in Suranaree University of Technology. He always brings me much belief, endless kindness and enthusiasm supports and orientation for me in lectures, researches and project. It is so pleasure and lucky for me with his guidance, research methodology and philosophy, author can have many improvements for research ability in my career in the future and also have more experience gains for sharing next generations.

The author would like to share many thanks and appreciate much Professor Suksun Horpibulsuk and Associate Professor Dr. Pornpot Tangseng, from School of Civil Engineering, Institute of Suranaree University of Technology for giving international students like us with high professional sympathy of lectures, enlightening Geomechnics, Advanced Foundation, Ground improvement technique, teach international students with kindness. I also give my deeply sincerely to my Prof. Do Quang Thien, dean of Geography and Geology, Hue University of Sciences for his

support and kindly advices, and more cooperation between 2 universities of Thailand and Vietnam.

My best wish and acknowledge to Mr. Tanakorn Rakkob, Ms. Rattana Salee, Mr. Somjai Youbonchi, Dr. Duc Bui Van, and Mr. Hoymeng Lim for their kindly support discussions and encouragement in my unforgettable 3 years in SUT. And much appreciates to Suranaree University of Technology for facilities, equipment and financial support.

I also giving great bless and wish to appreciate all the staffs and office members of the School of Civil Engineering, Suranaree University of Technology, Thailand for the academic, administrative and technical support during my PhD study in Thailand for document preparations and explanations every time with enthusiasm and friendly.

My appreciate and many thanks from warming heart to my family in Vietnam who always stays beside me and always support me with all the best and give me more inspiration and motivation for my studying time in Thailand.

Finally, it is no word to describe my deeply appreciate and big thank to all SUT and Thailand that give me a chance to improve as well as develop me in great ways.

La Duong Hai

TABLE OF CONTENTS

	Page
ABSTRACT (THAI)	I
ABSTRACT (ENGLISH).....	III
ACKNOWLEDGEMENTS	V
TABLE OF CONTENTS.....	VII
LIST OF TABLES	XI
LIST OF FIGURES	XII
ABBREVIATIONS AND SYMBOLES	XXII
CHAPTER	
I INTRODUCTION	1
1.1 Statement of the problem.....	1
1.2 Objectives of the study.....	4
1.3 Organization of the dissertation.....	5
1.4 References	6
II LITERATURE REVIEWS	9
2.1 Introduction	9
2.2 Soil water modelling for unsaturated flow regime	10
2.2.1 Steady state flow	10
2.2.2 Unsaturated flow model	13
2.3 MSE wall failure state problems	16
2.3.1 Back drain installation.....	16

TABLE OF CONTENTS (Continued)

	Page
2.3.2 Backfill soil properties	20
2.3.3 Extremely rainfall.....	27
2.4 Geocomposite material properties	44
2.4.1 Geotextiles properties.....	45
2.4.2 Geonet hydraulic transmissivity	52
2.5 MSE wall dimensions to seepage responses	58
2.6 Linear analysis for maximum water level (h_o) in protected area	75
2.7 References	77
III STEADY STATE GROUNDWATER IN MECHANICAL STABILIZED EARTH WALLS OF VARIOUS DIMENSIONS WITH GEOCOMPOSITE BACK DRAIN.....	83
3.1 Statement of problem.....	83
3.2 Governing equations	87
3.3 Materials and methods	89
3.4 Numerical simulations	96
3.5 Influence of shape parameters	101
3.5.1 The highest water level inside protected zone (h_o)	101
3.5.1.1 Dimensions of the protected zone.....	104
3.5.1.2 The distance from the wall base to the impervious boundary (D)	105

TABLE OF CONTENTS (Continued)

	Page
3.5.1.3 Length from upstream water to the drainage face (L)	109
3.5.2 Water saturation profile in the protected zone.....	109
3.6 Geocomposite drain properties.....	112
3.7 Conclusions	117
3.8 References	118
IV GROUNDWATER ESTIMATION IN MSE WALL WITH GEOCOMPOSITE BACK DRAINAGE: LINEAR ASSOCIATION ANALYSIS.....	124
4.1 Statement of problem.....	124
4.2 Materials and methods	126
4.2.1 Research methodology	126
4.2.2 Simulation set up for linear association analysis	127
4.3 Results.....	129
4.3.1 Estimating h_o against geonet transmissivity (T_{net}).....	129
4.3.2 Linear slope (S) and intercept (I) for h_o estimation.....	134
4.3.3 Linear equation establishing for h_o	137
4.4 Model verification results	138
4.5 Conclusions	140
4.6 References	141
V CONCLUSION AND RECOMMENDATIONS	144

TABLE OF CONTENTS (Continued)

	Page
5.1 Summarize and conclusions	144
5.1.1 Chapter III: Steady state groundwater in mechanical stabilized earth walls of various dimensions with geocomposite back drain installation	145
5.1.2 Chapter IV: Groundwater estimation in MSE wall with geocomposite back drainage: linear association analysis	146
5.2 Recommendations for future works.....	147
APPENDIX A	148
BIOGRAPHY	158

LIST OF TABLES

Table		Page
2.1	van Genuchten model parameters of the materials used in (Bui Van et al. 2017).....	25
2.2	Basic relevant properties of geotextile (Iryo and Rowe 2005).....	45
2.3	van Genuchten Parameters and Saturated Hydraulic Conductivity for Materials Used in the Modeling (Bahador et al. 2016).....	48
3.1	Basic and relevant physical and hydraulic properties of studied sandy soil, geotextile, geonet (adapted from Chinkulkijniwat et al., 2017) and lateritic soil (adapted from Bui Van et al., 2017) utilized in this study.....	94
3.2	Detail of 66 simulations conducted for shape parameters.....	100
3.3	Detail of 27 simulations conducted for T_{net} study.....	101
4.1	Relevant VG model parameters of studied materials.....	128
4.2	180 PLAXIS-2D simulation cases set up in this studied.	129
4.3	Variables assigned in 12 verification cases and the corresponding h_o values from Plaxis calculation and the linear proposed equation (Eq. 4.5).....	139

LIST OF FIGURES

Figure	Page
2.1 Large scale testing of MSE wall with geocomposite drainage system by rising water level upstream (Chinkulkijniwat et al. 2017 and Bui Van et al. 2017)	11
2.2 Side view of Plaxis 2D numerical model geometry and mesh discretization in Chinkulkijniwat et al. 2017 and Bui Van et al 2017	13
2.3 Typical plot of hydraulic conductivity or k-function (Mualem 1976) for studied geosynthetic materials in this thesis adapted from Bui van et al. 2017	15
2.4 Schematic diagram of soil water characteristic curve (SWCC) in adapted from Chinkulkijniwat et al. 2017 and used in Bui Van et al. 2017.	16
2.5 MSE wall section showing drainage geocomposite back drain and outlet system, geotextile filters, as well as a geomembrane surface waterproofing layer (Koerner et al. 2011).....	17
2.6 Back drainage set up behind MSE walls (Koerner et al. 2011).....	18
2.7 The drainage systems from within to behind the reinforced soil zone (Koerner et al. 2011, Koerner et al. 2013, Koerner et al. 2018).....	20
2.8 Wall geometry and trace of failure surface obtained from limit equilibrium analysis (Yoo and Jung 2006).....	22

LIST OF FIGURES (Continued)

Figure	Page
2.9 (a) SWCC; (b) k-function in Vahedifad et al. 2017.....	23
2.10 (a) Grain size distribution of the studied soils and (b) SWCC of the materials used in this study.....	24
2.11 Permeability ratio effect to the inner phreatic surface level adapted from Chinkulkijniwat et al. 2017 and Bui et al. 2017.....	26
2.12 Finite-element model with meshing used in seepage analysis (Yoo and Jung 2006).....	28
2.13 Pore water pressure distributions at different dates during June and July rainfalls (Yoo and Jung 2006).....	29
2.14 Wall construction with 200 mm thick layer of coarse soil cushion above drainage layers to placing of locally available backfill soil (Thuo et al. 2015).....	30
2.15 Experiment setup (a), (b) numerical model, and (c) seepage velocity vectors and pore pressure contour of the soil column infiltration test (Thuo et al. 2015).....	31
2.16 Variation of slope stability with cumulative rainfall for slopes 3-B and 4-B: (a) overall FS; (b) local FS for soils above the top geotextile layer (Thuo et al. 2015).....	32
2.17 Pore-water pressure contour inside slope with time factor (Robinson et al. 2017).....	33

LIST OF FIGURES (Continued)

Figure	Page
2.18 Simulated suction stress for baseline and projected precipitation extremes along three cross-sections of slope modelling (Robinson et al. 2017).....	34
2.19 Simulated effective degree of saturation (Se), along with percent relative change in time, for baseline and projected precipitation extremes along three cross-sections of the model slope (Robinson et al. 2017).....	35
2.20 Geometry of the model MSE wall used in Vahedifad et al. 2017.	36
2.21 Effect of change in intensity and duration of rain behind the wall on effective suction with initial suction of (a) 60 kPa; (b) 240 kPa (Vahedifad et al. 2017).....	37
2.22 Effect of rainfall intensity and duration behind the wall (x - xtoe $\frac{1}{4}$ 2 m) on effective degree of saturation with initial suction of (a) 60 kPa; (b) 240 kPa (Vahedifad et al. 2017).....	37
2.23 Effect of rain on change in the volumetric water content for initial suction of (a) 60 kPa; (b) 240 kPa (Vahedifad et al. 2017).....	38
2.24 Effect of rain on change in the mean effective stress for initial suction of (a) 60 kPa; (b) 240 kPa (Vahedifad et al. 2017).....	38

LIST OF FIGURES (Continued)

Figure	Page
2.25 Effect of rainfall intensity, duration and initial suction on the displacement of the wall: (a) displaced wall with initial suction of 60 kPa; (b) displaced wall with initial suction of 240 kPa (Vahedifad et al. 2017).....	39
2.26 Effect of change in intensity and duration of rain on the maximum reinforcement loads T_{max} : (a) maximum reinforcement load for initial suction of 60 kPa; (b) maximum reinforcement load for initial suction of 240 kPa (Vahedifad et al. 2017).....	39
2.27 Volumetric water content measured in the upper reinforced soil layer: (a) until 35,000 min and (b) until 10,000 min of test Portelinha et al. (2017).....	41
2.28 Cumulative water volumes into the reinforced soil wall under high precipitation Portelinha et al. (2017).....	42
2.29 (a) Effective saturation profiles along the vertical sections located 5 cm to either side of the soil - geocomposite interface, outside and inside the protected zone, for varying g_a values of the native lateritic soil for the L-S scenario and (b) varying a value of the compacted lateritic soil for the L-L scenario (Bui Van et al. 2017).....	43
2.30 Variation in the phreatic surface outside the protected zone for varying a (g_a) values for lateritic soil (solid line for the L-S scenario and dashed line for L-L scenario) (Bui Van et al. 2017).....	44

LIST OF FIGURES (Continued)

Figure	Page
2.31 (a) Wetting phase WRC curves of 13 geotextiles reported and of the geotextile used in the physical test, and (b) WRC curves of all geotextiles assigned to the numerical experiment by Iryo and Rowe (2003) (Chinkulkijniwat et al. 2017).....	46
2.32 Hydraulic properties for sand and geotextile. (a) Water characteristic curves. (b) Hydraulic conductivity functions (Iryo and Rowe 2005).	47
2.33 (a) Moisture characteristic curves; (b) unsaturated hydraulic conductivity curves (Bahador et al. 2016).....	49
2.34 Pore pressure contours in the profile: (a) without geocomposite; (b) with woven-fabric geotextile transport layer; (c) with non-woven geotextile transport layer (Bahador et al. 2016).	50
2.35 Installation lead failure problems for geotextile as drainage system: (a) Occurrence of large void beneath a highway pavement preventing intimate contact of the upstream geotextile, (b) Suggested remedy for backfilling large voids via hydraulically placed sand with the geocomposite edge drain moved to the shoulder side of trench (Koerner et al. 2015).	51
2.36 Geonet material in research of Dickinson (2010).	53
2.37 Flow rate through geonet with time (Dickinson 2010).	53

LIST OF FIGURES (Continued)

Figure	Page
2.38	Generic curve of hydraulic conductivity or transmissivity (logarithmic scale) as a function of hydraulic gradient (logarithmic scale) from Giroud et al. (2014).....
	54
2.39	(a) Tri-planar geonet; and (b) bi-planar geonet (Yarahmadi et al. 2017).....
	55
2.40	Transmissivity as a function of hydraulic gradient (Bourges-Gastaud et al. 2013).
	56
2.41	Flow vectors corresponding to the variably saturated model (Clement et al. 1996).....
	59
2.42	Variation of the phreatic surface predicted by the variably saturated model owing to changing downstream levels for the square (Clement et al. 1996).....
	60
2.43	Variations of the phreatic surfaces predicted by the variably saturated models owing to changing downstream open-water levels for the ‘elongated’ (Clement et al. 1996).....
	61
2.44	Sensitivity analysis of the variably saturated flow model to the Van Genuchten parameter a for the square slow problem (Clement et al. 1996).....
	62
2.45	Sensitivity analysis of the variably saturated flow model to the Van Genuchten parameter n , for the square embankment problem (Clement et al. 1996).....
	63

LIST OF FIGURES (Continued)

Figure	Page
2.46 Fluctuation of groundwater head in the leaky confined aquifer at $t = 3$ h with specific leakage $L = 0, 0.01$ and 0.05 (Saeedpanah et al. 2011).	64
2.47 Fluctuation of groundwater head in the leaky confined aquifer at $t = 3$ h with specific leakage $L = 0, 0.01$ and 0.05 (Saeedpanah et al. 2011).	65
2.48 Piezometer head fluctuations at 100 m from the coast with $L = 0.01, 0.05$ in 1 day (Saeedpanah et al. 2011).	65
2.49 MSE Failures at research area in Roy and Singh 2008.	67
2.50 MSE wall cross-section for failure report in Roy and Singh 2008.	68
2.51 Development of reinforcement strains and stresses as a percent of yield stress at the North MSE wall (Stuedlein et al. 2012).	69
2.52 Development of reinforcement strains and stresses as a percent of yield stress at the West MSE wall (Stuedlein et al. 2012).	69
2.53 Cross section of MSE wall (qualitative) (Kibria et al. 2014).	70
2.54 (a) Geometry of MSE wall; (b) mesh connectivity (Kibria et al. 2014)	71
2.55 Maximum horizontal displacement 287 mm (arrows indicate direction of movement of MSE wall) (Kibria et al. 2014).	72
2.56 Overall factor of safety of 1.2 (arrows indicate direction of movement of MSE wall) (Kibria et al. 2014)	72

LIST OF FIGURES (Continued)

Figure	Page
2.57	Effect of reinforcement length on horizontal displacement of MSE wall (Kibria et al. 2014). 73
2.58	Three-dimensional finite element model of laboratory test adapted from Xu et al. (2014)..... 74
2.59	Relationship between increment of hydraulic gradient and insertion depth ratio adapted from Xu et al. (2014). 75
3.1	Sketch of the physical test model and its instrumentation: (a) plan view of the model, (b) side view of the model, (c) sketch of bearing reinforcement (adapted from Chinkulkijniwat et al. 2017 with permission). . 90
3.2	(a) Grain size distribution, (b) WRC, and (c) permeability function of studied sandy soil, geotextile, geonet and lateritic soil utilized in this study (adapted from Bui Van et al. (2017) with permission). 92
3.3	(a) Water saturation profiles, phreatic level and (b) time series plot of water content adopted from the physical model test reported in adapted from Chinkulkijniwat et al. (2017) and the corresponding calculations. 95
3.4	Plaxis model of mesh discretization and the relevant shape parameters of MSE wall with back drain using geocomposite. 96
3.5	Variation of h_o subjected to change in all shape parameters for (a) <i>S-S</i> , <i>L-L</i> and <i>L-S</i> ; and (b) <i>L-L</i> and <i>L-S</i> scenarios. 103

LIST OF FIGURES (Continued)

Figure	Page
3.6	(a) Phreatic surface approaching drain interface and (b) reflection of flow directed from native soil to drain material. 105
3.7	(a) Setup of conditions a, b, and c for modeling of MSE wall without back drain installation and (b) variation of h_w with D for conditions a, b, and c. 106
3.8	(a) Setup of extra numerical experiment to model MSE wall with back drain installation keeping the entry length of upstream water unchanged and (b) variation of h_o with D 108
3.9	Water saturation profile subjected to variation of D , W , L shape parameter in (a) S - S and L - S scenarios, (b) L - L scenario and (c) for H shape parameter in 3 scenarios as S - S , L - L and L - S 111
3.10	Water saturation profile subjected to variation of geonet thickness (t_{net}) in S - S , L - L and L - S scenarios. 113
3.11	Suction profiles for (a) S - S scenario, (b) L - S scenario, and (c) 114
3.12	k-functions of the geotextile and native soil for (a) S - S scenario and (b) L - S scenario 115
3.13	Variation of h_o subjected to the effect geonet thickness (t_{net}) and geonet permeability in S - S , L - L , L - S scenarios (The number appeared on the corresponding line is ratio of h_o for the lowest t_{net} to h_o for the highest t_{net}). 116

LIST OF FIGURES (Continued)

Figure		Page
4.1	Linear relationship between h_o and $\log T_{net}$ for all 27 cases conducted in the second part of the numerical experiment.....	130
4.2	Linear relationship of h_o subject to $\log T_{net}$ and L shape parameter for (a) coarse sand, (b) sandy soil and (c) clayey sand.	132
4.3	Linear relationship of h_o subject to $\log T_{net}$ and L shape parameter for (a) lateritic soil and (b) clay.	133
4.4	Linear relationship of (a) $\log S $ and (b) $\log I $ subjected to L shape parameter.	135
4.5	Linear relationship of (a) $\log S/k$ and (b) $\log I/2k$ subjected to $\log L$ shape parameter.	136
4.6	Verification results between Plaxis simulation and Proposed equation.....	140

ABBREVIATIONS AND SYMBOLS

MSE	=	mechanical stabilized earth
VG	=	van-Genuchten
VGM	=	van-Genuchten Mualem
TDR	=	time domain reflectometry
WRC	=	water retention curve
D	=	distance from the wall base to the impervious boundary (m)
G_s	=	specific gravity (-)
H	=	MSE wall height (m)
H_w	=	height of upstream water level (m)
h	=	total head (m)
h_o	=	highest water level inside protected zone;
h_p	=	matric suction head (m)
h_w	=	height of phreatic level at wall face (m)
I	=	length of vertical impervious boundary line (m)
k	=	coefficient of permeability (m/sec.)
$k_{Latitude}$	=	coefficient of permeability of geotextile in the x directions (m/sec.)
$k_{Longitude}$	=	coefficient of permeability of geotextile in the y directions (m/sec.)
k_{net}	=	geonet permeability (m/sec.)
k_r	=	coefficient of relative permeability (-)

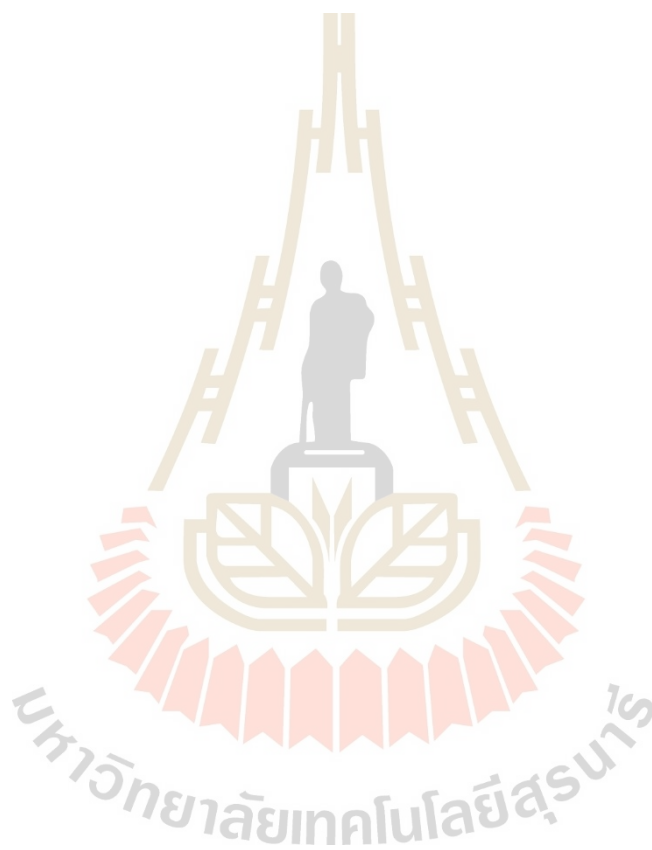
ABBREVIATIONS AND SYMBOLS (Continued)

k_x	=	coefficients of permeability in the x directions (m/sec.)
k_y	=	coefficients of permeability in the y directions (m/sec.)
L	=	length from upstream water to the drainage face (m)
LL	=	liquid limit (%)
m	=	VG model parameter (-)
n	=	VG model parameter (-)
PL	=	plastic limit (%)
S	=	degree of saturation (-)
S_e	=	effective degree of saturation (-)
S_{res}	=	residual saturation (-)
S_{sat}	=	saturated saturation (-)
T_{net}	=	geonet transmissivity (m ² /sec.)
t	=	time (sec.)
t_{net}	=	geonet thickness (m)
W	=	protected zone width (m)
α	=	VG model parameter (m ⁻¹)
β_1	=	incident angle or angle (deg.)
β_2	=	reflected angle (deg.)
γ	=	unit weight (kN/m ³)
θ	=	volumetric water content (-)

ABBREVIATIONS AND SYMBOLS (Continued)

θ_{res} = residual volumetric water content (-)

θ_{sat} = saturated volumetric water content (-)



CHAPTER I

INTRODUCTION

1.1 Statement of the problem

Nowadays, the mechanically stabilized earth (MSE) walls have been significant considerations as feasible in cut and fill works for highway construction through difficult terrains as mountainous areas. By unpredictable climate changes as high precipitation, that caused massive impacts to internal and external stability of wall reinforced area. That extremely weather condition caused underestimated failure of MSE wall through two hydrological key varied objectives such as water content distribution and the highest water level inside the reinforced zone. Some preliminary work was carried out several years ago reported failure modes in MSE walls (Yoo and Jung 2006; Koerner et al. 2011, Kim and Borden 2013, Koerner et al. 2013, Koerner et al. 2015; Thuo et al. 2015, Robinson et al. 2017, Koerner et al. 2018, Albino et al. 2019). Internal instability was partly caused by the wide distribution of water content inside the reinforced zone (Valentine et al. 2013, Koerner et al. 2018, Bui Van et al. 2017, Albino et al., 2019). Iryo and Rowe (2004) and Thuo et al. 2015 reported serious reductions in shear strength of the soil in the reinforced zone due to extreme precipitation. Koerner et al. 2018 reported that up to 41% of all internal failures were caused by the poor performance of the drainage system. It follows that the installed drainage system must have a high enough capacity to drain sufficient water in extreme conditions. To combine high drainage capacity and ease of installation, drainage systems installed in

many geological structures, including MSE walls, have frequently used a geocomposite comprising a geonet core with a large flow channel sandwiched by a nonwoven geotextile (Zornberg et al. 1995, McKean and Inouye. 2001, Koerner et al. 2011, Koerner et al. 2013). This type of geocomposite system installed as a back wall drain for an MSE wall is the focus of this study.

Although geocomposite drains in MSE walls have been spotlighted in various reports, their approach is not enough comprehensive, particularly the influence of factors affecting geonet transmissivity. In advance the year 2010, Dickinson determined the relationship between geonet transmissivity and geonet thickness. In research of Giroud et al. 2014 and Yarahmadi et al. 2017 studied the reduction of hydraulic transmissivity of geonet due to effects of creep deformation. Reports about the influence of geocomposite properties on hydrological responses in MSE walls are limited. Chinkulkijniwat et al. 2017 concluded that the capillary barrier phenomenon plays a role in the distribution of effective saturation at the soil–geotextile interface and Bui Van et al. 2017 found that the ratio between geonet permeability and permeability of the soil on the upstream side affected the phreatic level in the reinforced zone. Clearly, further knowledge about the influence of geocomposite properties on hydrological responses in and around MSE walls is still required to inform the design of geocomposite drains in MSE walls. Other than geocomposite properties, the hydrological properties of the relevant soils also play an important role in hydrological responses such as the distribution of water content and the location of the phreatic surface in MSE walls. A number of studies reported the effect of hydrological properties of the soil on hydrological responses in MSE walls (Zornberg et al. 1994, Christopher 1998, Valentine 2013, Portelinha and Zornberg 2013, Vahedifard et al.

2017). In mountainous terrain, where heavy rainfall could raise the upstream water level due to huge amounts of rainwater flowing from high ground towards an MSE wall (Bui Van et al., 2017), the hydrological responses in the MSE wall were also governed by the relevant shape parameters. These parameters included the level of the upstream water table, the distance from the upstream water to the drainage face, the depth below the wall of the impervious rock interface, and the width and height of the reinforced zone.

Refer steady-state unconfined flow in rectangular-flow systems, Clement et al. 1996 investigated the effect of flow domain aspect ratio on the height of the seepage face, which is the difference between the phreatic surface at the exit and the downstream water level. They found that effects on the seepage face were diminished for long, shallow flow domains, while the position of the phreatic surface was relatively insensitive to downstream water level for deep flow domains. Saeedpanah et al. 2011 reported that the length of the groundwater flow path plays a more important role in the flow rate than the upstream water level does. Despite their importance to hydrological responses, the relevant shape parameters are yet to be investigated thoroughly enough to comprehensively explain their influence on hydrological responses in an MSE wall. A well-calibrated numerical model, computed in the Plaxis environment and introduced by Chinkulkijiwat et al. 2017, was further elaborated with regard to the effect of scaling. To ensure the validity of the Plaxis-based model on different scales, it was established using identical shape ratios at double the size of the physical model. The calibrated model was further employed to perform a series of parametric studies focusing on the influence of the shape parameters and geonet transmissivity on hydrological responses in the modeled MSE wall.

Furthermore, research results of this thesis were also utilized for linear association analysis for adapting and provide a convenient and simple linear equation for estimation the variation of h_o following the relationship among many influenced parameters such as native and backfill soil permeability (k), MSE wall dimension (L), geonet transmissivity (T_{net}). The linear model provides an ease for practical via linear equation uses. Good linear estimation of h_o in relevant relationships is, therefore, vital for the best design of MSE wall against failure.

Based on practical problems, we conduct the research in this thesis with topic investigating influence of the dimensions of MSE walls and relevant geocomposite properties as well as for soil properties on steady-state hydrological responses and assist drainage design.

1.2 Objectives of the study

1.2.1 To investigate the influences of individual MSE wall geometric parameters and backfill soil properties to the changes of water saturation degree (S_{eff}) and the highest water level inside reinforced zone (h_o).

1.2.2 To study the influences of geocomposite back drainage properties through geonet transmissivity (T_{net}) via geonet permeability (k_{net}) and geonet thickness (t_{net}) to the variation of h_o and S_{eff} in MSE wall protected zone.

1.2.3 To propose linear equation for h_o estimation in relationship among the MSE wall dimension (L), soil permeability (k) and geonet transmissivity (T_{net}).

1.3 Organization of the dissertation

This thesis consists of 5 chapters and outlines of each chapter are presented as follows:

Chapter I: Introduction. The part of introduction, describing the statement of the problems, the objectives of the study and the organization of the dissertation.

Chapter II: Literature reviews

Chapter III: Steady state groundwater in mechanical stabilized earth walls of various dimensions with geocomposite back drain installation. In this chapter the influences of all considerable MSE wall geometric parameters and backfill soil properties to the changes of effective water saturation degree (S_{eff}) and the highest water level inside reinforced zone (h_o) are investigated comprehensively. In addition, a series of study the influences of geocomposite back drainage properties through permeability (k_{net}), transmissivity (T_{net}) and thickness (t_{net}) of geonet to (h_o) and (S_{eff})

Chapter IV: Groundwater estimation in MSE wall with geocomposite back drainage: linear association analysis. IN order to propose a linear equation for h_o estimation in relationship among the MSE wall dimension (L), soil permeability (k) and geonet transmissivity (T_{net}). The linear model provides an ease for practical via linear equation uses. Good linear estimation of h_o in relevant relationships is, therefore, vital for the best design of MSE wall against failure.

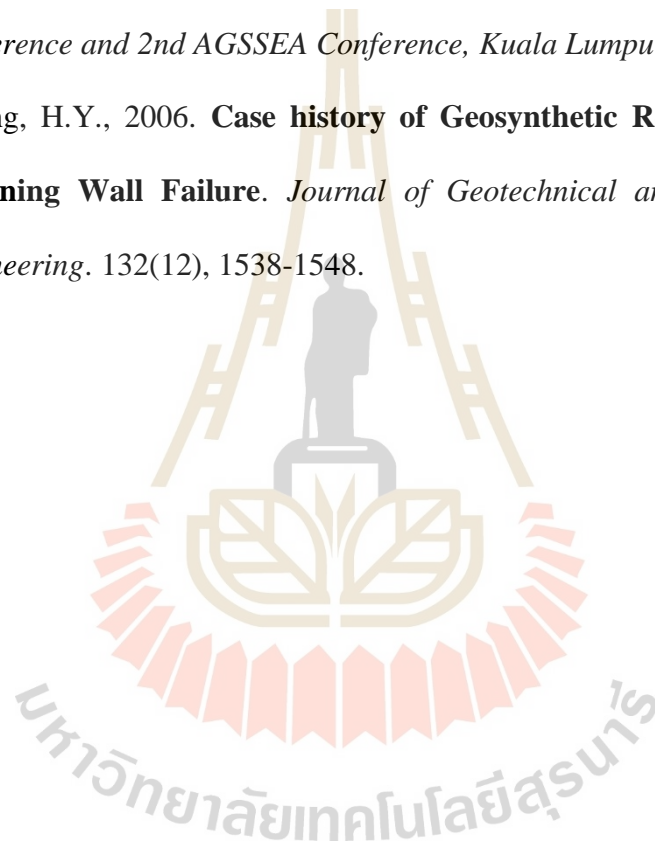
Chapter V: Concludes the present work and suggests the topics for further study.

1.4 References

- Albino, U.D.R., Portelinha, F.H.M., Zornberg, J.G., Futai, M.M., 2019. **Numerical simulation of infiltration into the fill of a wall reinforced with nonwoven geotextiles.** *Computers and Geotechnics*. 108, 27-39.
- Bahador, M.,1; Evans, T. M., and Gabr, M. A., 2016. **Modeling effect of geocomposite drainage layers on moisture distribution and plastic deformation of road.** *Journal of Geotechnical and Geoenvironmental Engineering*. 139(9).
- Bourges-Gastaud, S., Blond, E., Touze-Foltz, N., 2013. **Multiscale transmissivity study of drain-tube planar geocomposite: effect of experimental device on test representativeness.** *Geosynthetics International*. 20(3), 119-128.
- Bui Van, D., Chinkulkijniwat, A., Horpibulsuk, S., Yubonchit, S., Limrat, I., Arulrajah, A. and Jothityangkoon, C., 2017. **Steady flow in mechanically stabilised earth walls using marginal soils with geocomposite.** *Geosynthetics International*. 24(6), 590-606.
- Chinkulkijniwat, A., Horpibulsuk, S., Bui Van, D., Udomchai, A., Goodary, R., Arulrajah, A., 2017. **Influential factors affecting drainage design considerations for mechanical stabilised earth walls using geocomposite.** *Geosynthetics International*. 24(3), 224-241.
- Clement, T. P., Wise, W. R., Molz, F. J., & Wen, M., 1996. **A comparison of modeling approaches for steady-state unconfined flow.** *Journal of Hydrology*. 181(1-4), 189-209.
- Dickinson, S., Brachman, R. W. I., & Rowe, R. K., 2010. **Thickness and Hydraulic Performance of Geosynthetic Clay Liners Overlying a Geonet.** *Journal of Geotechnical and Geoenvironmental Engineering*. 136(4), 552-561.

- Giroud, J. P., & Kavazanjian, E., 2014. **Degree of Turbulence of Flow in Geosynthetic and Granular Drains.** *Journal of Geotechnical and Geoenvironmental Engineering.* 140(5), 06014001.
- Iryo, T., Rowe, R., 2005. **Numerical Study of Infiltration Into a Soil–Geotextile Column.** *Geosynthetics International.* 11(5), 377-389.
- Koerner, R.M., Koerner, G.R., 2011. **The Importance of Drainage Control for Geosynthetic Reinforced Mechanically Stabilized Earth Walls.** *Journal of Geoengineering.* 6(1), 3-13.
- Koerner, R.M., & Koerner, G.R., 2013. **A data base, statistics and recommendations regarding 171 failed geosynthetic reinforced mechanically stabilized earth (MSE) walls.** *Geotextiles and Geomembranes.* 40, 20-27.
- Koerner, R.M., & Koerner, G.R., 2015. **Lessons learned from geotextile filter failures under challenging field conditions.** *Geotextiles and Geomembranes.* 43(3), 272-281.
- Koerner, R.M., & Koerner, G.R., 2018. **An extended data base and recommendations regarding 320 failed geosynthetic reinforced mechanically stabilized earth (MSE) walls.** *Geotextiles and Geomembranes,* 46(6), 904-912.
- La Duong, H., Chinkulkijniwat, A., Horpibulsuk, S., Do Quang, T., Yaowarat, T., 2020. **Steady state groundwater in mechanical stabilized earth walls of various dimensions with geocomposite back drain installation.** *International Journal of geomechanics.*

- Xu, Y.-S., Shen, S.-L., Ma, L., Sun, W.-J., & Yin, Z.-Y. (2014). **Evaluation of the blocking effect of retaining walls on groundwater seepage in aquifers with different insertion depths.** *Engineering Geology*. 183, 254-264.
- Yarahmadi, N., Gratchev, I., Jeng, D.S., Gibbs, D., 2017. **Effect of Thickness Reduction on Hydraulic Transmissivity of Geonets used in Leachate Collection Systems in Landfills.** *The 19th Southeast Asian Geotechnical Conference and 2nd AGSSEA Conference, Kuala Lumpur, Malaysia.*
- Yoo, C., Jung, H.Y., 2006. **Case history of Geosynthetic Reinforced Segmental Retaining Wall Failure.** *Journal of Geotechnical and Geoenvironmental Engineering*. 132(12), 1538-1548.



CHAPTER II

LITERATURE REVIEWS

2.1 Introduction

The mechanically stabilized earth (MSE) wall becomes wider applying in cut and fill works in the word since several years ago due to their advantages in engineering and economic benefits that mentioned in many reports. However, under the unpredictable climate change as heavy rainfall caused the high development of hydrological risks that can impact to the internal stability of wall construction. A growing body of literature has examined the failure of MSE wall due to lack of sufficient water drain out of reinforced soil as well as poor drainage capacity. That kind of failure accounted quite domain number of failure cases in comparative to other failure reasons.

Several authors have attempted to define the appropriate material to design and installation of MSE wall back drain. The composite material which consist of comprising a geonet core with a large flow channel sandwiched by a nonwoven geotextile has been indicated in many researches as being high potential for MSE back drainage. Thoroughly, much work study on the potential of geocomposite drainage has been carried out for proving appropriate water drain capacity.

Reports about the influence of geocomposite properties on hydrological responses in MSE walls are limited. Besides, the influence of factors affecting geonet transmissivity become a concern of researchers link to the comprehensive approach of

geocomposite drainage system. Their reports emphasized the geonet core drain play as domain water drain channel through its relevant hydrological properties such transmissivity in linking to geonet thickness and permeability.

Various researches highlighted the hydrological responses of MSE wall with back drain geocomposite are not only affected by hydrological properties of geocomposite especially geonet but the influence of others factors in term of dimensions such as geonet transmissivity and MSE wall geometric parameters; Backfill soil hydrological properties inside reinforced zone.

2.2. Soil water modelling for unsaturated flow regime

2.2.1 Steady state flow

A steady flow mode was selected to calculate the final groundwater states due to elevated upstream water. Steady-state flow conditions were focused in this to quantify the final state of ground flow in MSE wall. Steady-state of unconfined aquifer is considered as flow regime expressed that when the magnitude and direction of flow is constant with time throughout the entire domain. With steady state flow appearance, time is no longer an independent variable and thus the storage term in the groundwater flow equation disappears; Since there is no change in the amount of water stored in the domain (i.e. the hydraulic head and pressure at any points get constant value over time

The relationship of soil water is expressed to in term of total head and total suction as well as. This kind of curve indicate the properties and relationship of soil suction material and water content. Essential parameters which are used for estimation the SWCC come from the determination of water content and suction for

specific conditions maximum saturation degree (S_{sat})/maximum volumetric water content (θ_{sat}), residual saturation degree (S_{res})/residual volumetric water content (θ_{res}) and air-entry value (α), and pore size distribution (n).

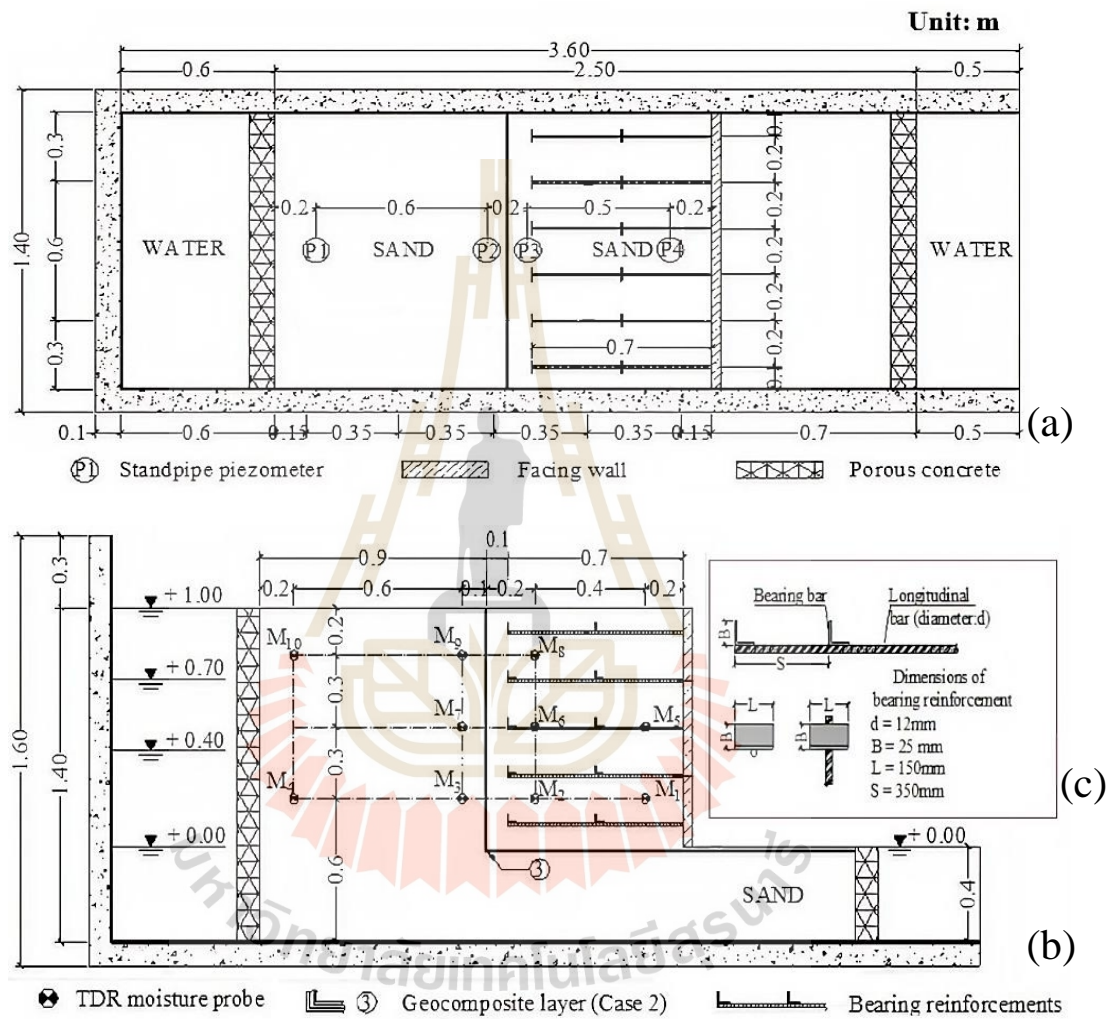


Figure 2.1 Large scale testing model of MSE wall with geocomposite drainage system by rising water level upstream (Chinkulkijniwat et al. 2017 and Bui Van et al. 2017).

In this thesis, core content is that under the impacts of groundwater level behind the wall rise due to extreme precipitation, the phreatic surface changes and water content distribution at steady-state condition present and determine critical conditions at a particular upper stream state since the increase of water level in research. From numerical model of MSE wall from highlight research of Bui Van et al. 2017 and Chinkulkijniwat et al 2017, the high precipitation was reflected via the change of groundwater behind the reinforced area. By conducting a series of Plaxis environment for MSE wall modelling (**Figure 2.2**) in verification and calibration with physical large-scale test in **Figure 2.1**. Their examination indicates the steady state VG parameter of flow conditions; upstream soil permeability, and upstream water level influenced majorly to the phreatic line inside and out side reinforced area, and for variation of water saturation profile along vertical cross-section around geocomposite. However, they did not comprehensively quantify the change of groundwater changes and water saturation under for other influenced factor as MSE wall geometries and more geocomposite properties.

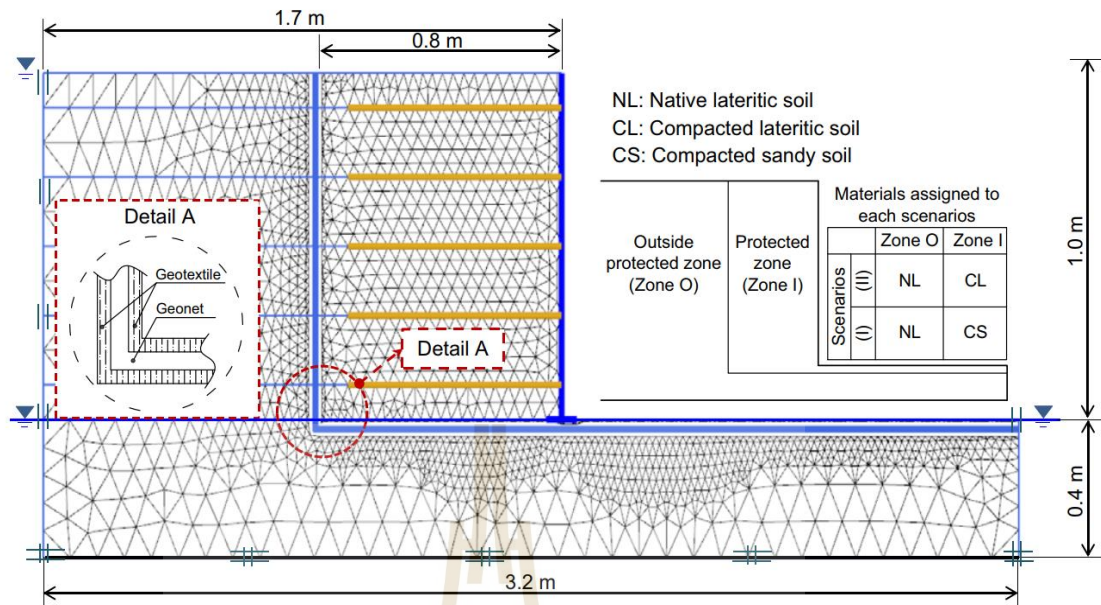


Figure 2.2 Side view of Plaxis 2D numerical model geometry and mesh discretization in Chinkulkijniwat et al. 2017 and Bui Van et al 2017.

2.2.2 Unsaturated flow model

There are many recent developments flow models in attempt to catch the behavior of soil water characteristic at steady-state flow assumption through porous media. One of the most outstanding and suitable models named Van Genuchten (VG) (van-Genuchten 1980) (Eq. 2a) and expressed van Genuchten-Mualem model (Mualem, 1976) (Eq. 2b) show themselves feasible using and closed catching hydraulic behavior of soil material. Specifically, those models are noticed as close-form, smooth curve and consist three-parameter model, which relate to particular physical meaning, for indicating the relationship between soil suction capacity and water content. This model has ability to approximate in wide ranges of soil types. They are employed to fit the water retention curve (SWSS) and permeability functions ($k - function$) for every porous media in the MSE wall problem typical shown in **Figure 2.3**.

$$S_e = \frac{S - S_{res}}{S_{sat} - S_{res}} = \frac{\theta - \theta_{res}}{\theta_{sat} - \theta_{res}} = \left[1 + (\alpha |h_p|)^n \right]^{-m} \quad (2.2a)$$

$$k_r(S_e) = S_e^{0.5} [1 - (1 - S_e^{1/m})^m]^2 \quad (2.2b)$$

In the above equations, S_e is effective degree of saturation, S is degree of saturation, S_{res} is residual saturation at very high values of suction, S_{sat} is the maximum saturation of saturated soil, θ_{res} is residual volumetric water content, θ_{sat} is maximum volumetric water content of saturated soil, h_p is matric suction head, and k_r is the relative permeability coefficient: α [m^{-1}] and n are fitting parameters which represent respectively the air-entry value of the soil and the rate of water extraction from the soil once the air entry value has been exceeded: m , according to the Mualem hypothesis (Mualem, 1976), is assigned the value $1-1/n$. Steady-state flow conditions were the focus of our study in order to quantify the final state of groundwater flow in the porous media.

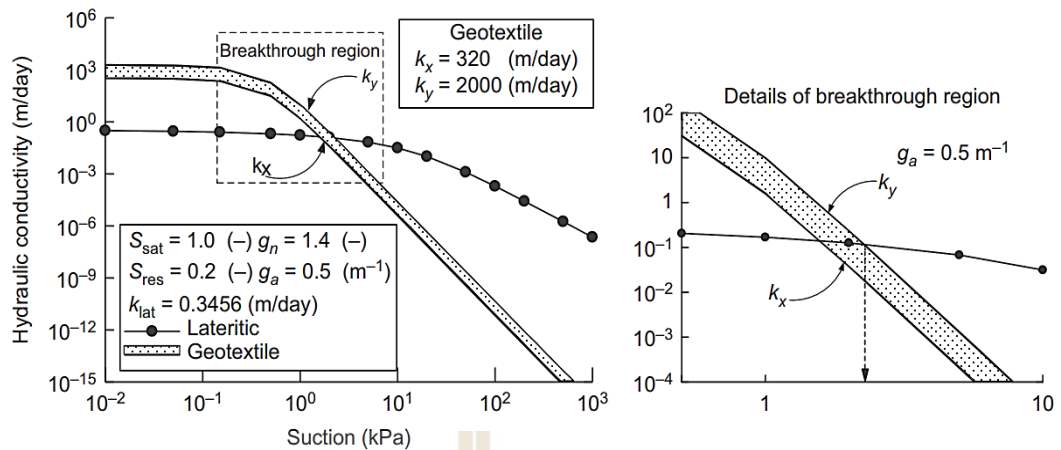


Figure 2.3 Typical plot of hydraulic conductivity or k-function (Mualem 1976) for studied geosynthetic materials in this thesis adapted from Bui van et al. 2017.

Typical plot of VG model fit curve or SWCC (soil water characteristic curve) is shown in **Figure 2.4**. In addition, all available pore/void space or pore size distribution (n) of material is considered as effect to the shape of SWCC fitting curve (Chinkulkijniwat et al. 2017). There are such many previous, related to hydrological responses to MSE wall, applied the steady unsaturated flow. Domain changing of van Genuchten (van-Genuchten 1980) parameter such as α and n directly effect to hydrological response such as water content and soil suction. Many changes indicate the saturation profile especially for earth structural as MSE wall. However, with geosynthetic material reflects high value of α and n , which also represent to high draining capacity. That material become hot picking as replacement drain method by using high permeability soil in practical conditions.

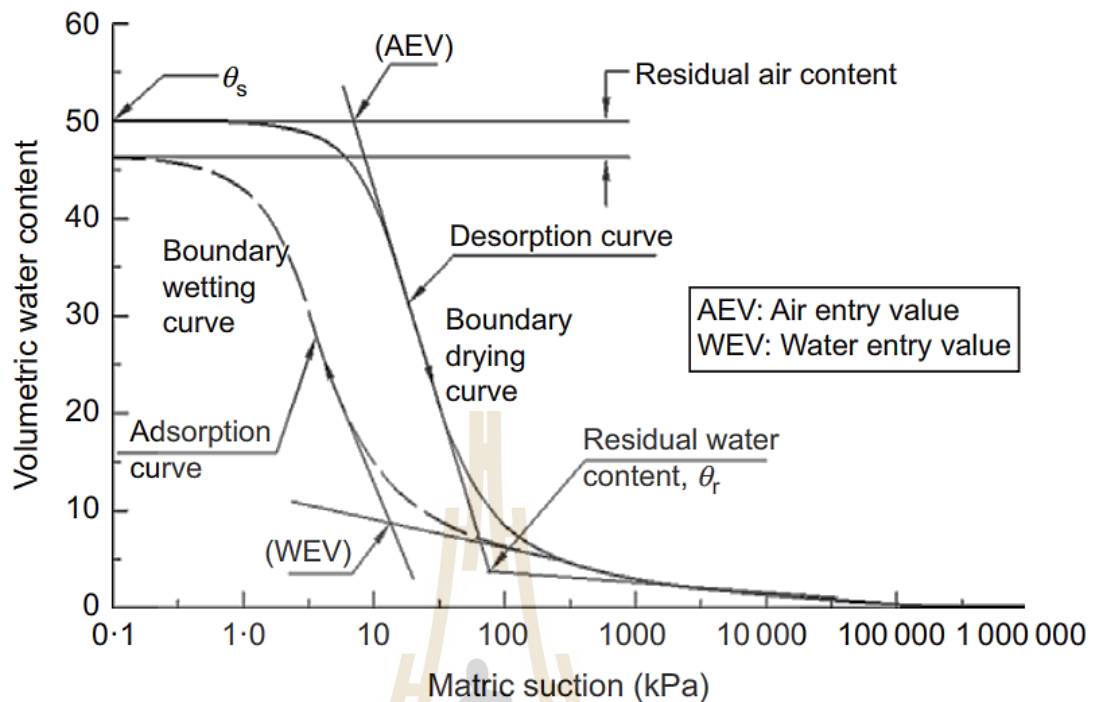


Figure 2.4 Schematic diagram of soil water characteristic curve (SWCC) in adapted from Chinkulkijniwat et al. 2017 and used in Bui Van et al. 2017.

2.3. MSE wall failure state problems

2.3.1 Back drain installation

Experts have always seen core reasons caused the failure of many MSE walls regard to thigh exceed pore water pressure due to high water content and ground water level behind MSE wall that caused hydrological risks. Koerner et al in the year 2011 emphasized the importance of considering drainage control for geosynthetics reinforced mechanically stabilized earth (MSE) walls (**Figure 2.5**). The geosynthetic for reinforcing MSE wall consist of horizontal geogrid combine with geotextile (**Figure 2.6**). In their research the maximum vertical length of geocomposite back drain just read 2/3 or lower in comparative to the total wall height. Based on this point, for conditions

of long-term rainfall, the groundwater domain rise over the top of back drain and forward to backfill area behind the wall face.

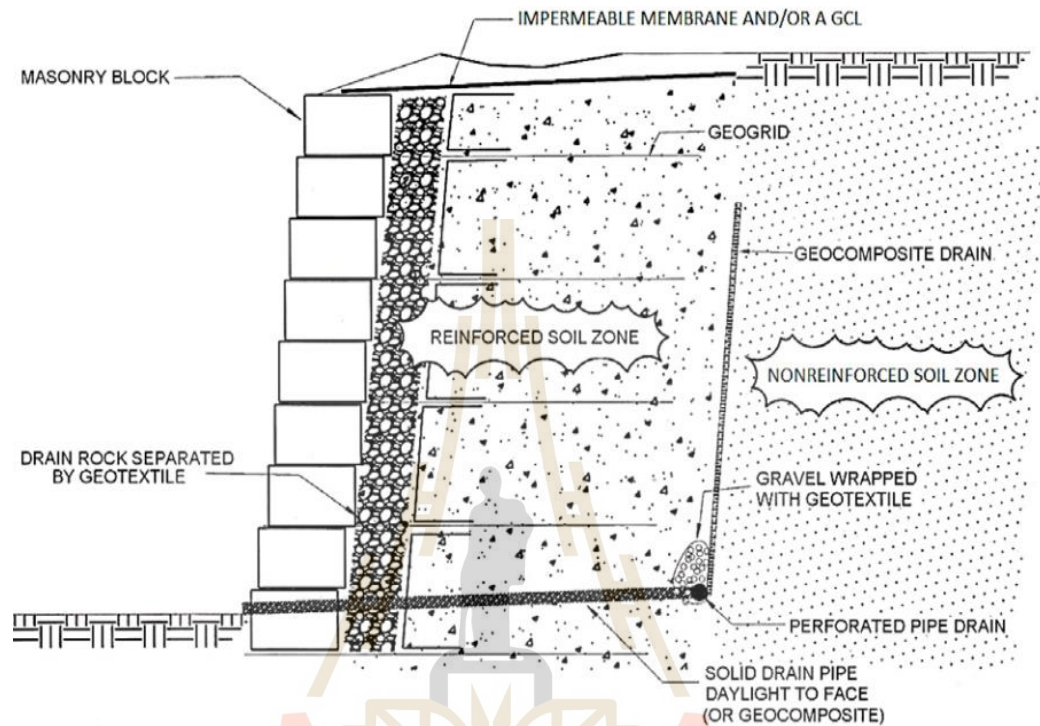


Figure 2.5 MSE wall side section showing geocomposite back drain and outlet system, geotextile filters, as well as a geomembrane surface waterproofing layer (Koerner et al. 2011).

Koerner et al. 2011 aimed on statistic internal water drainage issues within the protected soil mass within the reinforced soil mass by 46% and external water drainage serious happened around the soil behind wall by 22% count in total 82 MSE wall failure cases as research base data. There were 2 key drain controls mode which they investigated such as high phreatic surface variation from the upstream to the wall face and soil drainage capacity. His statement also concentrates on the importance of water

drainage capacity for MSE wall construction. If without sufficient water drain out that highly water rise near or close MSE wall construction is considerable because a bunch of hydrostatic pressure happens caused lateral pressure leading MSE wall collapse. Whenever MSE walls are built adjacent to, or even near to, of course standing or flowing water, for especially extremely hydrological conditions as stream river, flood, storm, must concern over a rising water surface must be taking care.



Figure 2.6 Back drainage set up behind MSE walls (Koerner et al. 2011).

Addition in their research (Koerner et al. 2011) with low permeability backfill soil will cause the mobilization of hydrostatic pressures and expansion of wet profile behind wall face. Stand on their comprehensive research, the new proper method of drainage control for MSE wall was proposed and suggested to mitigate the realistic failures. Through that method, the hydrostatic pressure developed from improper drainage control can be either internal or external with respect to the reinforced soil mass.

In hypotheses regarding of Koerner et al. 2011, base drainage by assigning high permeability soil types such as sand and/or gravels must extend beneath the reinforced soil zones for cases where high water in adjacent streams and rivers are anticipated. Furthermore, the backfill soil in the reinforced zone consists of fine-grained silts and/or clays, it is felt to be a very dangerous practice to bring the surface water into the reinforced soil zone. This research empathized the soil properties at wall base position bring various impact to the groundwater drawdown.

Various approaches have been proposed from preliminary reports of Koerner was carried out a series investigation for identifying in total 171 failure cases of MSE wall due to poor drainage capacity in period from 2013 to 2018 (Koerner et al. 2013, Koerner et al. 2018). Since 2013, there were noticeable 25 of the 63 (40%) internal water failures of MSE wall and up to 41% of all internal failures were caused by the poor performance of the drainage system indicated in Koerner report of the year 2018. This reports also recommended necessary move the drainage system to behind the reinforced soil zone and further more to couple it with the back and base drains (**Figure 2.7**). By applying this reinforced method, all possible water sources (with their

accompanying hydrostatic pressures) are eliminated from penetrating the reinforced soil zone.

Continuously, their research revealed and highlighted the various types of soils used in the reinforcement zone with more than 171 case history failures of MSE wall. Noticeably, it can be seen that approximate 103 (61%) of the failure cases used fined grained soils such containing silt and clay. The reason for use of such soils is felt to be their availability at allow or even zero cost in comparison to the cost of sand gravels which usually have to be imported to the site.

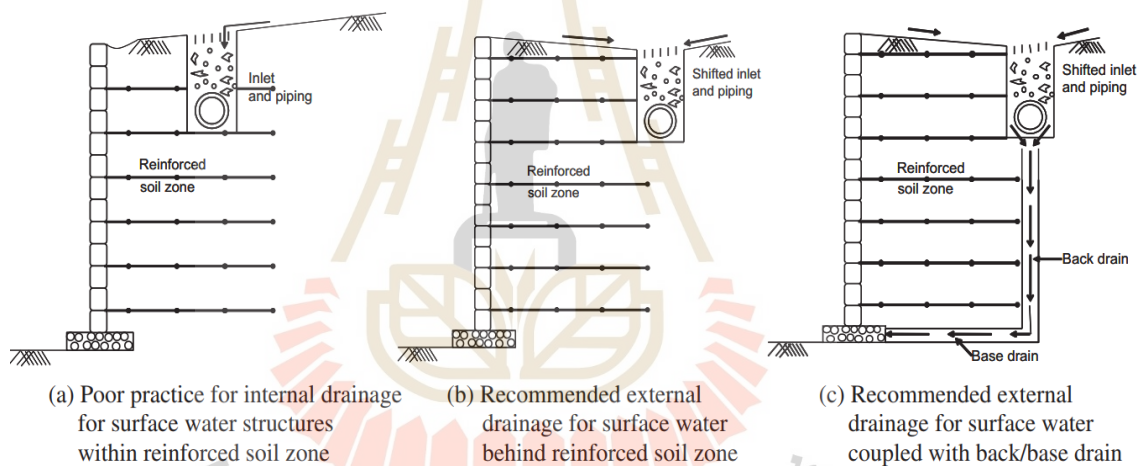


Figure 2.7 The drainage systems from within to behind the reinforced soil zone

(Koerner et al. 2011, Koerner et al. 2013, Koerner et al. 2018).

2.3.2 Backfill soil properties

In highlights of Yoo and Jung in the year 2006, they presented various serious failure cases of a geosynthetic reinforced segmental retaining wall (SRWs). Specifically, the failure of SRWs was monitored in moon soon period time in Korea. Wall geometry was 7.4 m high from leveling pad to the top of the wall crest, and

appeared to have been reinforced with 5 m-long reinforcement layers at a uniform spacing of 0.6 m in **Figure 2.8**. Mentioned wall construction was approach design to adapt to internal, external and local stability.

By comprehensive stress-pore pressure coupled finite-element analysis was additionally conducted with due consideration of both positive and negative pore pressures in saturated and unsaturated zones of the wall (Yoo and Jung 2006). They determined the essential reason causing wall collapse due to many effects of backfill soil properties and others. Their research stated a low-quality soil, with a significant percentage of fines, available at the site was used as the select fill, presumably assigning an internal friction angle to the soil that is considerably greater than the actual value. From reason determination, some suggestions were given as the first is geotechnical properties of backfill soils must be frequently evaluated for their appropriateness before let them into practical fill construction. In addition, their report emphasized complex wall geometries took considerable influences to the global slope stability analysis should be carried out for design cases with complex geometry.

Zornberg and Mitchell in the year 1994 indicated their paper about the assessment on the utilize of marginal soils as natural material through evaluating the performance of structures reported in case histories. The marginal soil contains high percentage of silt and clay or low permeability, which need high consideration when applying as backfill soil for reinforced soil structures.

From their research, permeable geotextile reinforcements may be especially useful and suggested for soil structures with poorly draining backfills because the drainage capabilities of the geotextile help to increase the structure's stability by dissipating excess pore water pressures.

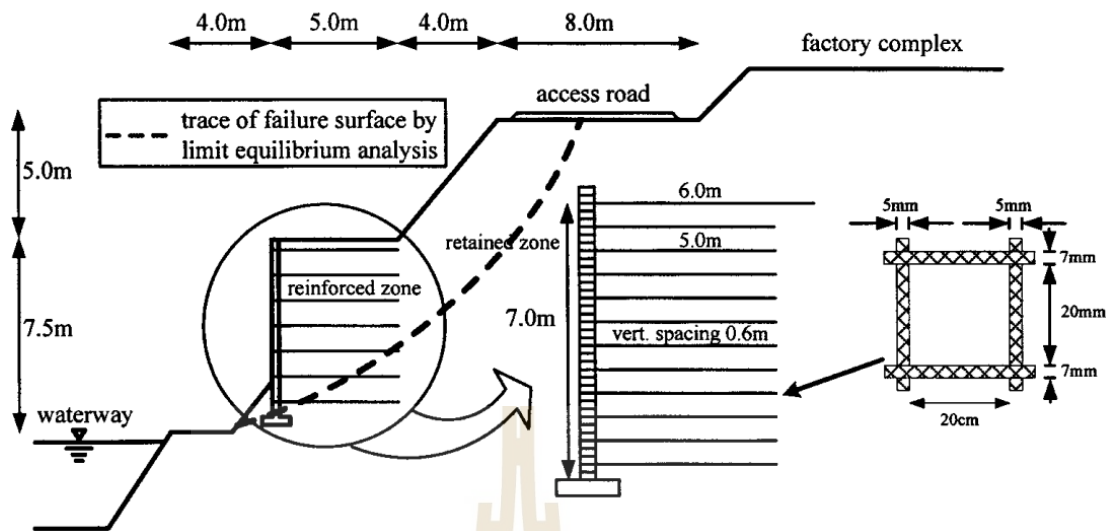


Figure 2.8 Wall geometry of failure surface obtained from limit equilibrium analysis in Yoo and Jung 2006.

From their research, permeable geotextile reinforcements may be especially useful and suggested for soil structures with poorly draining backfills because the drainage capabilities of the geotextile helps to increase the structure's stability by dissipating excess pore water pressures. Although reported results have led to some contradictory conclusions on the effects of impermeable reinforcement layers, there is already strong experimental evidence that permeable reinforcements can effectively reinforce poorly draining backfills (Zornberg and Mitchell 1994).

Vahedifad et al. 2017 utilized the fine-grained soil for his MSE wall model with high fines content (over 30% of fines passing a sieve #200 sieve). This research was performed on a wall constructed with marginal backfill (with high fines content) due to rapidly increasing interest in using marginal backfills in construction of MSE walls to reduce construction costs. The specific backfill soil properties are indicated in SWCC and k-function in **Fig 2.9**. His research stated decrease in the effective suction implies

reduction in the shear strength of the backfill soil, which can lead wall failure. Or mechanical strength parameters closely hinge on the pore water or water content spread into soil mass behind the wall. As can be seen that water content development capacity as controlling factor impact to soil strength in term of hydrological responses.

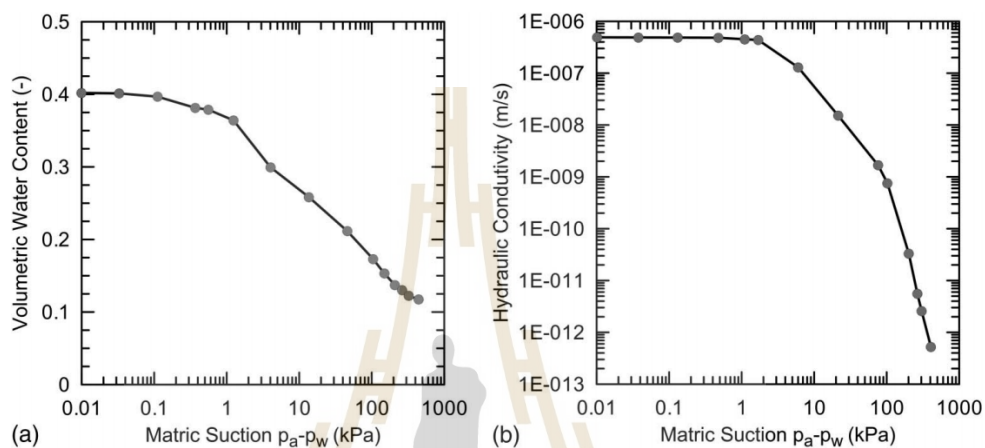


Figure 2.9 (a) SWCC, (b) k-function in Vahedifad et al. 2017.

The backfill soil nowadays is usually noticed as marginal soil (lateritic soil) due to the low construction cost of transportation especially in term of highway and earth retaining structures. This type of soil, possesses suitable hydrological properties but fail when meeting highly fined content and plasticity index requirements for mechanical stabilized earth (MSE) walls, are of particular interest to the construction industry as a potential replacement for granular backfill materials (Bui et al. 2017). The soil in Bui et al. (2017) comprises 26% fine particles (-0.075 mm) with a PI of 16%; thus, this soil fails to meet the requirement for backfill materials (AASHTO 2002), which limits the fine particles to no greater than 15%. The hydraulic conductivity of the lateritic soil at the saturated state was found to be 0.34 m/day.

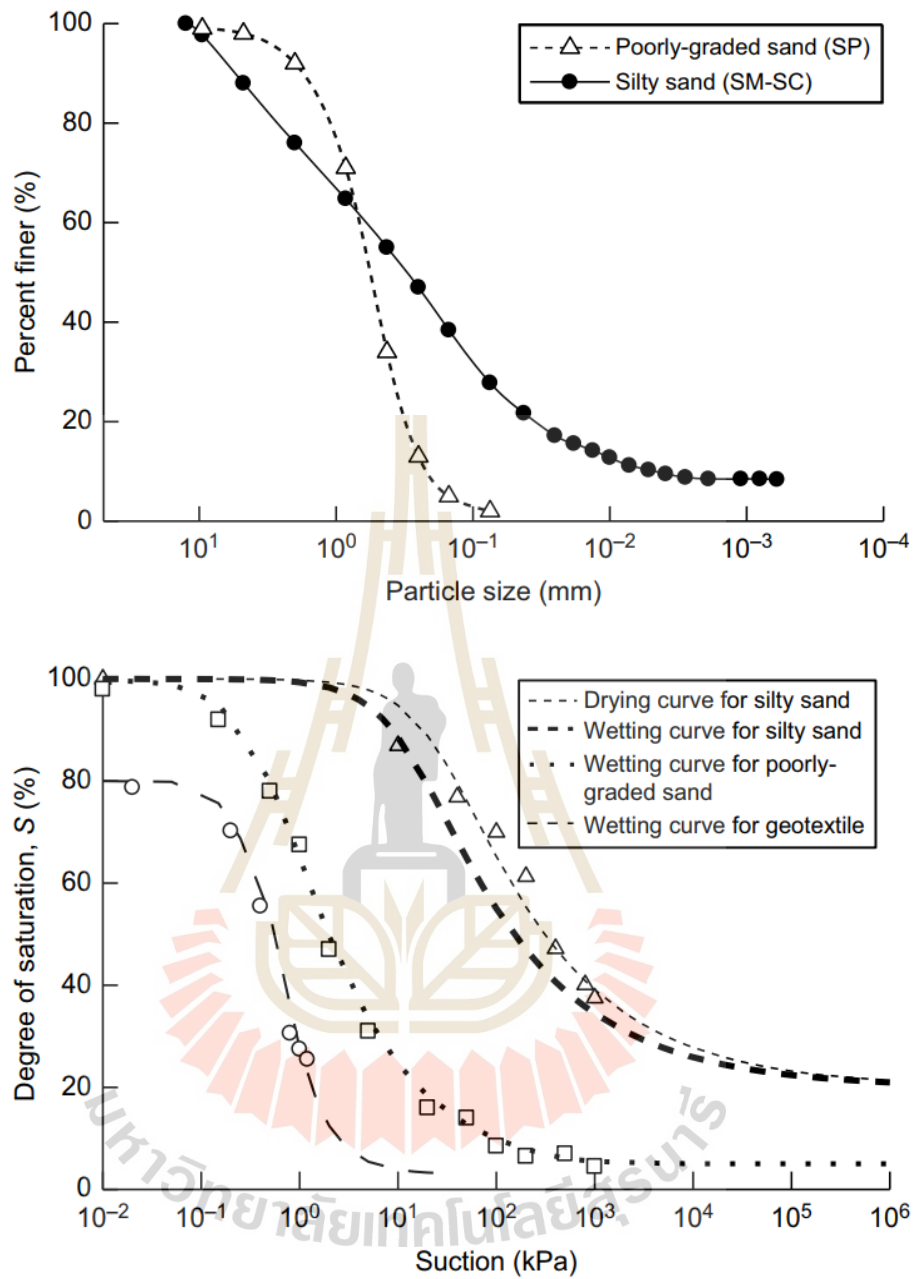


Figure 2.10 (a) Grain size distribution of the studied soils and (b) SWCC of the materials used in this study

Table 2.1 van Genuchten model parameters of the materials used in Bui Van et al. 2017.

Materials	VG-VGM model parameters				
	g_a (m^{-1})	g_n (-)	S_{res} (-)	S_{sat} (-)	k (m/day)
Sandy soil	20	1.5	0.03	1	17
Lateritic soil	0.8	1.4	0.2	1	0.3456
Geotextile	20	2.5	0.03	0.8	2000 (320) ^a
Geonet	600	40	0	1	69120

^aHydraulic conductivity of geotextile in lateral direction.

His research also utilized poor-graded sand soil (SP) from research of Chinkulkijniwat et al. (2017), which brings high drainage capacity via high permeability than lateritic soil for numerical model calibrating. Those conceptual backfill soil types (lateritic soil and poor-graded sandy soil) seem as the input data for MSE wall numerical modelling in Plaxis 2D environment. The VG parameter for all soil types in his researches and their SWCC as well as grain size distribution of each soil are shown in **Figure 2.10** and **Table 2.1**.

Highlight from (Bui et al. 2017) that the WRCs of a soil outside the protected zone has a negligible effect on the hydrological conditions of the soil inside the protected zone, and vice versa. A greater fine particle content (lower g_a (α) and g_n (n) values) in the soil outside the protected zone results in a wider distribution of the high-water-content area. Careful geocomposite installation is required for this soil type, since increasing water content results in the loss of suction forces and therefore decreased interface strength. Moreover, as for geonet properties and backfill soil properties, his research figures out the ratio of the hydraulic conductivity of the geonet to that of the soil outside the protected zone (K_{outer}) has an important role on the variation of the inner phreatic surface (**Figure 2.11**). The capillary barrier affects the level of the outer

phreatic surface, particularly if the soil outside the protected zone has a high fine particle content.

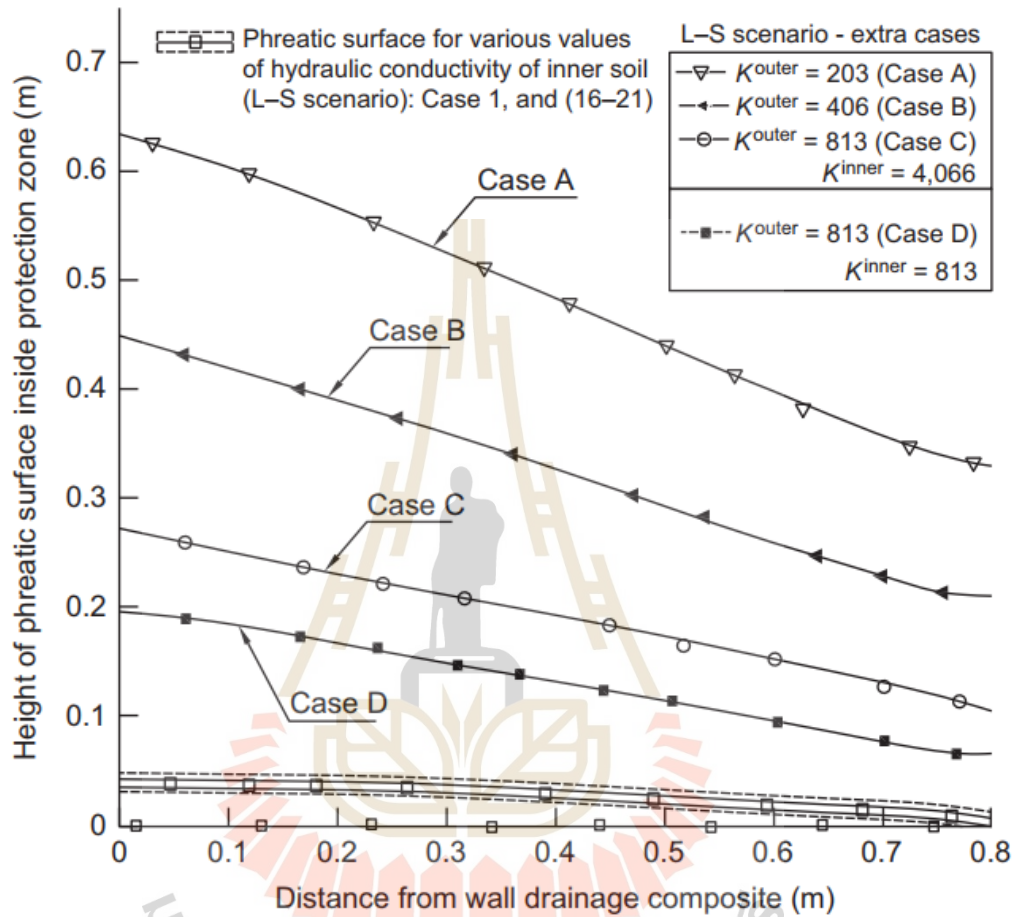


Figure 2.11 Permeability ratio effect to the inner phreatic surface level adapted from Chinkulkijniwat et al. 2017 and Bui et al. 2017.

Similarly, Albino et al. (2019) conducted numerical simulation to investigate of water infiltration into a fine-grained reinforced soil wall using geotextiles in type of non woven. A large-scale reinforced soil wall was constructed in the laboratory and subjected to water irrigation to impose a controlled infiltration. The numerical investigation was performed to provide insight into the overall infiltration process, with

a particular focus on the hydraulic behavior at soil geosynthetic interfaces that was not properly captured in the laboratory model. His results emphasized that geotextile reinforcements were found to develop a capillary break, leading to the development of positive pore water pressures in the soil overlying the reinforcements.

2.3.3 Extremely rainfall

Nowadays, with the unpredictable climate changes specially as heavy rainfall, it is becoming negative effect to the stability of cutting or filled construction as specific as MSE wall. There were many of researches attempted simulating raining period to investigate the regime of ground flows which act through MSE wall. Severe rainfall events result in substantial and unprecedented changes in the degree of saturation within the unsaturated backfill of MSE walls, which can lead to failure of these structures.

Also mentioned in research of Yoo and Jung in 2006, they conducted infiltration analysis to quantify pore pressures in the reinforced and retained soils arising from the rain water infiltration in a transient manner for use in the subsequent limit equilibrium-based slope stability analyses for geosynthetic reinforced segmental retaining wall. Finite-element modelling, for wall (**Figure 2.12**), as SEEP/W environment was used to conducted a series of numerical simulation and undergo with series of numerical results that various profile indicated the change of porewater pressure behind the wall were established (**Fig 2.13**). They applied transient flow condition with period time from June 1st to July 30th. Those important profile bring appropriate and comprehensive for new retaining wall design approaching under heavy rain periods.

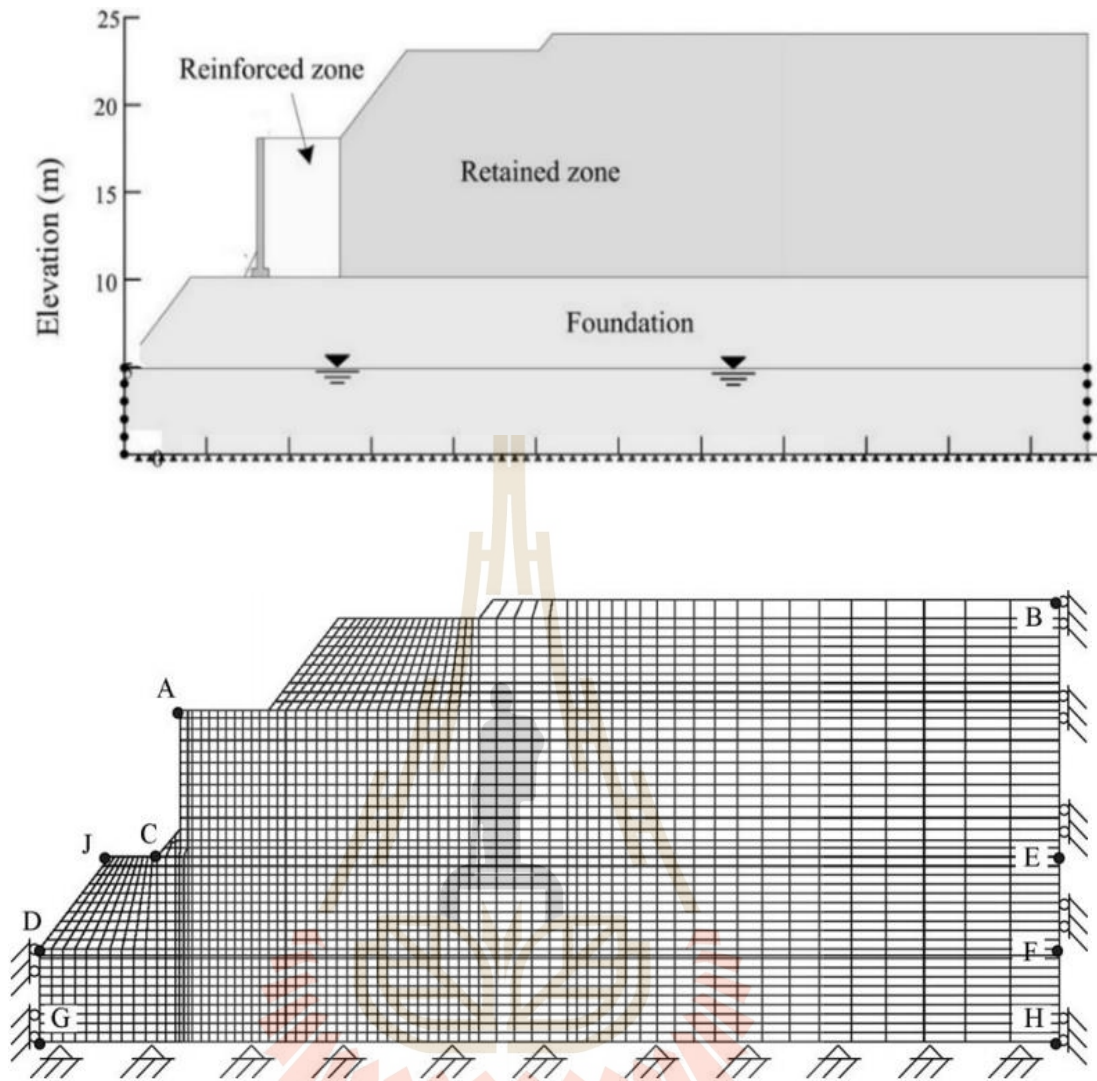


Figure 2.12 Finite-element model with meshing used in seepage analysis

From Yoo and Jung 2006.

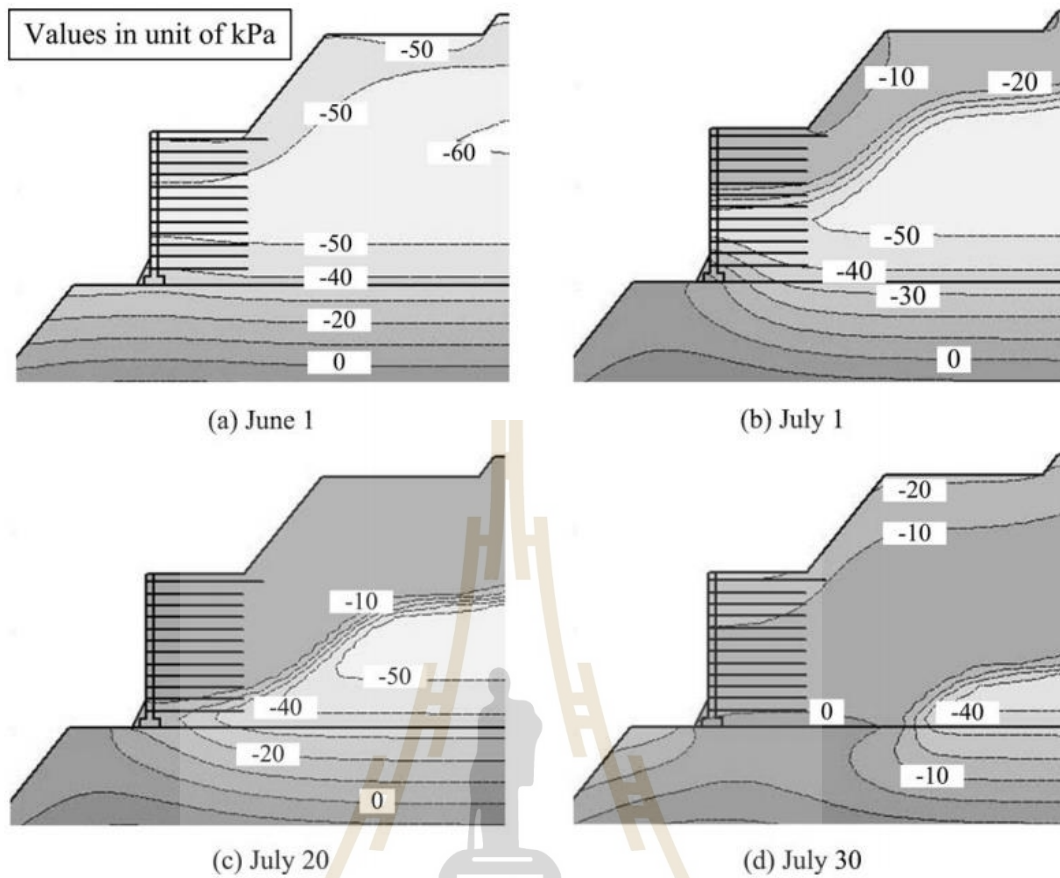


Figure 2.13 Pore water pressure distributions at different dates during June and July rainfalls in Yoo and Jung 2006.

Thuvo et al. 2015 studied numerical models of ground reinforced soil (GRS) with nonwoven geotextile drains (**Figure 2.14**). Research assumption subjected to rainfall infiltration were developed to investigate the unsaturated hydraulic behavior and stability of slopes constructed with nonwoven geotextile drains in thin layers of highly permeable sand (i.e. sand cushions). The precipitation was simulated with many scenarios to adapt to realistic weather condition. The numerical results indicated that the sand cushions reduced the development of the capillary barrier effect by acting as an intermediate material between the backfill and the nonwoven geotextile, which

bridged the gap between two materials with very different unsaturated hydraulic characteristics. The reduction of the development of the capillary barrier effect led to the accumulation of pore water pressure above the nonwoven geotextile being effectively dissipated downward.

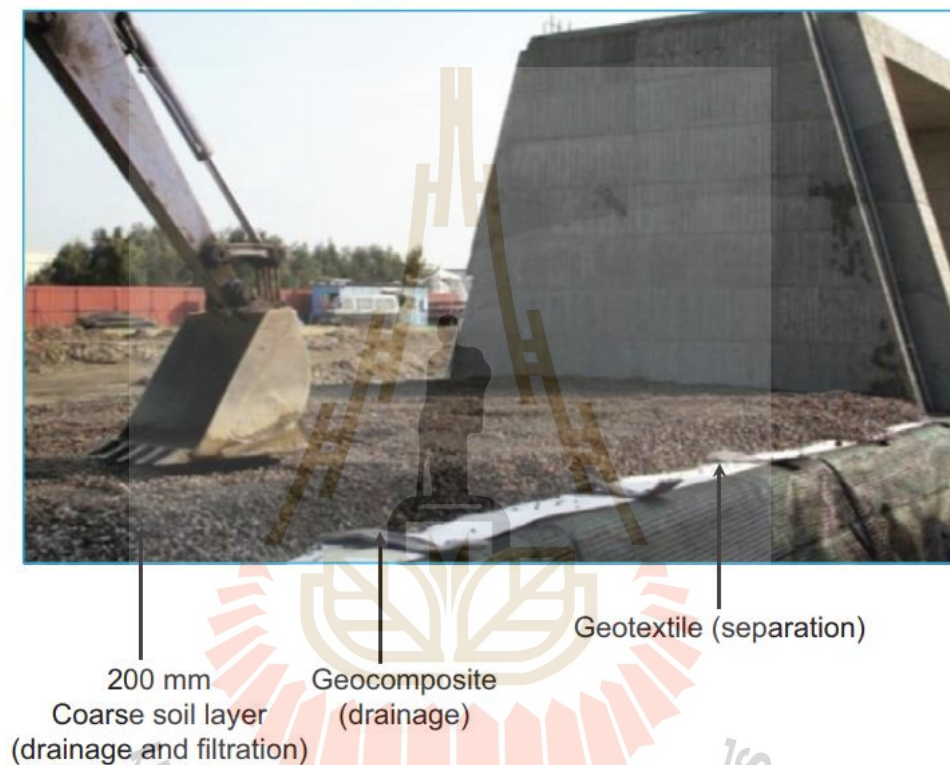


Figure 2.14 Wall construction with 200 mm thick layer of coarse soil cushion above drainage layers to placing of locally available backfill soil (Thuo et al. 2015).

The sand cushions also acted as additional drain layers to facilitate the drainage of water within the slope system (**Figure 2.15** and **2.16**). Thus, the inclusion of sand cushions enhanced the local slope stability for soils above the top geotextile layer. Based on the numerical results, methods for determining the occurrence of the capillary

barrier effect are identified from the literature and discussed. The slope stability indicated through the factor of safety (FS) reduction along with the increase of rainfall intensity (**Figure 2.13**).

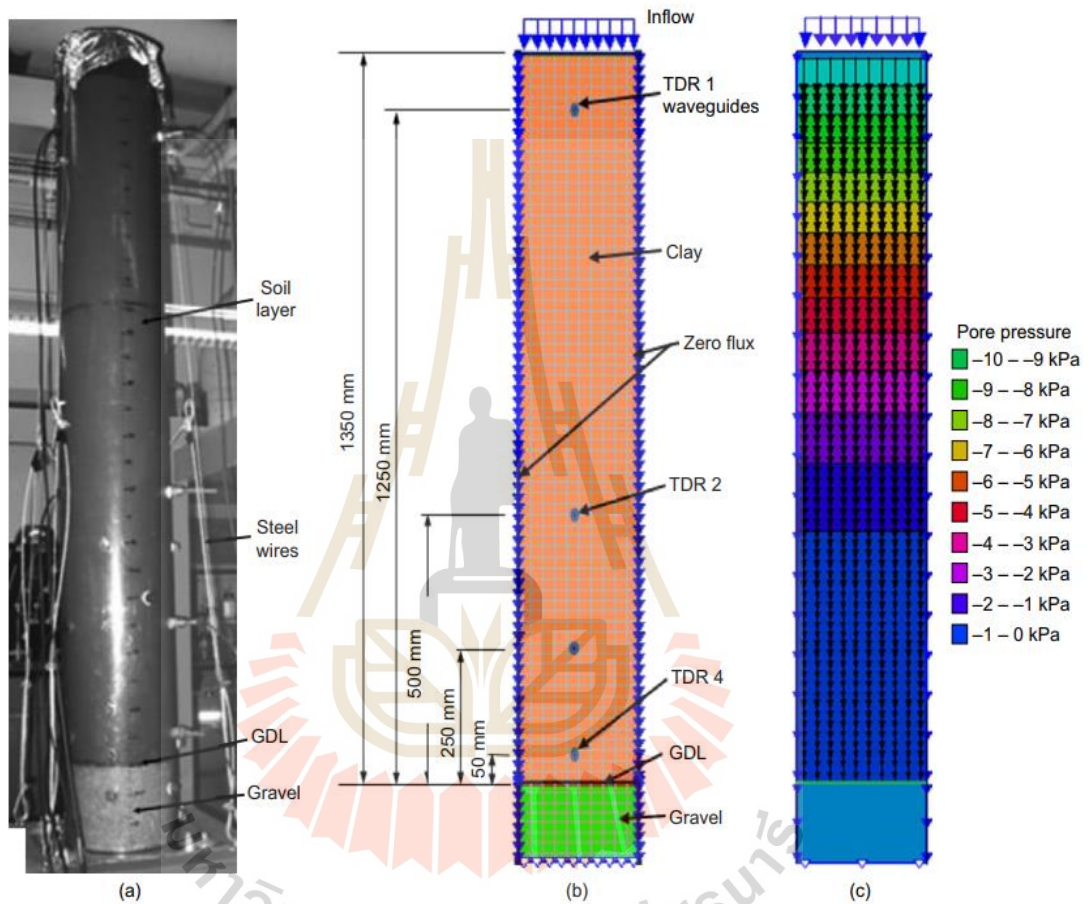


Figure 2.15 Experiment setup (a), (b) numerical model, and (c) seepage velocity vectors and pore pressure contour of the soil column infiltration test (Thuo et al. 2015).

From his research, the importance, for considering the hydrological responses variation due to extreme precipitation, is repeat focused and emphasized especially with earth retaining structural.

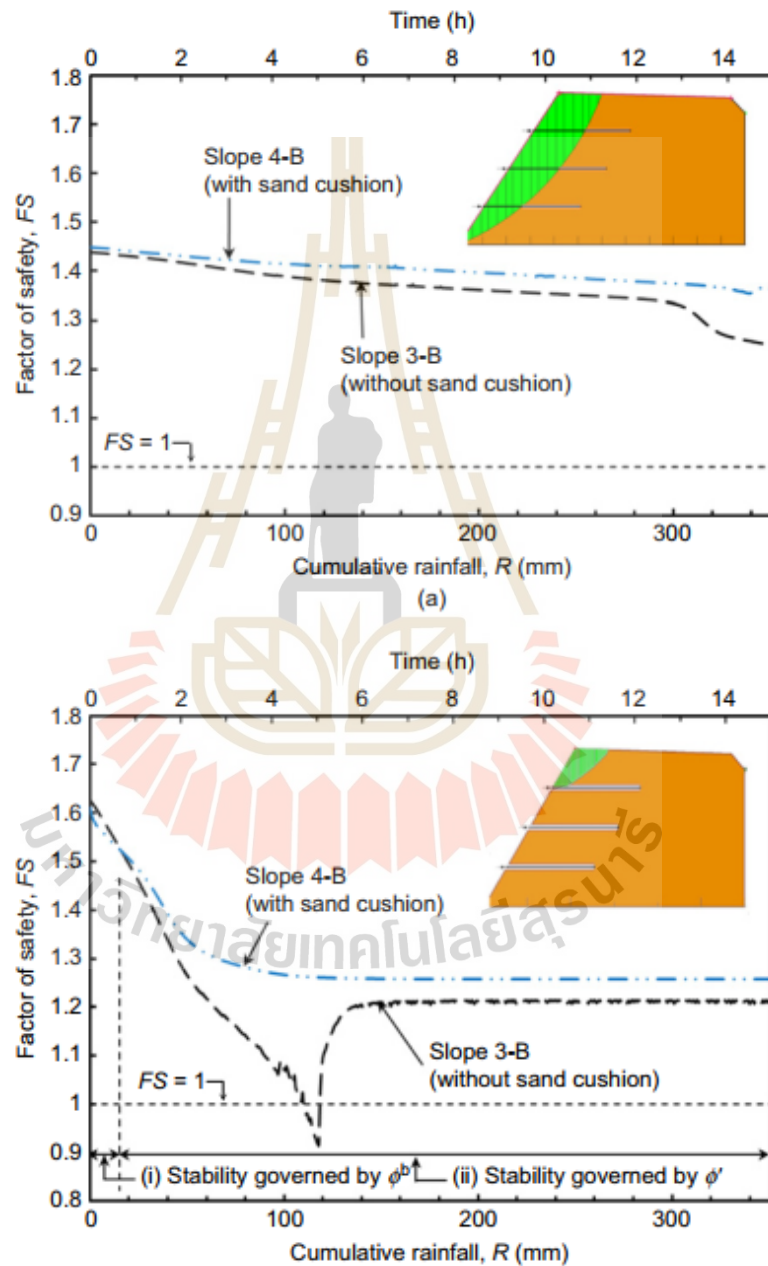


Figure 2.16 Variation of slope stability with rainfall as (a) overall FS, (b) local FS for soils above the top geotextile layer (Thuo et al. 2015).

In cutting edge research of Robinson et al (2017), a series of numerical simulation for investigating the impact of rainfall trigger (from long time precipitation) to instability of slope through high development of pore water pressure increase inside natural soil of slope. Their results are investigated along with time dependent with increment of rainfall intensity. A numerical modeling are approached for more comprehensive and appropriate in constancy to practical conditions in this research.

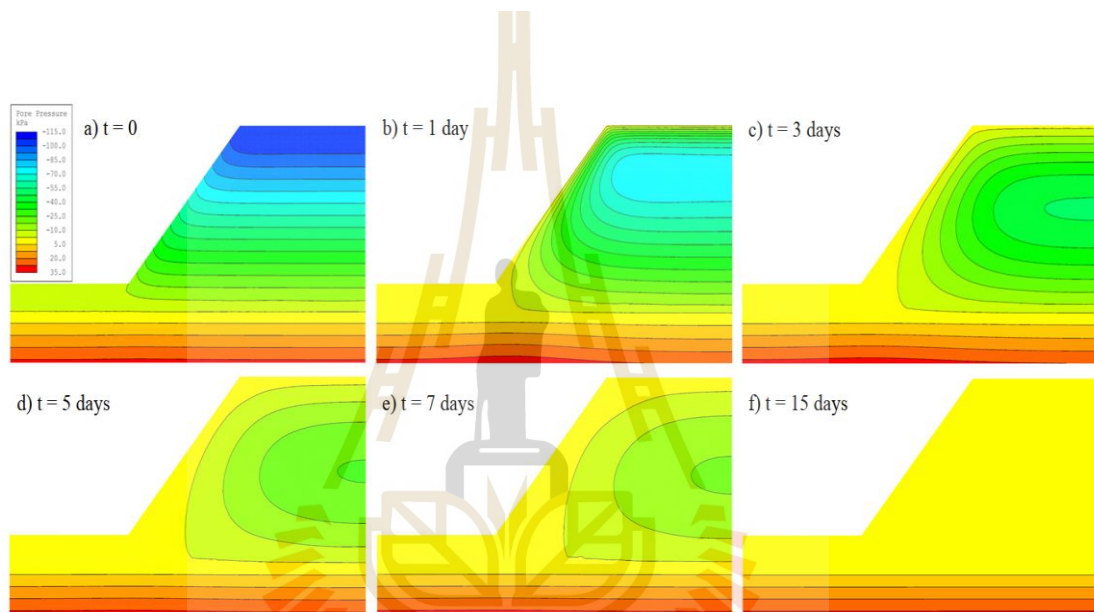


Figure 2.17 Pore-water pressure contour inside slope with time factor (Robinson et al. 2017).

Research hydrological objects comprise as effective saturation degree and pore-water pressure increment in their conceptual cross-section of slope. Under high a higher rain intensity happened in long time that causes an engineered slope or specific earth retaining wall construction contain much water in void space in nature soil or more rising of pore water pressure. That lead natural soil rapid is saturated and strength reduction majorly and failure occurrences. In short time period, there were many

significant rises of effective saturation degree in studied cross-section. The changes of research objectives distributed along with the depth from top slope to the toe and to the basic water level at slope base. Magnitude of that changes also varied considerable following vertical and horizontal direction.

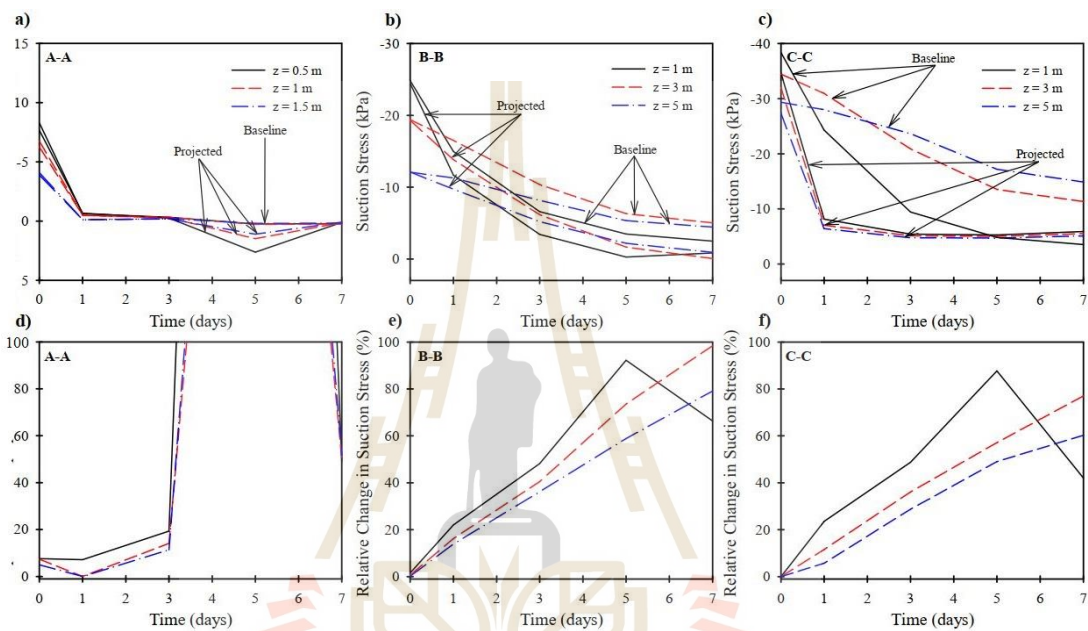


Figure 2.18 Simulated suction stress for precipitation extremes along three cross-sections of slope modelling (Robinson et al. 2017).

The statement from Robinson et al. 2017 that there was an integration of hydrological factors combined with climate analysis to serve for geotechnical work design. A quantitative method also to compute the amount and quantify climate change-induced changes in extreme precipitations may affect the performance of earth retaining structures. The modeling approach introduced in this paper can be applied to other geotechnical engineering structures, other regions and climate extremes as well, to address the direct impact of climate change on geotechnical infrastructure.

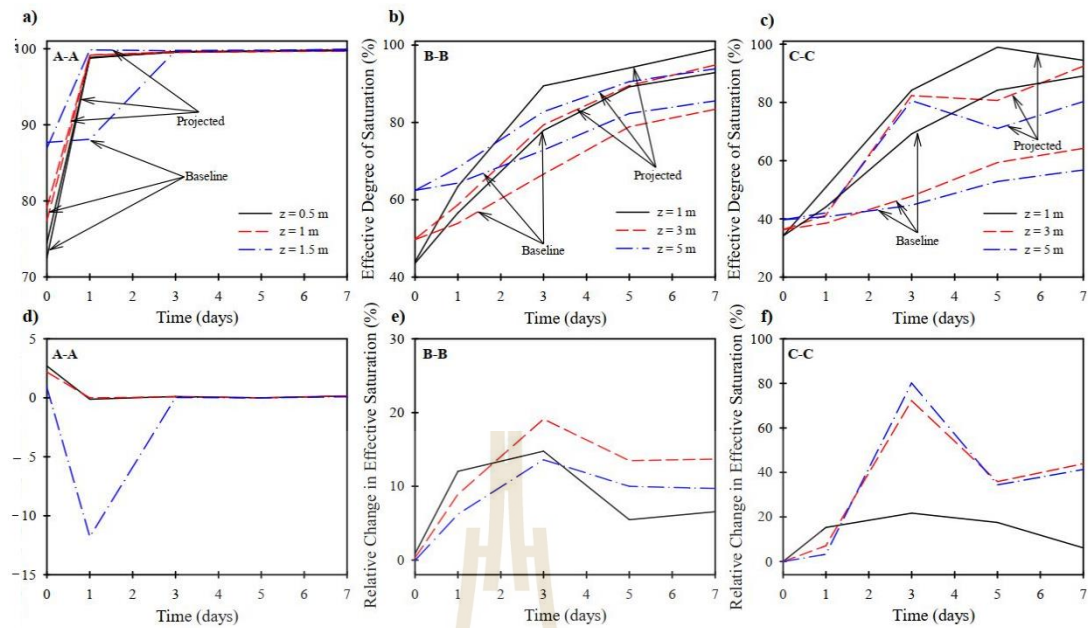


Figure 2.19 Simulated effective degree of saturation (S_e), along with percent relative change in time, for baseline and projected precipitation extremes along three cross-sections of the model slope (Robinson et al. 2017).

From Vahedifad's research of the year 2017 recognized the high precipitation in long time period become an extreme challenge for MSE wall construction. Various figures of increased rain intensity due to climate change as well as occurrence of several precipitation-induced failures in MSE walls emphasize the need to assess the resilience of MSE walls in a changing climate. Increased rain intensity increases the degree of saturation of unsaturated backfill, leading to a reduction in soil suction and soil strength, and an increase in lateral earth pressures behind wall face and load to reinforcement area. Some of typical model failure phenomena such as uplift (heave), subsidence, internal erosion piping and slope instability (Vahedifad et al. 2017).

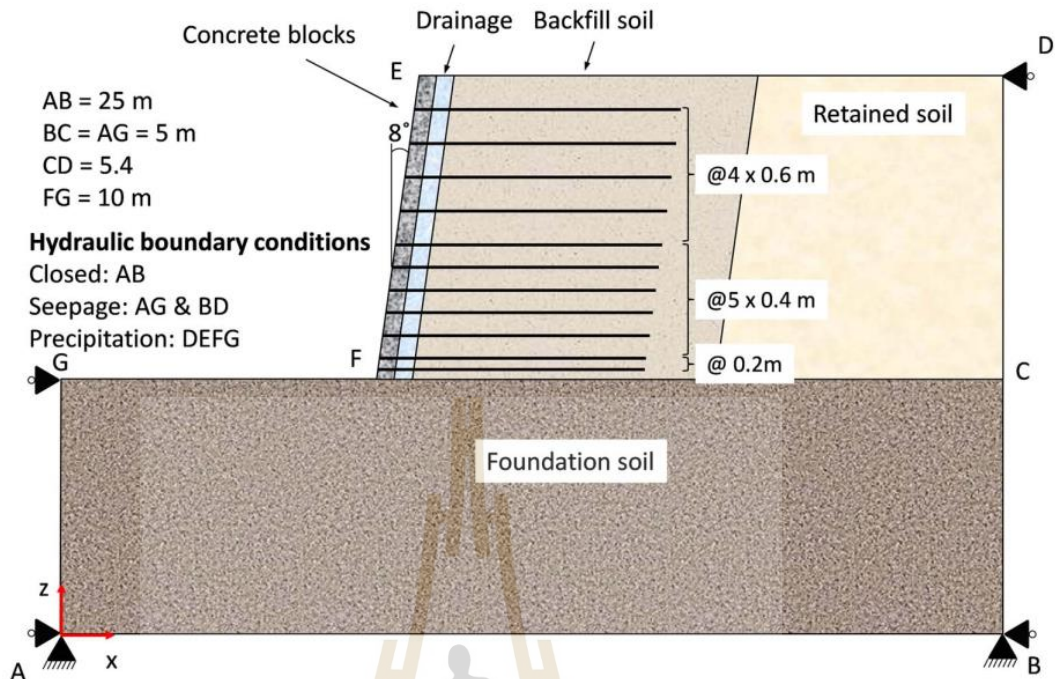


Figure 2.20 Geometry of the model MSE wall used in Vahedifad et al. 2017.

His study conducted couple analysis as hydro-mechanical responses of a mechanically stabilized earth (MSE) wall modelling (**Figure 2.20**) constructed with marginal backfill to extreme rainfall events under a changing climate. Their results highlight the importance of assessing potential impacts of climate change and variability on the performance of MSE walls (**Figure 2.21** to **Figure 2.26**).

This effect was more notable for 7-day rainfalls, in which up to 157% change in effective degree of saturation was reached behind the wall when the initial suction is 60 kPa. Such an increase is even greater for the case with initial suction of 240 kPa, where up to 667% change in effective degree of saturation was reached behind the wall (Vahedifad et al. 2017).

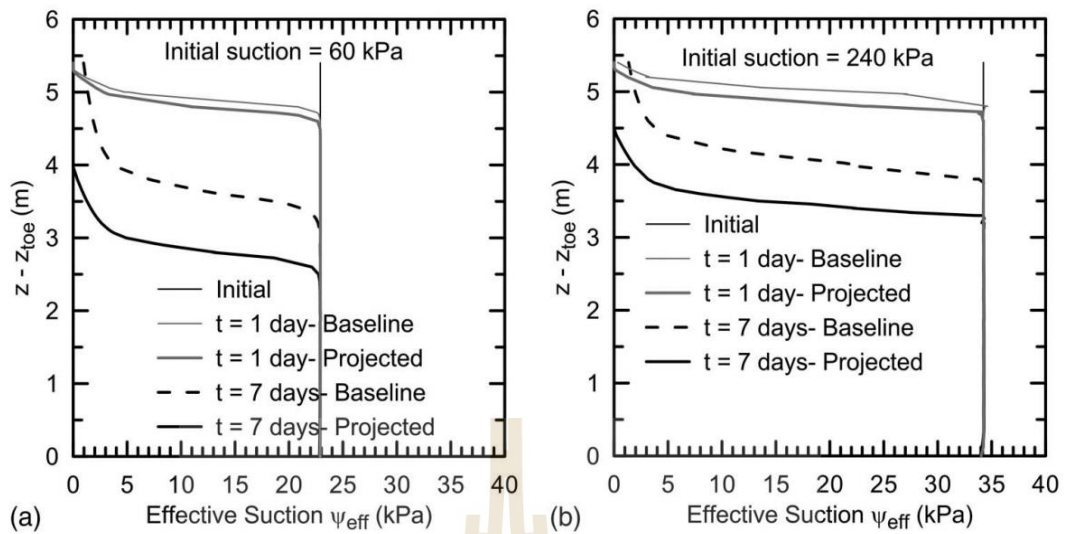


Figure 2.21 Effect of change in intensity and duration of rain behind the wall on effective suction with initial suction of (a) 60 kPa; (b) 240 kPa (Vahedifad et al. 2017).

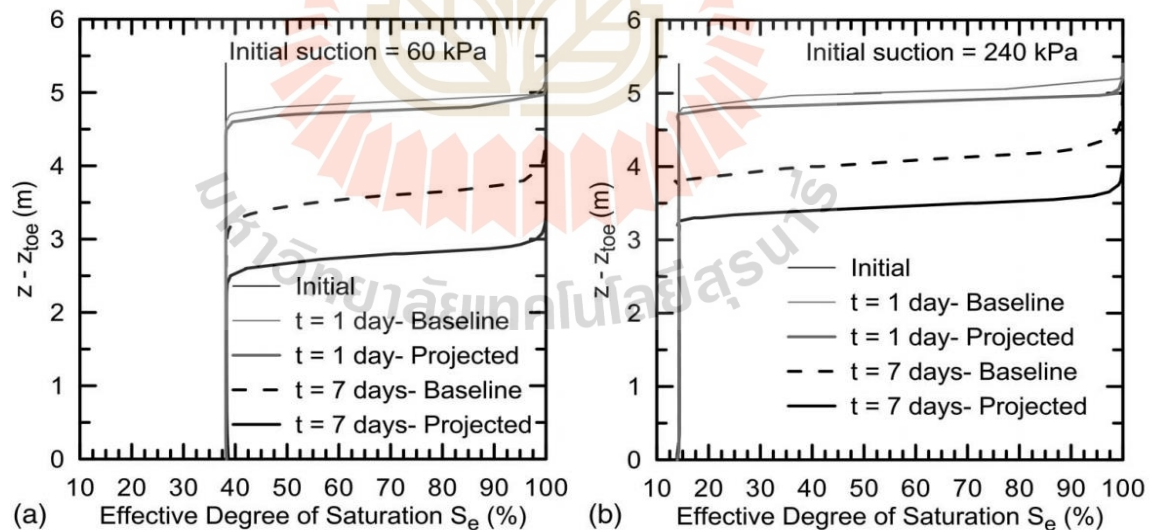


Figure 2.22 Effect of rainfall intensity and duration behind the wall ($x - x_{toe} \frac{1}{4} 2$ m) on effective degree of saturation with initial suction of (a) 60 kPa; (b) 240 kPa (Vahedifad et al. 2017).

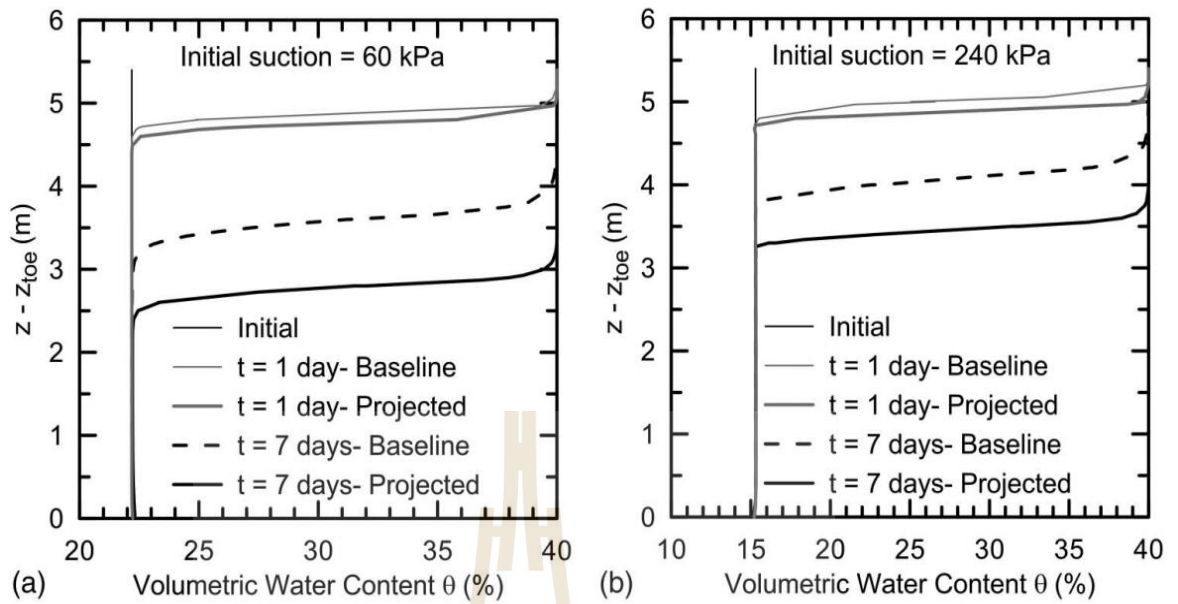


Figure 2.23 Effect of rain on change in the volumetric water content for initial suction of (a) 60 kPa; (b) 240 kPa (Vahedifad et al. 2017).

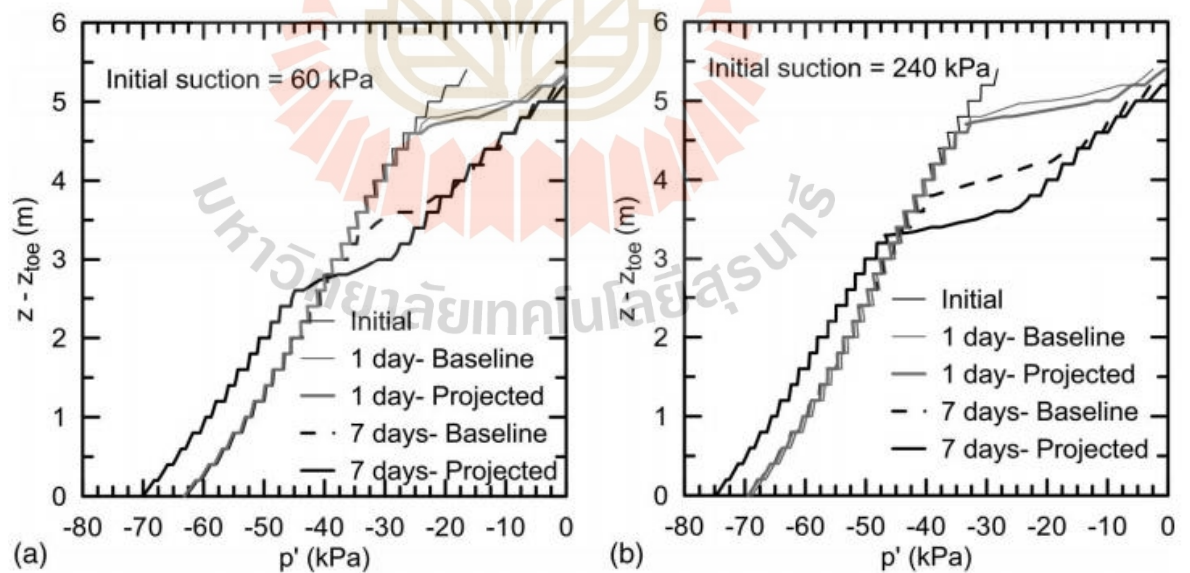


Figure 2.24 Effect of rain on change in the mean effective stress for initial suction of (a) 60 kPa; (b) 240 kPa (Vahedifad et al. 2017).

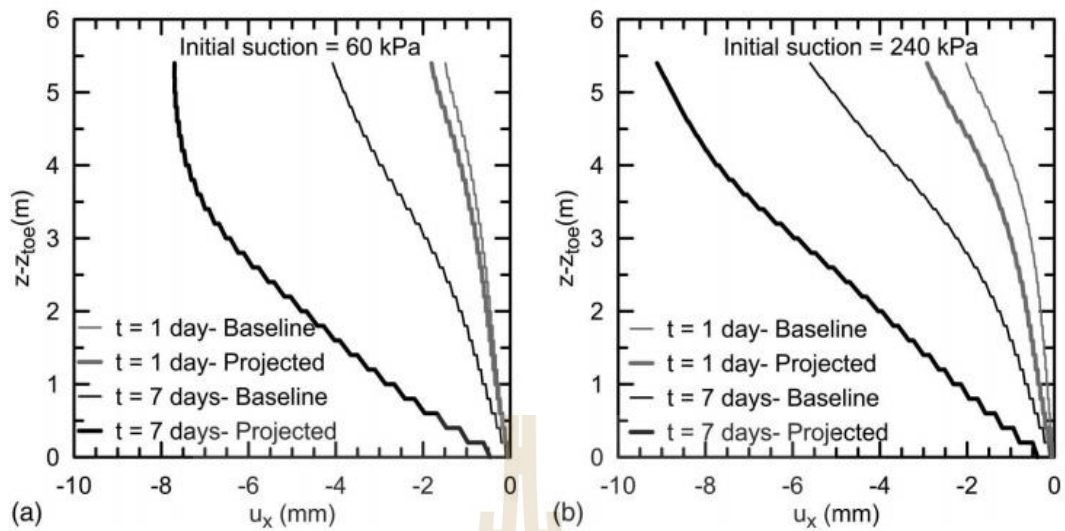


Figure 2.25 Effect of rainfall intensity, duration and initial suction on the displacement of the wall: (a) displaced wall with initial suction of 60 kPa; (b) displaced wall with initial suction of 240 kPa (Vahedifad et al. 2017).

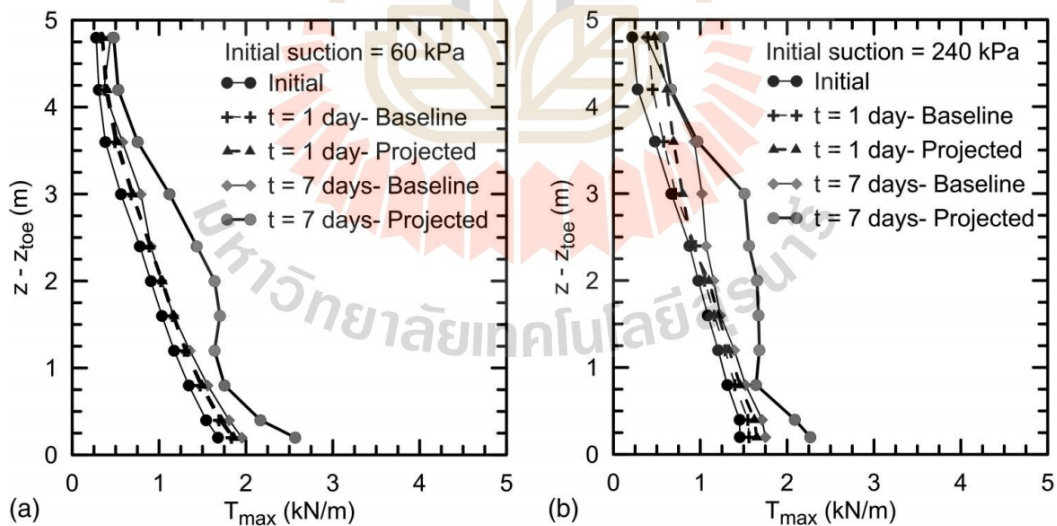


Figure 2.26 Effect of change in intensity and duration of rain on the maximum reinforcement loads T_{max} : (a) maximum reinforcement load for initial suction of 60 kPa; (b) maximum reinforcement load for initial suction of 240 kPa (Vahedifad et al. 2017).

One of the outstanding from (Vahedifad et al. 2017) that by greater influence of extremely rainfall on the upper part of the wall was attributed to the hydraulic properties of the marginal backfill used in finite element approach. It is obviously for the duration of rain also could be used for determining factor of safety in MSE wall performance. Furthermore, it was shown that the wall with higher initial suction was influenced more by the extreme rainfalls than was the wall with lower initial suction.

Portelinha et al. (2017) conducted a full-scale geotextile-reinforced soil wall in order to assess the characteristics of water infiltration and its effect on the structure performance. An irrigation system was used to simulate controlled rainfall events and the monitoring program allowed the evaluation of the advancement of infiltration and internal geosynthetic drainage.

After breakthrough, water was also found to migrate along the geotextiles, suggesting that the reinforcement layers ultimately provided in-plane drainage capacity. While generation of positive pore water pressures (**Figure 2.27**) was not evidenced during his tests, the advancing infiltration front was found to affect the performance of the wall. The development of capillary breaks was found to retard the infiltration process for the conditions in this study, retardation was 4 days per reinforced layer (**Figure 2.28**).

Specifically, the infiltration front was observed to reach the bottom of the geotextile-reinforced soil wall after approximately 30 days of irrigation. On the other hand, the infiltration front was expected to reach the base of the wall in approximately 10 days without the development of capillary breaks.

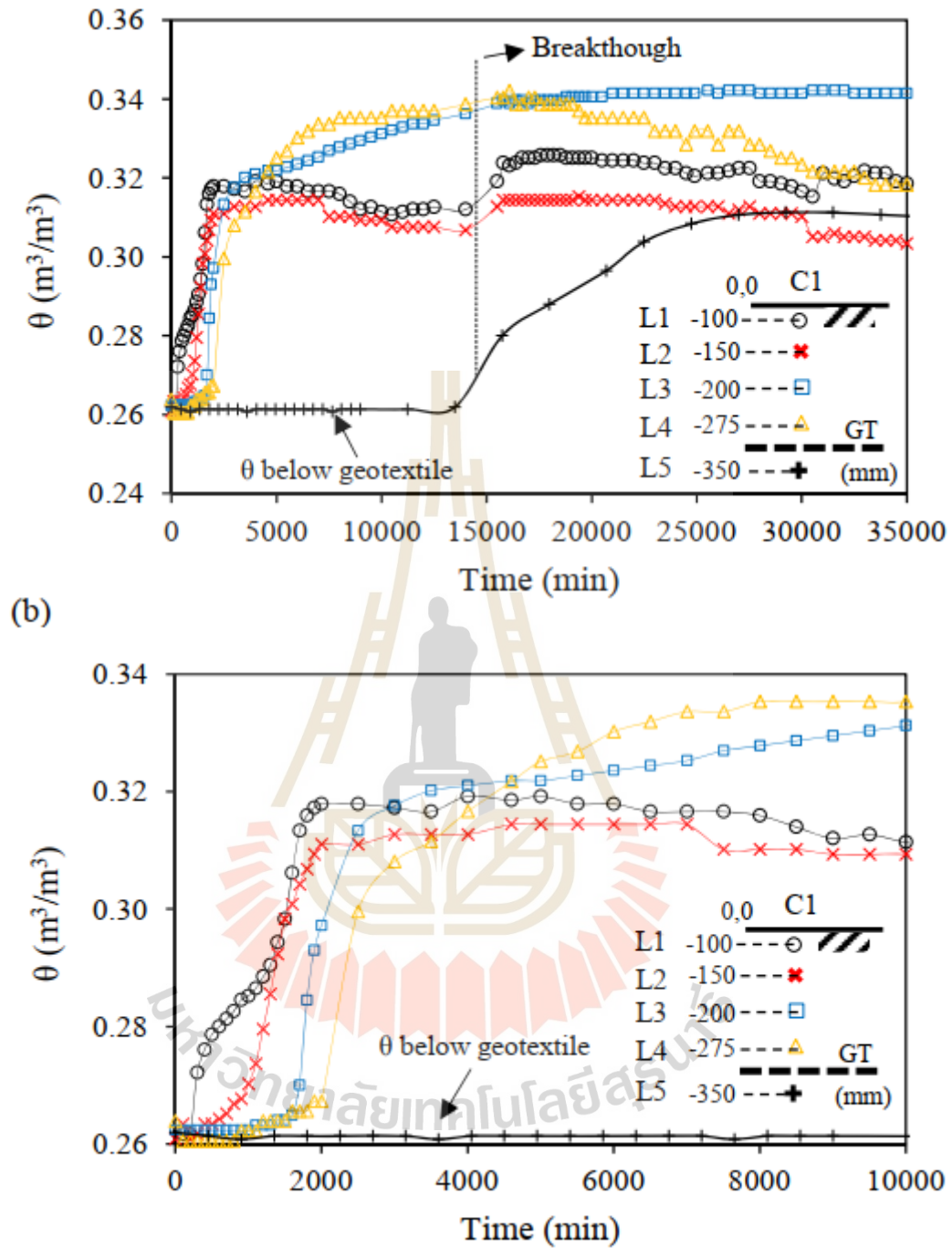


Figure 2.27 Volumetric water content measured in the upper reinforced soil layer: (a) until 35,000 min and (b) until 10,000 min in test from Portelinha et al. 2017.

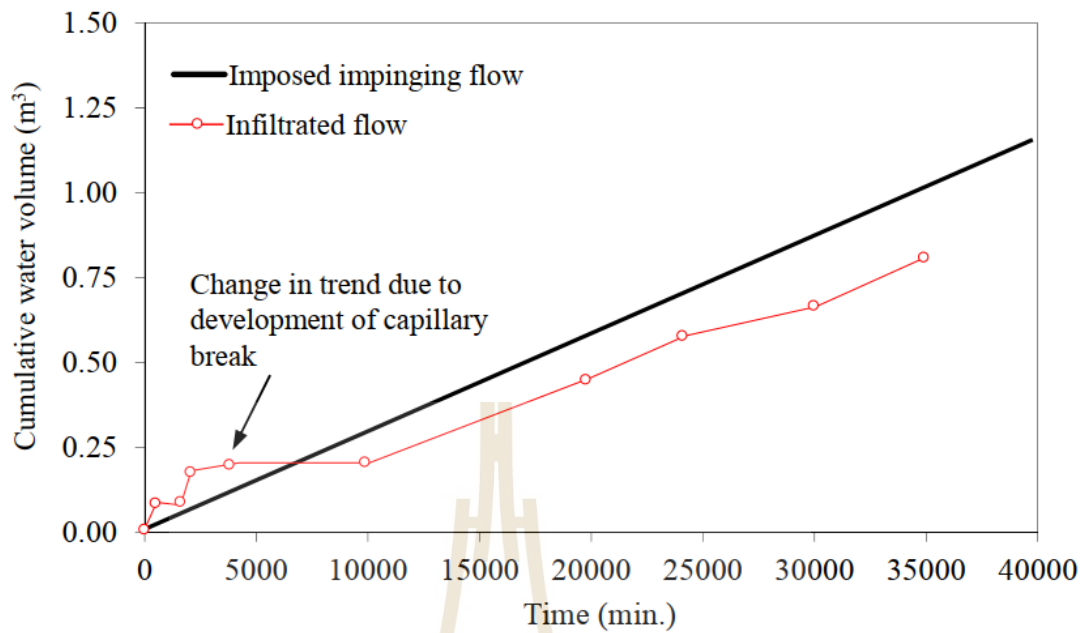


Figure 2.28 Cumulative water volumes into the reinforced soil wall under high precipitation from Portelinha et al. 2017.

In research of Bui Van et al. 2017 mentioned and simulated the effect of heavy rainfall through the change of water level rise behind the MSE wall construction. In their numerical model of MSE wall, the groundwater level behind an MSE wall is very high, similar to the situation that may occur in mountainous areas during heavy rainfalls. The water level at upstream tank was increased stepwise from heights of +0.0 m, +0.4 m, +0.7 m, and +1.0 m. The upstream water level was increased after reaching a steady state in which there was no change in the water content values, read from the TDR probes, for a period greater than 24 hours. VG parameter influenced to changes of water saturation around protected area with different soil type scenarios along elevation from the wall height are shown in **Figure 2.29**.

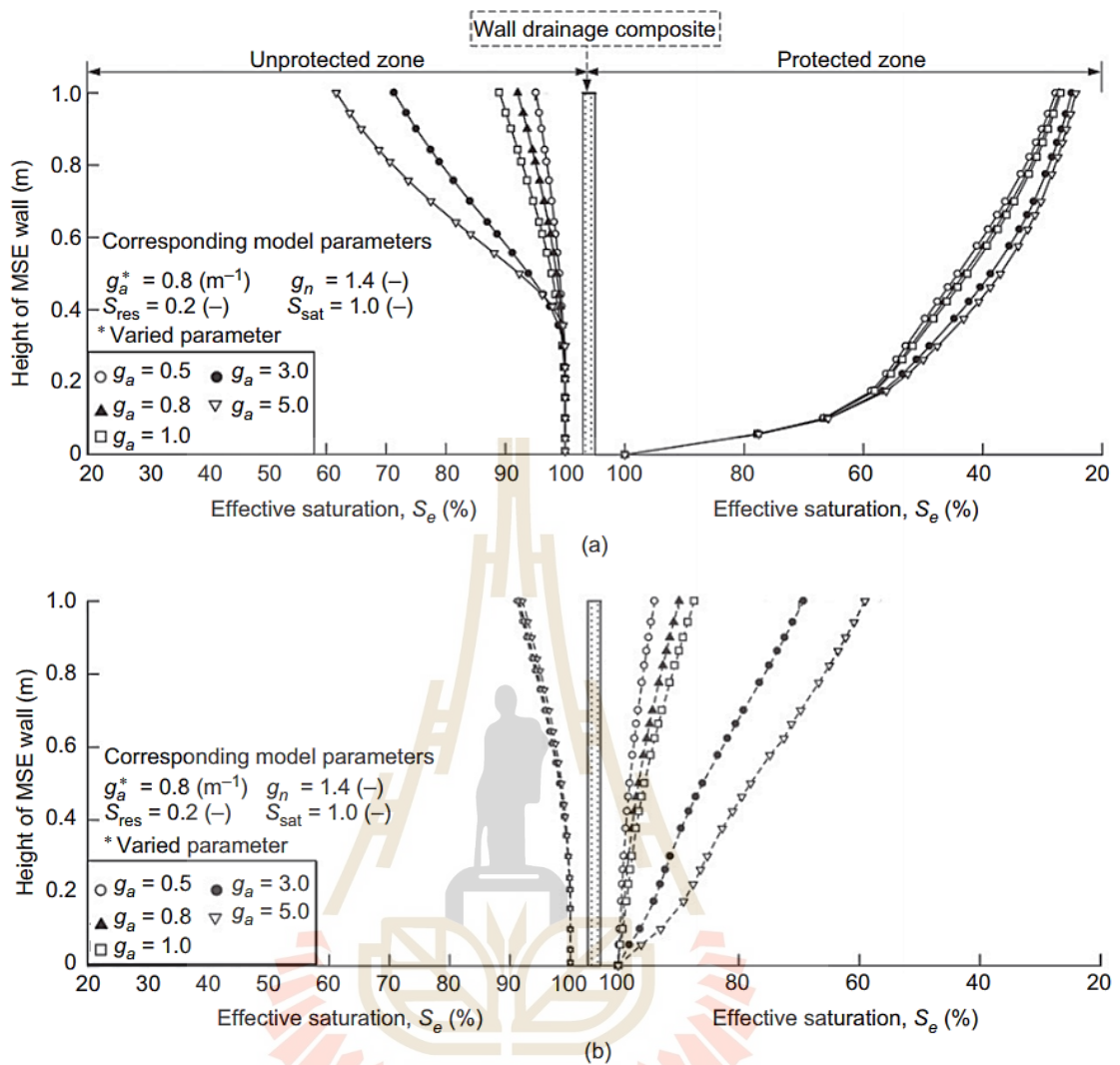


Figure 2.29 (a) Effective saturation profiles along the vertical sections around geocomposite interface for varying g_a values of the native lateritic soil for the L-S scenario and (b) for the L-L scenario in Bui Van et al. 2017.

In his research the phreatic line alternation is examined under the research scenarios for different types of soil inside and outside reinforced area. By differential native soil permeability of lateritic soil and sandy soil at upstream, the change of phreatic line varying also indicate as different inside and outside, also lower phreatic line inside reinforced area come from the high water drain out when water move to

geocomposite drainage system. The specific change of phreatic line via series of variation VG model parameters as shown in **Figure 2.30**.

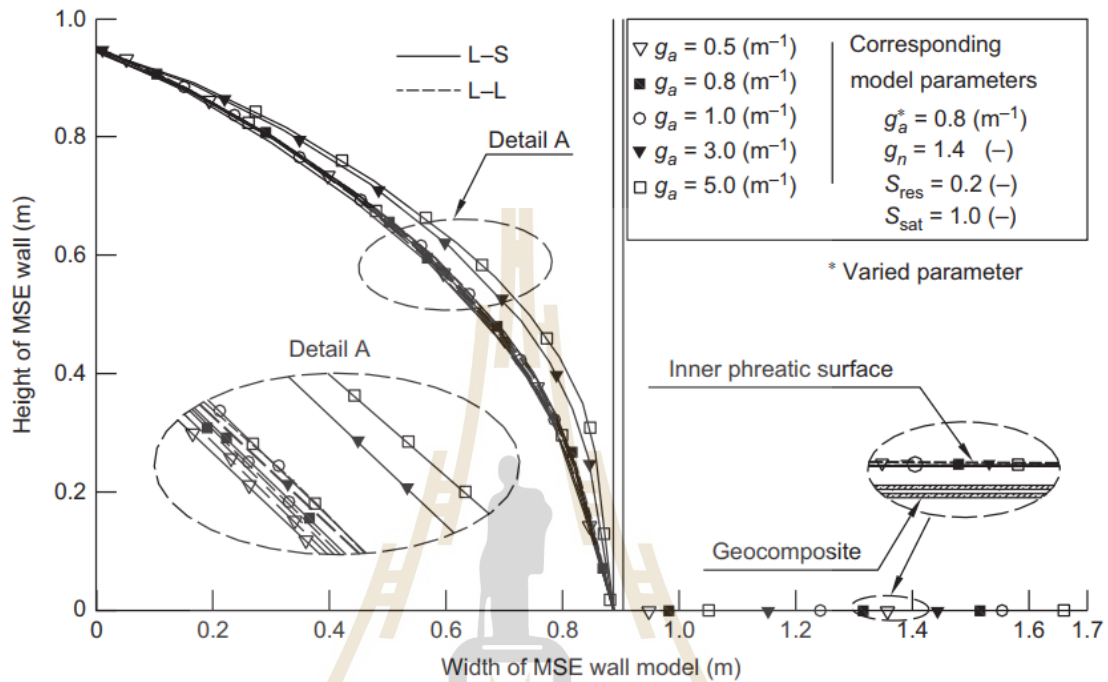


Figure 2.30 Variation in the phreatic surface outside the protected zone for varying $\alpha (g_a)$ values for lateritic soil from Bui Van et al. 2017.

2.4 Geocomposite material properties

The geocomposite material, which include geonet as core drain and covered sandwiched geotextiles, appears very high drainage capacity due to their high permeability with high open-sized mesh in comparative to normally backfill soil. Typical application of many kinds geosynthetics are appropriated system or porous layers in order to reinforce earth fill construction/retaining wall/MSE wall drain out water or reduce water content separate widely behind wall face. Depend on specific surrounded hydrological condition, geocomposite material has various way of

hydraulic behavior to adapt and reduce the negative of hydrological responses. The hydraulic behavior of permeable geosynthetics within unsaturated embankments subjected to infiltration is examined using the finite element method is becoming concern in many literatures.

There were many researches attempted to investigate comprehensively hydraulic properties of geocomposite material especially be the main drainage core geonet. Dickinson (2010) determined the relationship between geonet transmissivity and geonet thickness through a series of laboratory testing and in-situ large-scale testing. Giroud et al. (2014) and Yarahmadi et al. (2017) studied the reduction of hydraulic transmissivity due to creep deformation.

2.4.1 Geotextiles properties

The geotextile properties were outstanding in research of Iryo and Rowe (2005) and their results of hydraulic behavior of geotextile material become the basic information in term of hydrological properties for many research. The specific detail of hydraulic properties as shown in **Table 2.2**. In this paper, they used van Genuchten – Mualem (Mualem 1976) unsaturated flow model is employed to evaluate unsaturated hydraulic characteristics for both the soil and nonwoven geotextile.

Table 2.2 Basic relevant properties of geotextile (Iryo and Rowe 2005).

Mass per unit area, m_a (g/m ²)	310
Thickness of geotextile, $t_{\text{geotextile}}$ (mm)	3
Porosity, n_p	0.92 ^a
Saturated hydraulic conductivity in plane direction, $k_{\text{sat geotextile plane}}$ (m/s)	2.3×10^{-2}
Saturated hydraulic conductivity in cross plane direction, $k_{\text{sat geotextile cross}}$ (m/s)	3.5×10^{-3}
Tensile strength in machine direction (kN/m)	21.6
Tensile strength in cross to machine direction (kN/m)	17.2

^aEstimated value assuming unit weight of polyester $\gamma_{\text{polyester}} = 12.75 \text{ kN/m}^3$.

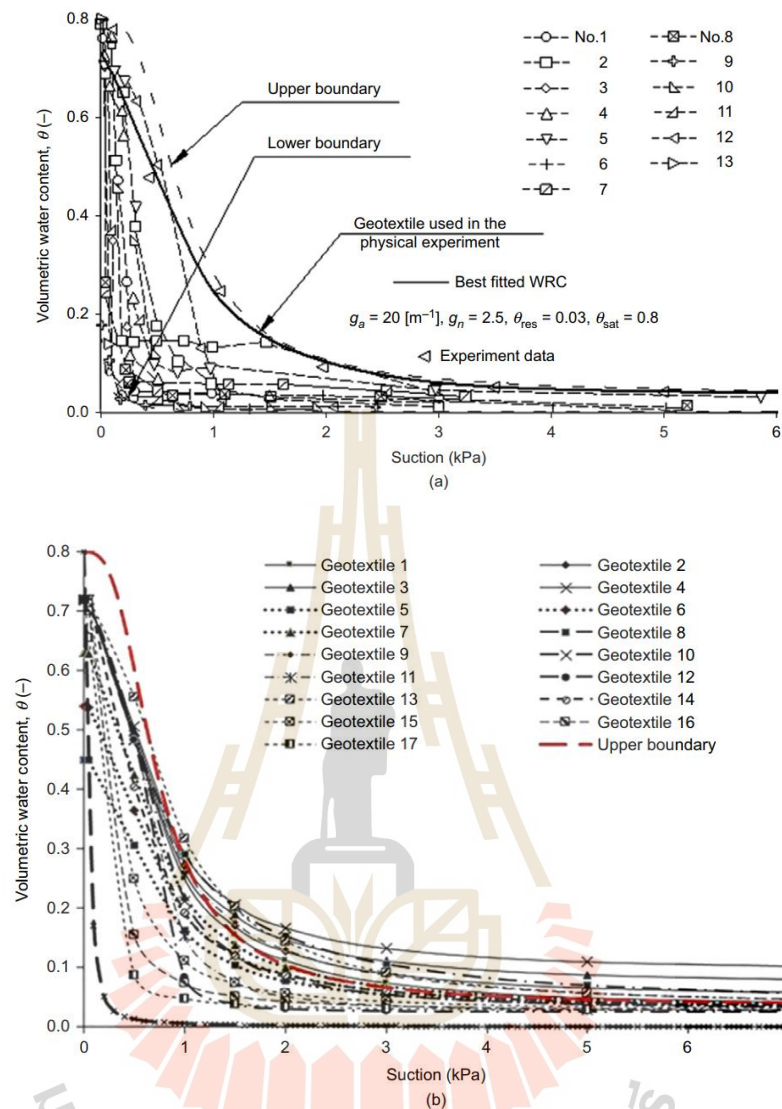


Figure 2.31 (a) Wetting phase WRC geotextiles reported and of the geotextile used in the physical test, and (b) WRC of all geotextiles assigned to the numerical experiment by Iryo and Rowe (2003) (Chinkulkijniwat et al. 2017).

Their study shows that nonwoven geotextiles contact water flow possible in conditions where the pore pressure is negative as seem as no water inside void space. That point proves they acted as a sufficient drainage material in above conditions. The paper is also shown that the contribution of the nonwoven geotextile to the stability for

embankment as a horizontal layer drainage material, is much less substantial than its role as a reinforcing material.

Iryo and Rowe 2005 varied van Genuchten – Mualem model parameters for the soil were obtained based on consideration of typical published values combined with a parametric study of the infiltration into unreinforced embankment. Varied values consist $n = 1.5, 2.0, 2.5$; $\alpha = 0.25, 0.4, 0.8$ (1/kPa); $k_{sat} = 1.0, 1.3, 2.0, 4.0, 6.0, 10.0 \times 10^{-5}$ (m/s); and $S_{res\ max} = 90, 92, 95$, and 100%. The most significant parameters were n and α . A suitable combination was selected based on a comparison of the behavior and volumetric water content profiles to the observed values. The water characteristic curve and the hydraulic conductivity function for the soil deduced from this study are shown in **Figure 2.31** and **Figure 2.32**. These water characteristic curve and the hydraulic conductivity function are deployed and cited in many research papers as Chinkulkijwat et al. 2015 and Bui Van et al. 2017.

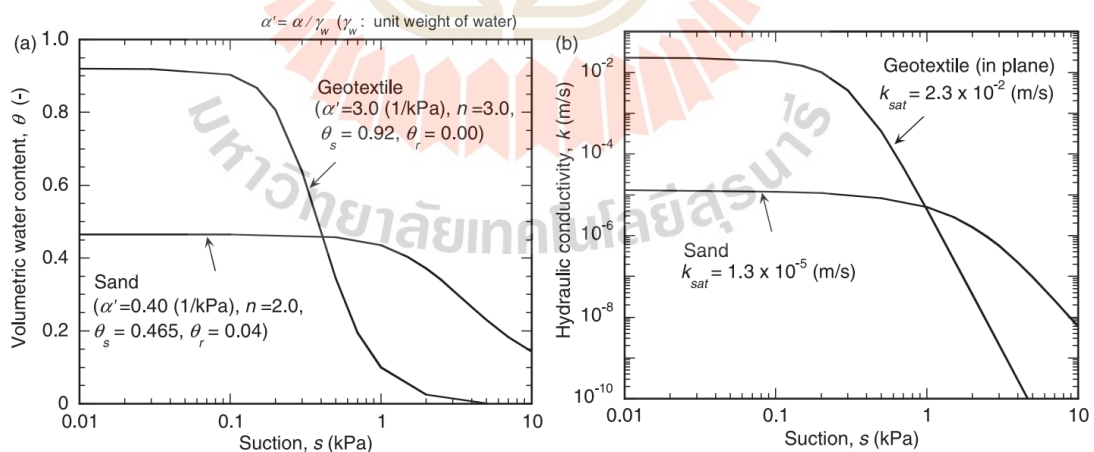


Figure 2.32 Hydraulic properties for sand and geotextile: (a) Water characteristic curves. (b) Hydraulic conductivity functions in Iryo and Rowe 2005.

Bahador et al. (2016) studied numerical simulation to investigate the effect of geosynthetic layers on moisture distribution and plastic deformation of paved and unpaved road sections. This geosynthetic layers consisted of a geonet, and a nonwoven geotextile with VG model parameter. Their properties, VG model parameter and SWCC is shown in **Figure 2.33** and **Table 2.3**.

Table 2.3 van Genuchten parameters and hydraulic conductivity for materials in the modeling of Bahador et al. 2016.

Material	Saturated water content, θ_s	Residual water content, θ_r	α (1/kPa)	n	Saturated hydraulic conductivity (m/s)	References
Silty sand (subgrade)	0.270	0.0	0.012	1.331	1.02×10^{-5}	<i>EICM</i>
Crushed stone (ABC)	0.239	7.8×10^{-2}	0.320	2.750	1.30×10^{-4}	Henry et al. (2001)
WF geotextile	0.754	0.0	2.577	1.680	3.44×10^{-3}	Stormont and Ramos (2004)
NWP geotextile	0.60	0.0	3.891	6.900	6.60×10^{-3}	Stormont and Morris (2000)
Geonet	0.850	5.0×10^{-3}	50.251	2.190	1.00×10^{-1}	Ramos (2001)
Asphalt	0.13	—	—	—	1.22×10^{-5}	Cooley et al. (2002)

Highlight conclusion from his research that the seepage analysis showed that during the simulated rainfall infiltration, the geocomposite increases the suction in subgrade by up to 8 kPa and decreases the suction by up to 3,6 kPa in **Figure 2.34**. The stress-deformation analysis showed that increasing the pavement thickness increases the hydraulic effect and decreases the mechanical effect of the geocomposite with regard to the total plastic deformations in both the paved and unpaved road sections. The geosynthetic, as for high permeability or high drainage capacity, is considered as appropriate replacement for traditional water drain out method than as soil drain or other material.

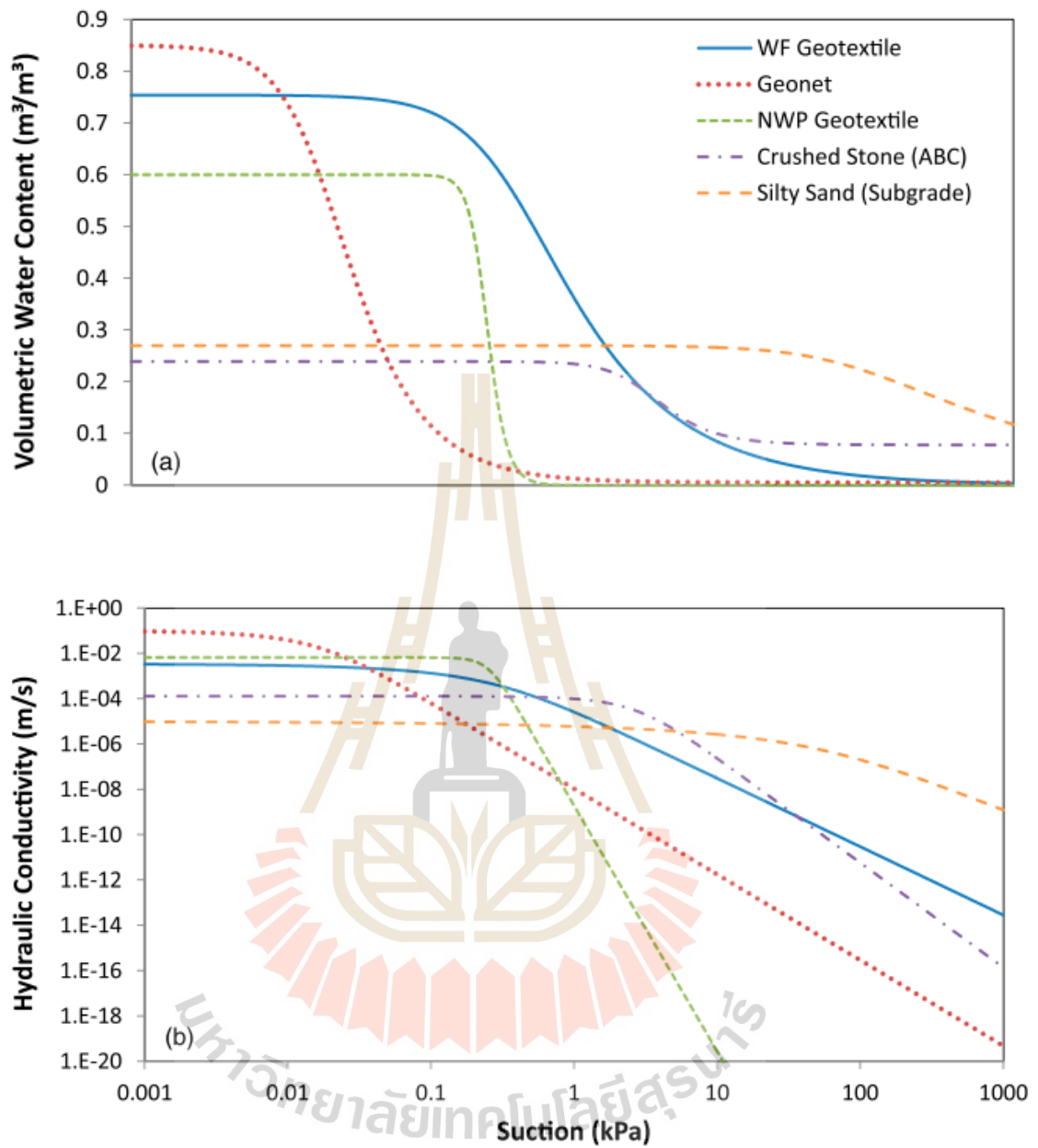


Figure 2.33 (a) Moisture characteristic curves; (b) unsaturated hydraulic conductivity curves (Bahador et al. 2016).

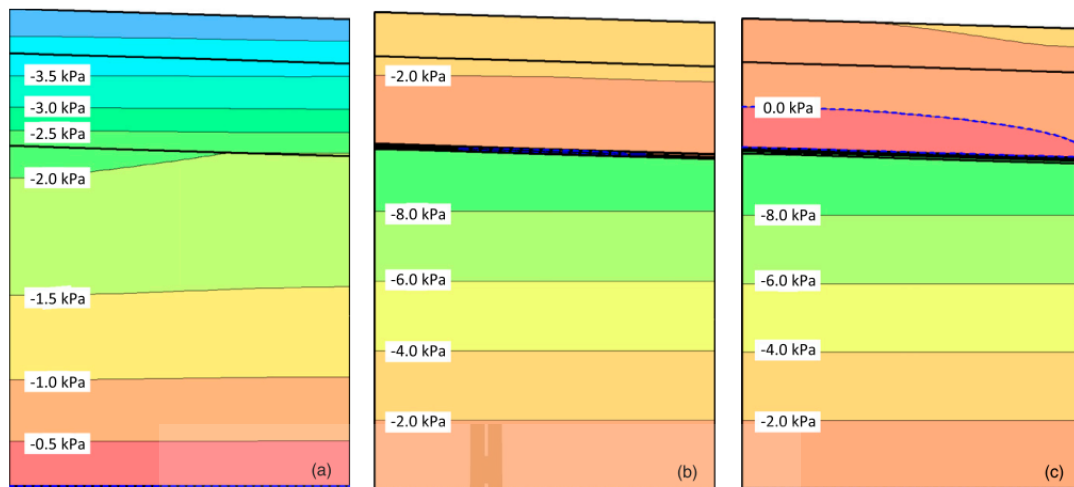


Figure 2.34 Pore pressure contours in the profile: (a) without geocomposite; (b) with woven-fabric geotextile transport layer; (c) with non-woven geotextile transport layer (Bahador et al. 2016).

In research work of Koerner et al. 2015 is an overview of design and using suitable geotextile in practical wall construction. Inadequate performance of geotextile filters under difficult and challenging field conditions are also figured out in this research. His research data based on series of collecting in-situ for failure of earth structures with geotextile installation. Highlights of his research include detail statement about 4 key criteria that caused practical failure of earth construction as design plan; typical soil related to failure; unusual permanent related to failure; and installation related to failure. Without excessive using of geotextile for covering and installing inside soil wall, bring more stable and effective drain out water capacity. Inter term of natural soil behind the wall contain much poorly graded granular soils such sand and gravel with high permeability, the problem of either designing a more open geotextile allowing fine soil such as silt and clay to penetrate or conversely a tighter geotextile resulting in excessive clogging. In addition, flow conditions wherein the

water is alternating much when across the geotextile from many factors as rainfall, steam, river, that need design in carefully and comprehensive. In related to this thesis, the point form Koerner et al 2015 enlighten the distance from installed location of drainage system to wall face, as well as soil backfill and natural play an importance role to whole construction perform in against to negative hydrological impacts (**Figure 2.35**).

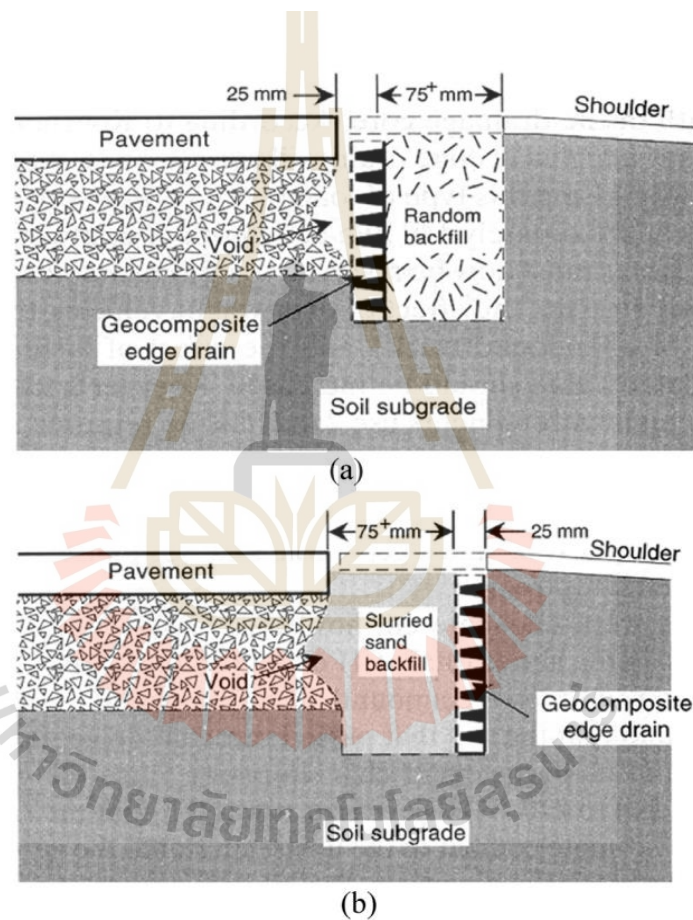


Figure 2.35 Installation lead failure problems for geotextile as drainage system: (a) Occurrence of large void beneath a highway pavement preventing intimate contact of the upstream geotextile, (b) Suggested remedy for backfilling large voids via hydraulically placed sand with the geocomposite edge drain moved to the shoulder side of trench (Koerner et al. 2015).

2.4.2 Geonet hydraulic transmissivity

In some cutting edges of various papers, they emphasized the highly effects of geonet thickness or the open-sized of geonet material variation to the changes of hydrological responses such as permeability and transmissivity of drainage system. Three well-known researches of them include Dickinson (2010), Giroud et al. (2014) and Yarahmadi et al. (2017).

In research of Dickinson (2010), he determined the relationship between geonet transmissivity and geonet thickness. By conducting a series of experimental results from physical testing to examine the thickness and hydraulic performance of three geosynthetic clay liners (GCLs) overlying a geonet (**Figure 2.36**) when subjected to vertical stresses with time (i.e. creep test). Results from fixed ring flow tests suggest that the indentations in the GCL caused by intrusion into the underlying geonet do not appear to negatively impact the hydraulic performance permittivity or resistance to internal erosion of the particular GCLs tested for the conditions examined. The flow capacity of the geonet in these tests was found to depend not only on the amount of GCL intrusion but also on the orientation of the geonet relative. The steady state permittivity of the GCL when underlain by a geonet was $3.8 \times 10^{-9} \text{ (s}^{-1}\text{)}$ and when underlain by saturated sand was $2.0 \times 10^{-9} \text{ (s}^{-1}\text{)}$. The permittivity was likely higher with a geonet because there is less consolidation in between the geonet ribs. The increase in permittivity for a GCL overlying a geonet need not be a problem provided that the slightly higher permittivity is taken into account in design. Permittivity of the GCL with time was calculated from the imposed flow rate and measured cell pressure using Darcy's Law (**Figure 2.37**).

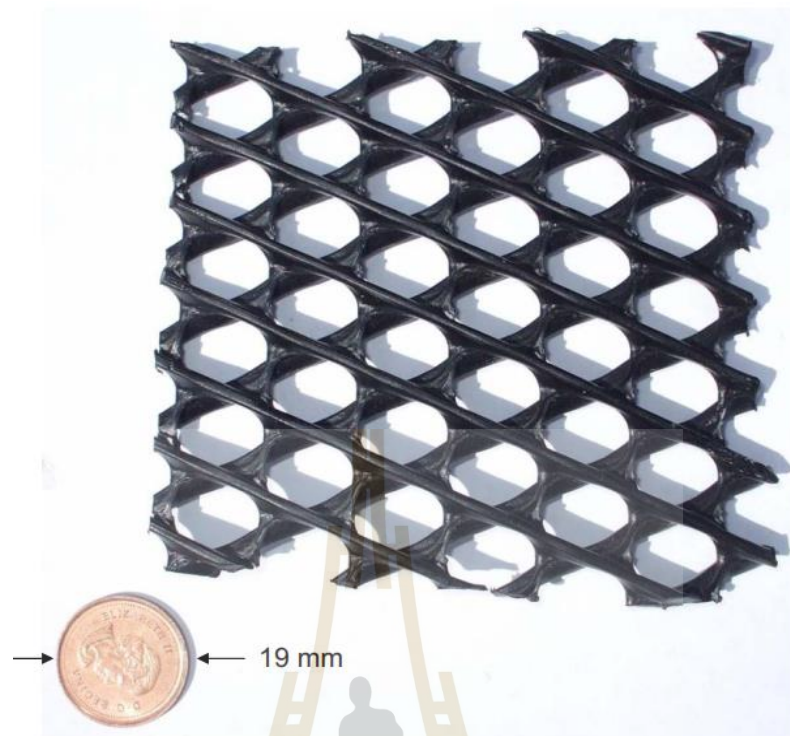


Figure 2.36 Geonet material in research of Dickinson (2010).

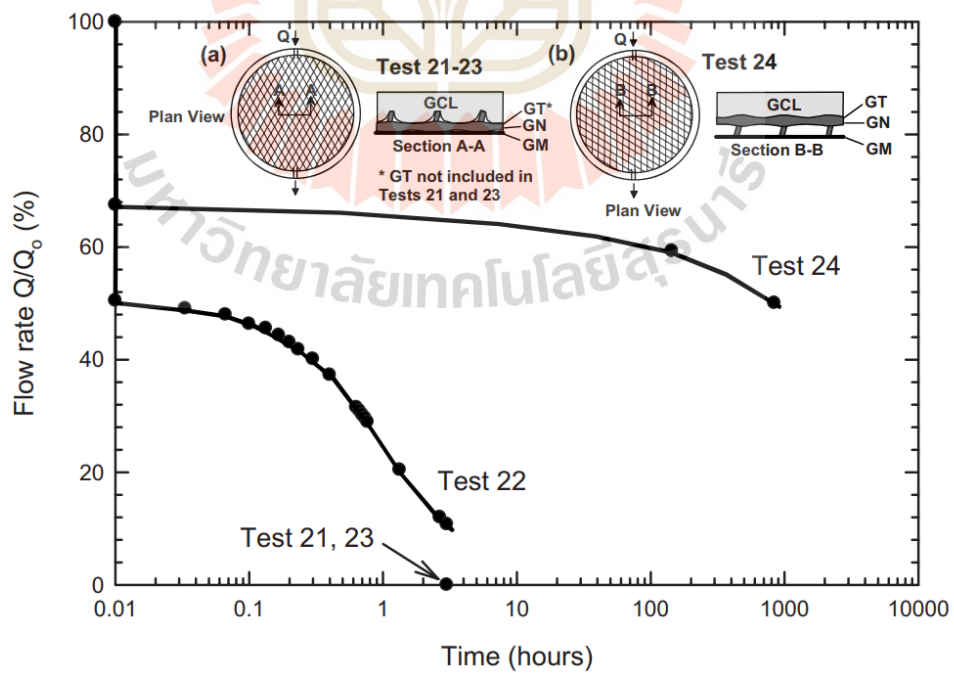


Figure 2.37 Flow rate through geonet with time (Dickinson 2010).

Giroud et al. (2014) stated that the flow in porous media, such as geosynthetic and granular drains, is often nonlaminar. That nonlaminar flow can vary in character from semi-turbulent to turbulent, depending upon the flow velocity, which is related to the hydraulic gradient. An exponent on the hydraulic gradient is used in the relationship among the hydraulic gradient, the apparent flow velocity, and the saturated hydraulic conductivity or transmissivity to quantify the degree of turbulence of the flow in porous media. They confirmed that flow is very turbulent for geonets between two plates that are both rigid and smooth (exponent on hydraulic gradient = 0.53 - 0.546) and for rockfill (for 0.54). That change of hydraulic gradient against hydraulic conductivity is shown in **Figure 2.38**.

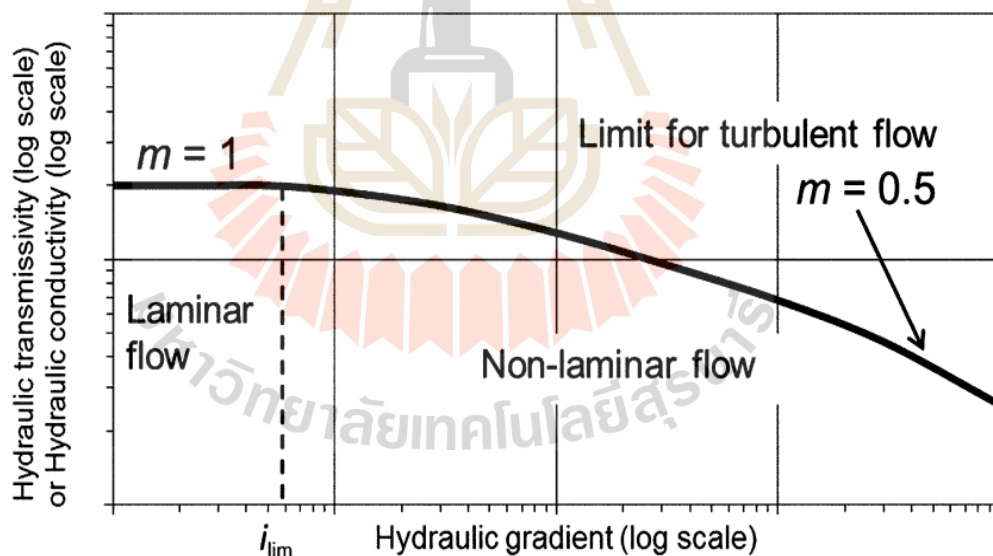


Figure 2.38 Generic curve of hydraulic conductivity or transmissivity (logarithmic scale) as a function of hydraulic gradient (logarithmic scale) from Giroud et al. (2014)

This conclusion was not as intuitively apparent as the parallel conclusion for granular soil because geonets are compressible and, as a result, the size of the flow channels decreases as the compressive stress increases, reducing flow velocity. In addition, in their research, However, geonets are modern geonets with low compressibility, the flow regime does not appear to be affected by compressive stress over the range of stresses considered herein.

Yarahmadi et al. (2017) studied the reduction of hydraulic transmissivity due to creep deformation (Long-time compressive stress on geosynthetic material). Specifically, in this study the effect of ribs geometry on hydraulic behavior of geonet materials was investigated. geonets are classified to two main categories named tri-planar geonets and bi-planar geonets (**Figure 2.39**).

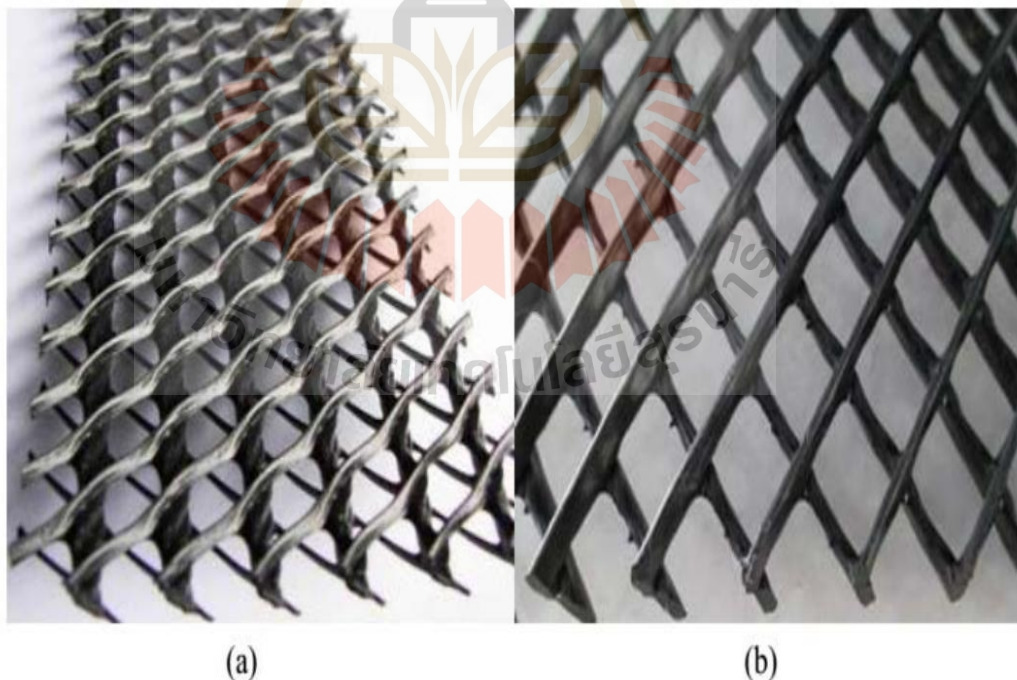


Figure 2.39 (a) Tri-planar geonet; and (b) bi-planar geonet

(Yarahmadi et al. 2017).

As for the hydraulic behavior of the two types of geonet was almost similar in low compressive stresses up to 200kPa regardless of their ribs geometry. However, the reduction in flow capacity was dependent on the structure of the geonet in compressive stress higher than 200kPa, and was smaller for the tri-planar geonet in which flow is governed by the main ribs set. The drainage capacity of the tri-planar sample was 2.3-3.0 times of that of the bi-planar sample at all four values of hydraulic gradient for the higher stress level. Additionally, in bi-lanar geonets, the sudden drop in drainage capacity is attributed to ribs reorientation. Although the lower ribs orientation remains almost unchanged, upper ribs slip over the lower ones and their orientation changes from almost vertical in low compressive stresses to almost horizontal in high compressive stresses.

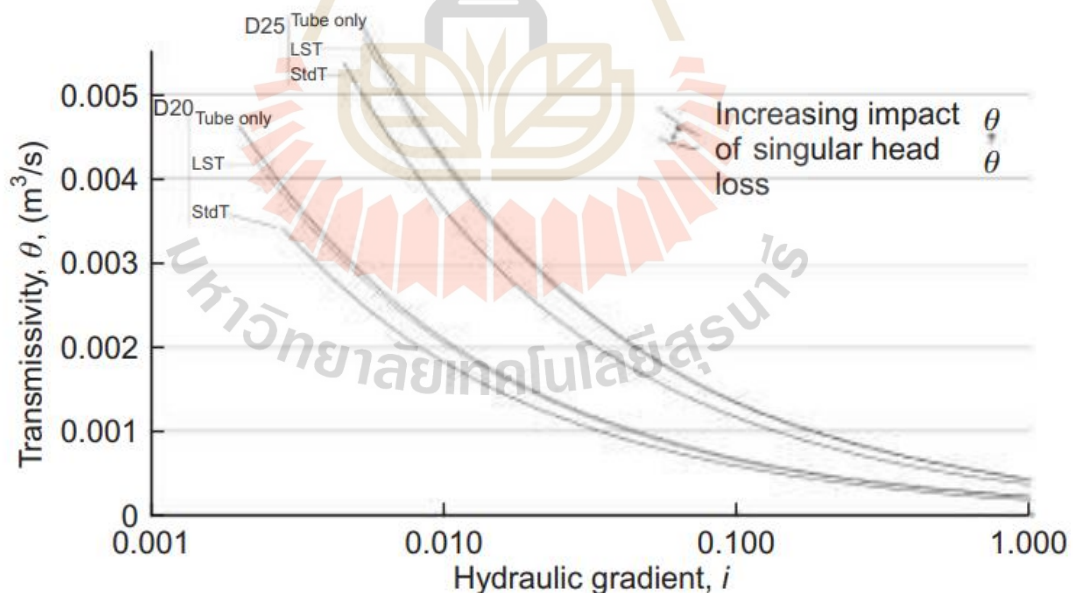


Figure 2.40 Transmissivity as a function of hydraulic gradient

(Bourges-Gastaud et al. 2013).

Bourges-Gastaud et al. (2013) investigated numerical method for the transmissivity study of drain-tube planar geocomposite which includes many kinds of geosynthetic material especially geonet as main core drain due to its high transmissivity. The head loss was the research objective. The transmissivity, albeit controversial if not correlated to one specific hydraulic gradient, is commonly used as a guide in designing geocomposites. Transmissivity is defined as the ratio of the flow capacity of a single tube to the hydraulic gradient and so depends on the hydraulic gradient because of non-laminar conditions (**Figure 2.40**).

From research of Chinkulkijniwat et al. 2017 and Bui et al. (2017), they investigated the properties that predominantly affect the hydraulic behaviors of the MSE wall with geocomposite installation are the hydraulic conductivity of the geocomposite, the variation in the hydraulic conductivity with the degree of saturation, the water retention characteristics of the soil and the geocomposite components (geotextile and geonet). As the geonet has a very open structure, VG and VGM models with the following considerations were assigned to the geonet (1) has a large and single pore size attribute (2) can be completely dried and saturated under suitable magnitudes of suction.

One of the hydrological responses, the phreatic surface in the protected zone is governed by the ratio between the hydraulic conductivity of the geonet and that of the soil ($K_{r,net}$). The lower magnitude of $K_{r,net}$ results in a higher phreatic surface level in the protected zone (Chinkulkijniwat et al. 2017 and Bui et al. 2017). As the phreatic surface level in the protected zone is vital for the stability of the MSE wall, a proper magnitude of permeability for the geonet must be used such that the water table level inside the protected zone is low and close to the base of the protected zone.

2.5 MSE wall dimensions to seepage responses

The shape variation of MSE wall play an essential role in the hydrological responses and the internal as well as external instability. This term is mentioned and become a hot topic in many researches. Moreover, the research methodology has been applying popularly by numerical simulation due to its convenient and reasonable.

In this thesis, a well-calibrated numerical model, computed in the Plaxis environment and introduced by Chinkulkijiwat et al. (2017), was further elaborated with regard to the effect of scaling. To ensure the validity of the Plaxis-based model on different scales, it was established using identical shape ratios at double the size of the physical model. The calibrated model was further employed to perform a series of parametric studies focusing on the influence of the shape parameters and geonet transmissivity on seepage responses in the modeled MSE wall

Clement et al. (1996) investigated the effect of flow domain aspect ratio on the height of the seepage face, which is the difference between the phreatic surface at the exit and the downstream water level. His research used a series of finite element analysis in order to investiagte the groundwater behavior at steady state via the change of model dimension. Also in this research, the main objects are comprise as the flow vector through the rectangular domain (**Figure 2.41**).

They found that effects on the seepage face were diminished for long, shallow flow domains, while the position of the phreatic surface was relatively insensitive to downstream water level for deep flow domains. The aspect ratio of rectagular domain flow is also exmined for the changes of phreatic line curve in ter of geometric investiagtion.

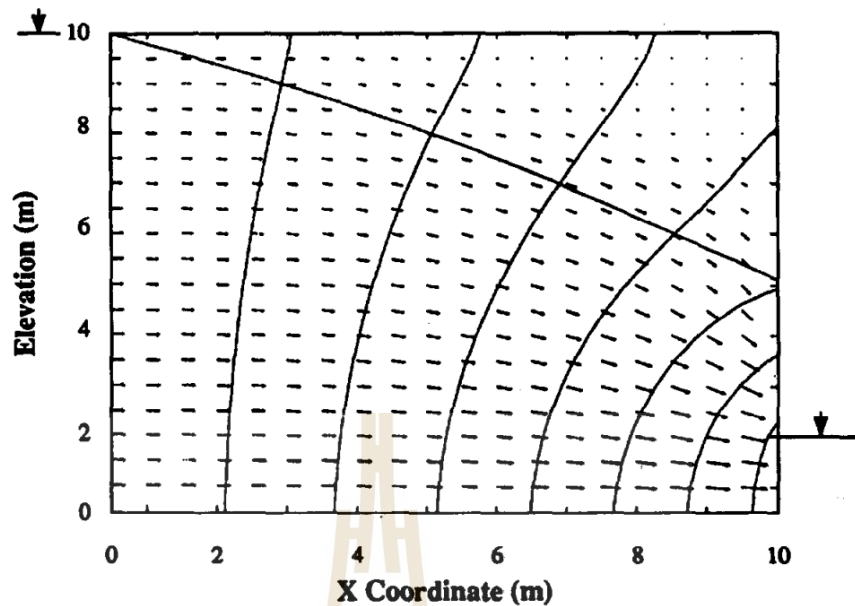


Figure 2.41 Flow vectors corresponding to the variably saturated model
(Clement et al. 1996).

In his research, the rectangular flow is affected by the scale of flow dimension, model aspect ratio, sensitivity of soil properties. The sensitivity of seepage face height to the scale of the problem was observed in this research. problem using a two-dimensional, finite-element, variably saturated flow model, and observed that the seepage face did not scale to the problem dimensions. In term of flow scale, several squarely flow domain problems were solved using both the variably saturated and the fully saturated flow models. His statement concluded as more water flows through the vadose zone (where the nonlinearity arises) in a smaller-scale problem than in a larger-scale problem. Hence, the disparities between the fully saturated flow model and variably saturated flow model results are more pronounced in smaller-scale problems. This

effect should be of particular interest to those trying to model laboratory-scale experiments.

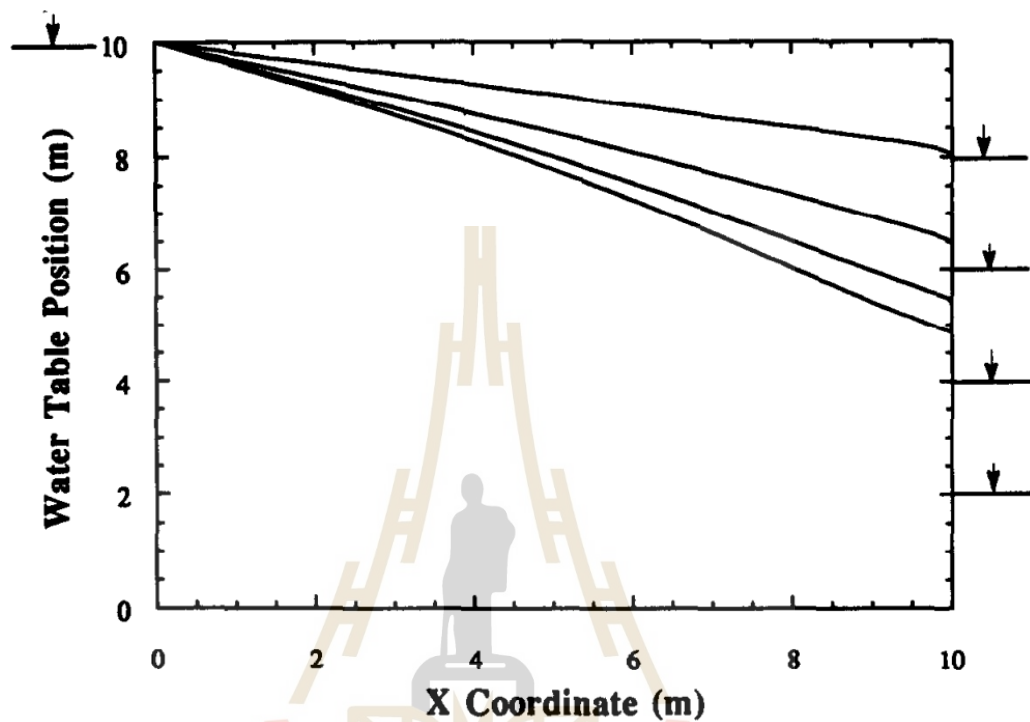


Figure 2.42 Variation of the phreatic surface predicted by the variably saturated model owing to changing downstream levels for the square (Clement et al. 1996).

As for the influences of aspect ratio to seepage sensitivity in Clement et al. 1996, Three rectangular-flow area as considered as 10 m x 10 m, 5.0 m x 25 m, and 25 m x 5.0 m. The length-to-height aspect ratio of the problems are 1,0.2, and 5, respectively. His results in **Figure 2.42** reflected that in square problem with an aspect ratio of unity, the absolute length of the seepage face decreases significantly with an increase in the tail-water level. That come from the decline for seepage-face height get to be due to a decrease in the discharge through the system at lower hydraulic gradients coupled with the concurrent increase in cross-sectional area for flow at higher tail-water levels. For

the long problem, with an aspect ratio of five, no seepage faces are discernible for the various downgradient conditions (**Figure 2.43**) indicating that the effects of seepage faces are diminished for long, thin problems.

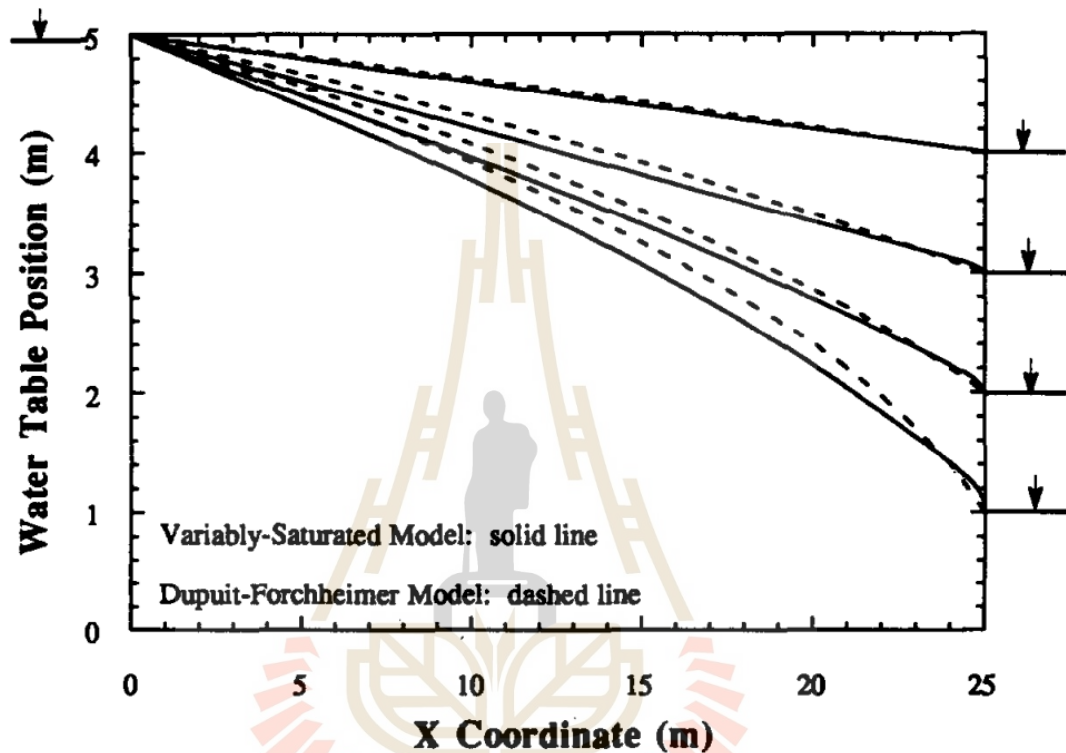


Figure 2.43 Variations of the phreatic surfaces predicted by the variably saturated models owing to changing downstream open-water levels for the ‘elongated’ (Clement et al. 1996).

Refer to the influences of soil properties head to rectangular flow, Clement et al. 1996 agreed for that steady-state water tables and seepage faces are insensitive to changes in the hydraulic conductivity. His studies results indicated varied discharges are directly proportional to the changes saturated hydraulic conductivity of assign soil model. As similar to this thesis, hydraulic properties of an unsaturated soil are described

by soil-water retention and relative-permeability functions, as described earlier as the Van Genuchten (1980) and Mualem (1976). Conceptual VG parameter results in **Figure 2.44** and **Figure 2.45**.

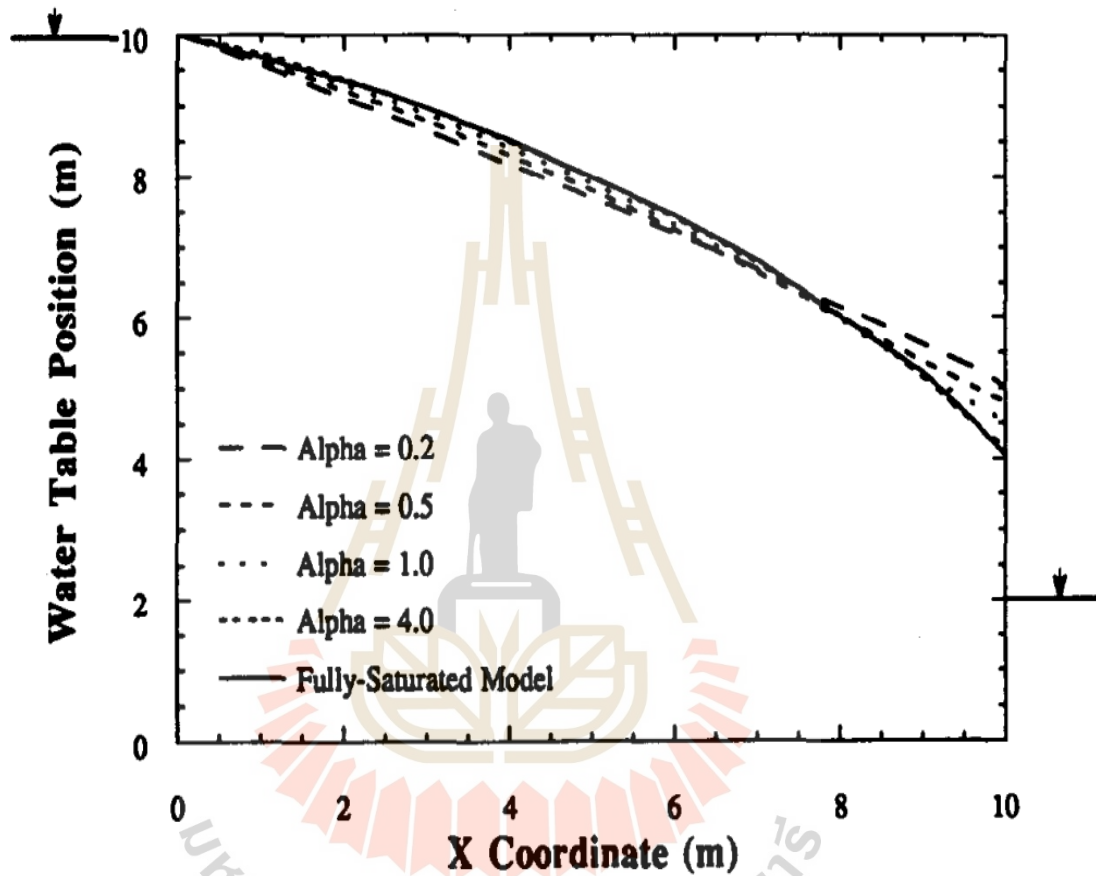


Figure 2.44 Sensitivity analysis of the variably saturated flow model to the Van Genuchten parameter α for the square slow problem (Clement et al. 1996).

His research noted that for small VG parameter values as n in presentative for poorly sorted media, the low permeability of the unsaturated zone forces the variably saturated flow model to behave like a fully saturated flow model. By contrast, for high

values of n , the low water content in the vadose zone forces the variably saturated flow model predictions to approach those of the fully saturated flow model.

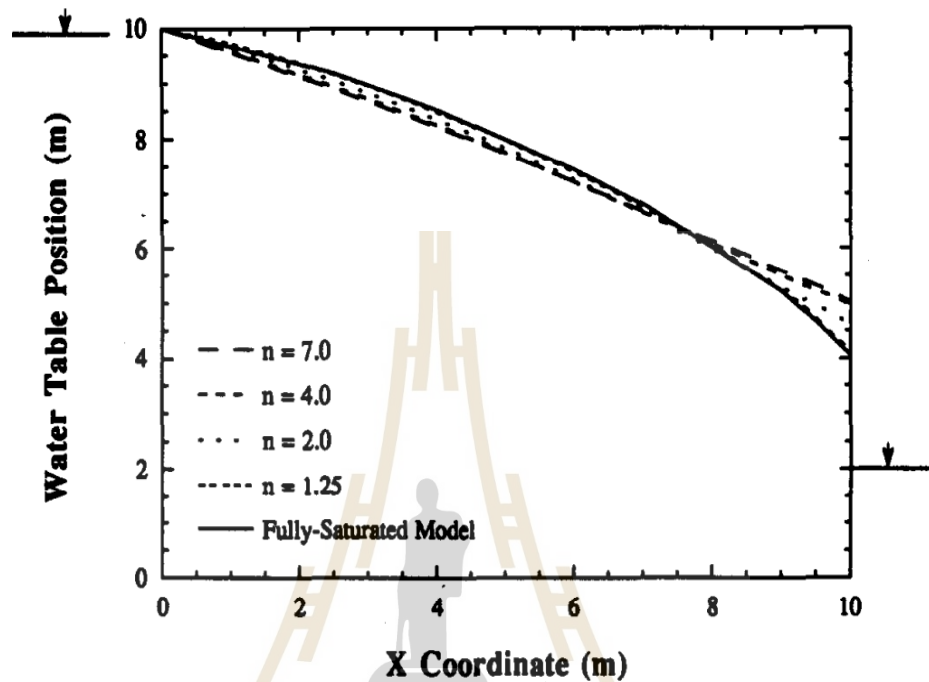


Figure 2.45 Sensitivity analysis of the variably saturated flow model to the Van Genuchten parameter n , for the square embankment problem (Clement et al. 1996).

Saeedpanah et al. 2011 reported that the length of the groundwater flow path plays a more important role in the flow rate than the upstream water level does. Despite their importance to seepage responses, the relevant shape parameters are yet to be investigated thoroughly enough to comprehensively explain their influence on seepage responses in an MSE wall. In this research, the groundwater level is examined under the impact from many factors such as shape function via finite element method (FEM) and finite volume method (FVM) are popular numerical schemes for the solution of

ground water flow problems. Some of satisfied results from Saeedpanah et al. 2011 as shown **Figure 2.46, 2.47 and 2.48** for the change groundwater level under impacts of leakage phenomena, distance from the tidal source as stream source.

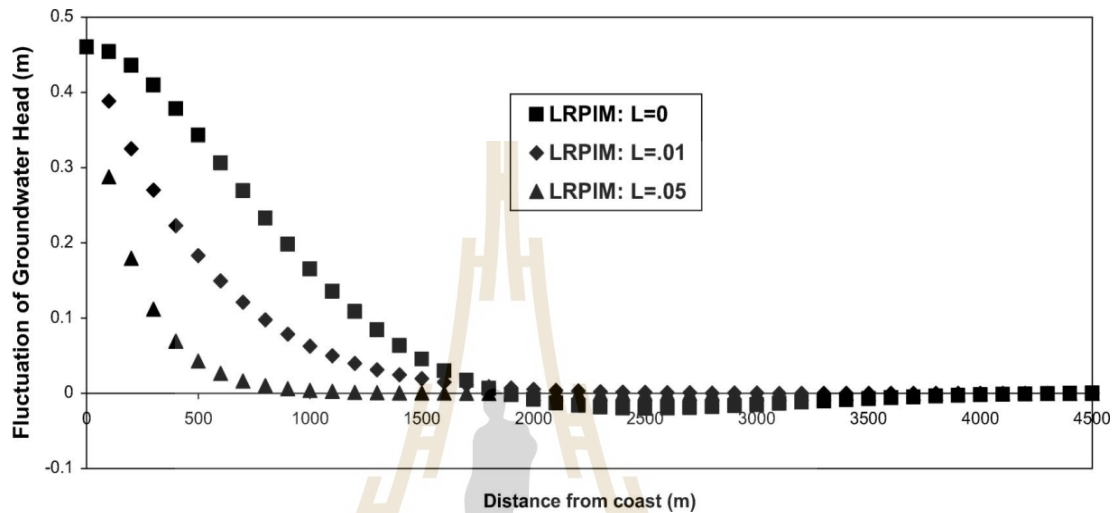


Figure 2.46 Fluctuation of groundwater head in the leaky confined aquifer at $t = \frac{1}{4} \cdot 3 \text{ h}$ with specific leakage $L = 0, 0.01$ and 0.05 (Saeedpanah et al. 2011).

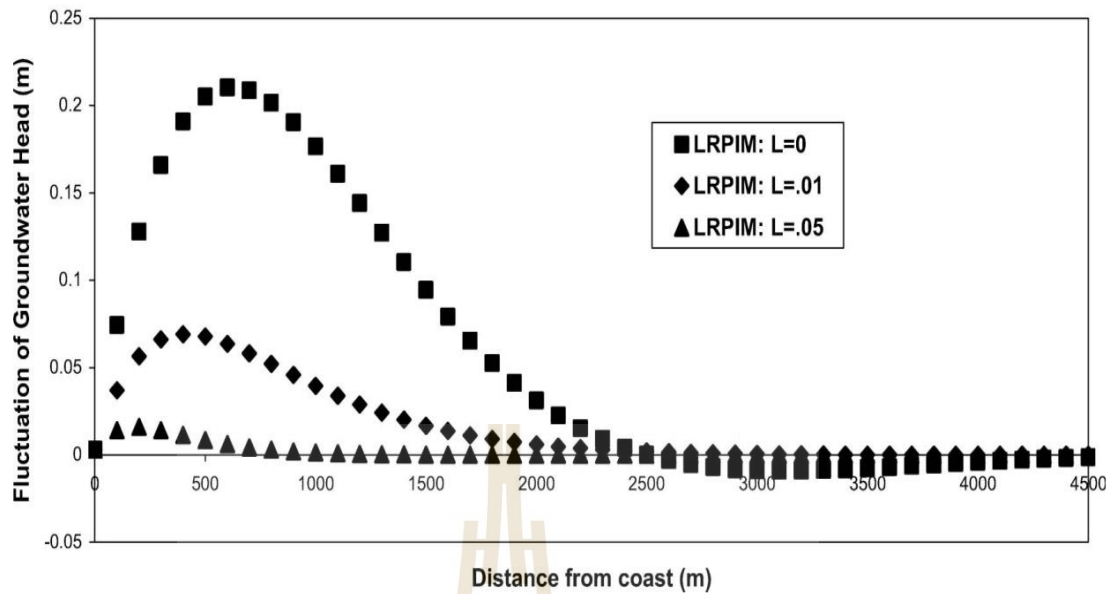


Figure 2.47 Fluctuation of groundwater head in the leaky confined aquifer at $t = 3$ h with specific leakage $L = 0, 0.01$ and 0.05 (Saeedpanah et al. 2011).

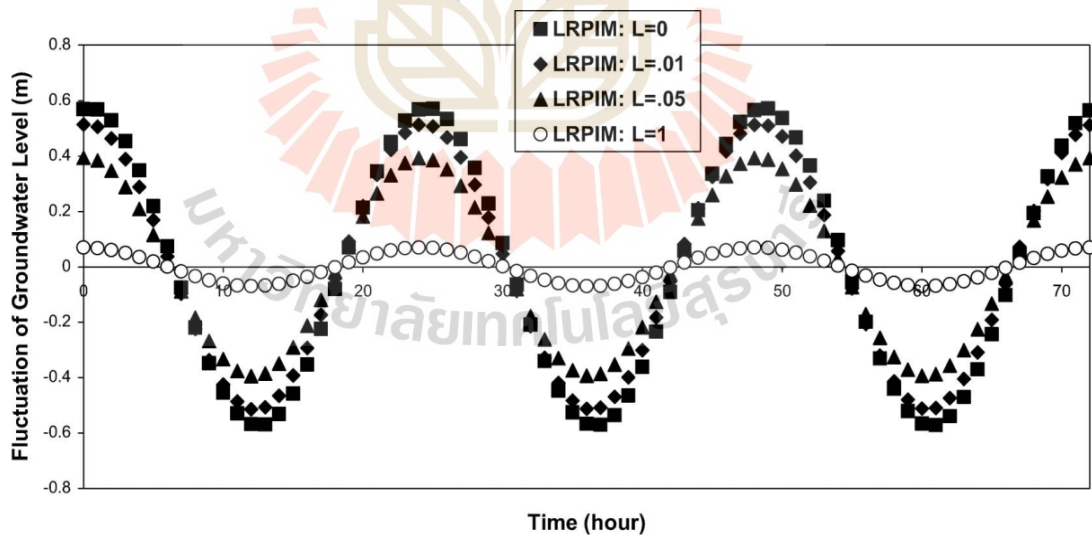


Figure 2.48 Piezometer head fluctuations at 100 m from the coast with $L = 0.01, 0.05$ in 1 day (Saeedpanah et al. 2011).

A novel of Saeedpanah et al. 2011 research approach is for radial point interpolation meshless (LRPIM) method is introduced to investigate the influence of leakage on coast tidal response in a coastal leaky to confined aquifer system, based on a local weighted residual method with the Heaviside step function as the weighting function over a local sub-domain.

It is widely agreement with that wall shape parameters play important roles in the mechanical responses, and hence internal and external stabilities of an MSE wall (Roy and Singh 2008; Stuedlein et al. 2012; Kibria et al. 2014). However, the effect of these shape parameters on the seepage responses in an MSE wall are not yet to be investigated or even very few. That point of above literatures encourage this thesis will focus on the effect of wall dimension or wall shape parameter to seepage response. This research point is based on the effect wall dimension noticed in reserch of Roy and Singh 2008; Stuedlein et al. 2012; Kibria et al. 2014.

Roy and Singh 2008 examined MSE walls cases, which failed in the final stages of its construction, was constructed after foundation soils were strengthened with prefabricated vertical drain installation and preloading. Using pre and post consolidation shear strengths the MSE walls were redesigned. Reconstruction involved prefabricated vertical drain installation at the second site and construction of stabilizing berms at both locations. The facilities are now operational and appear to be performing satisfactorily. Also, the series failure cases occur for MSE wall investigation as can be seen typically in Figure2.



Figure 2.49 MSE Failures at research area in Roy and Singh 2008.

Soil material in this research as considered as sand backfill material, a friction angle of 35° , and belong to cohesionless soil were deemed necessary for internal stability of the MSE wall. The reinforcing bars in this research as strips were bolted to 180 mm thick interlocking reinforced concrete facing panels with four strips connected to a single facing panel. Their report of MSE wall failure cases for each construction steps are shown by graphic in cross-section of **Figure 2.50**.

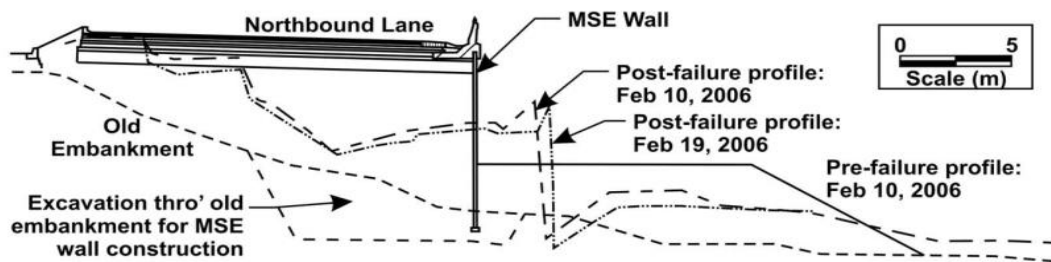


Figure 2.50 MSE wall cross-section for failure report in Roy and Singh 2008

Stuedlein et al. (2012) concluded the effect of MSE wall shape to the wall construction instability as the reinforcement load within the very tall west MSE wall increased at a rate greater than that predicted by theoretical overturning stresses alone. Given that MSE walls behave as relatively flexible rather than rigid structures, the reinforcement stiffness may have significantly contributed to the development of high reinforcement loads within the bottom tier of the west MSE wall as well as the observed differential settlement **Figure 2.51** and **Figure 2.52**. In most cases and considering the plane strain friction angle estimated from the measured direct shear friction angle, but capped at 44° , the Ehrlich and Mitchell method provided the most accurate overall estimate of reinforcement loads for both walls, especially at full height and intermediate wall heights greater than 20 m. The mean bias values ranged from 0.79 to 1.27.

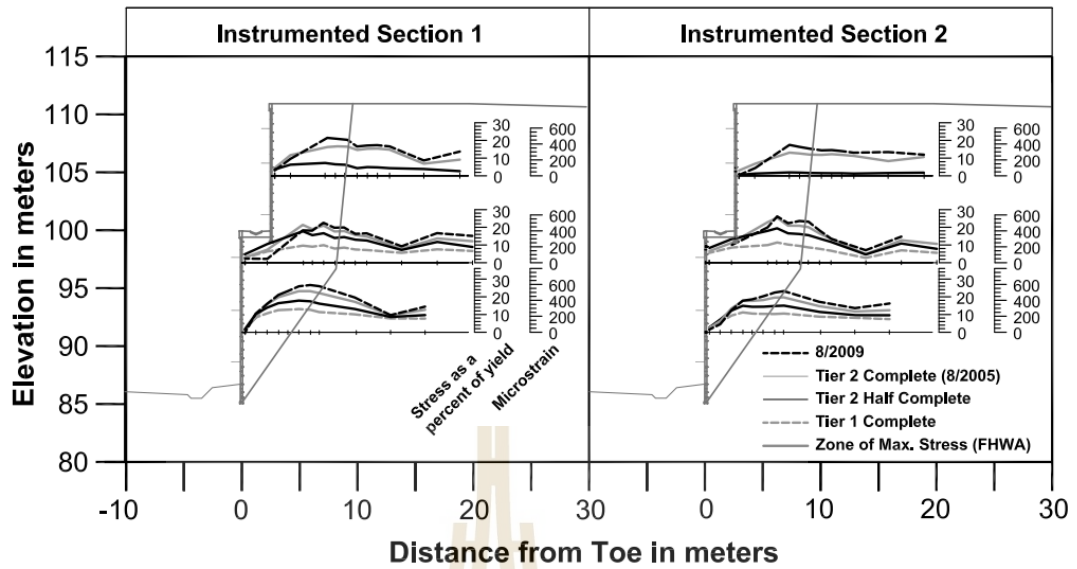


Figure 2.51 Development of reinforcement strains and stresses as a percent of yield stress at the North MSE wall (Stuedlein et al. 2012).

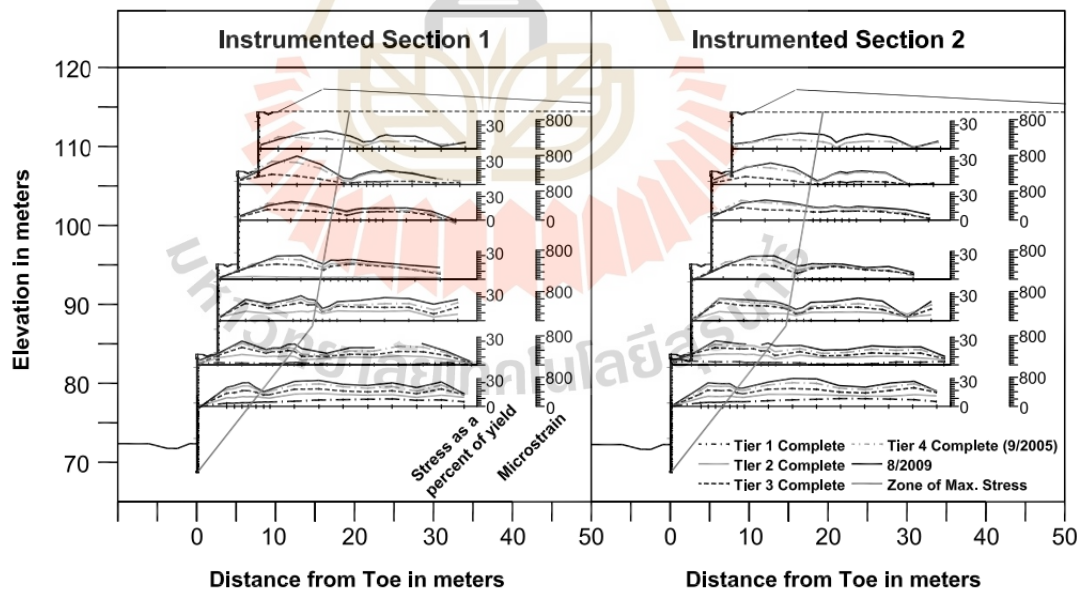


Figure 2.52 Development of reinforcement strains and stresses as a percent of yield stress at the West MSE wall (Stuedlein et al. 2012).

The Mechanically stabilized earth (MSE) walls offer simple construction techniques, pleasing aesthetics, and cost-effective solutions as an alternative to conventional gravity walls (Kibria et al. 2014). Their research processed a case study is presented on a MSE wall located on State Highway 342 in Lancaster, Texas and conduct the numerical model simulation (**Figure 2.31**). The horizontal movement of the MSE wall was monitored between 300 and 450 mm within 5 years of construction. Through research results, inadequate reinforcement length was one of the contributing factors that caused horizontal displacement of the MSE wall.

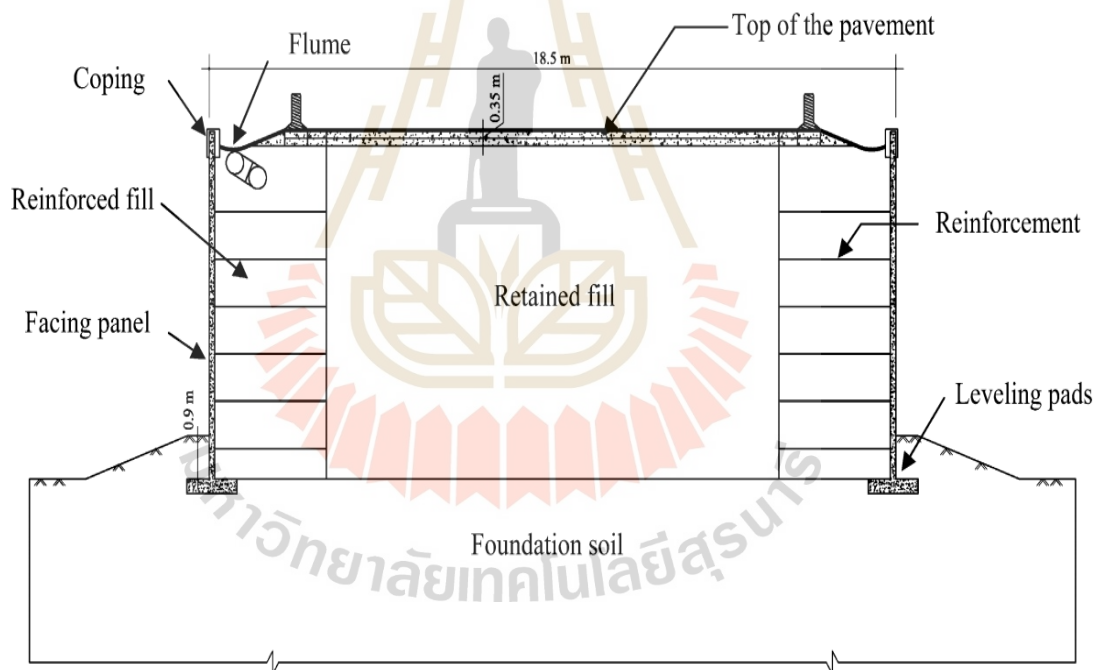


Figure 2.53 Cross section of MSE wall (qualitative) (Kibria et al. 2014).

The effects of soil in reinforced on excessive movement of the MSE wall play an important role (**Figure 2.53**). So that their research pick that effect as main objective research and conducted numerical analysis to simulate it. Overall stability of the MSE

wall was determined using the phi-c reduction method in PLAXIS 2D finite element software (Figure 2.54). The variations in displacement with reinforcement length suggested that a substantial decrease in displacement occurred for an increase in L/H ratio from 0.5 to 0.7 (Figure 2.55 and 2.56).

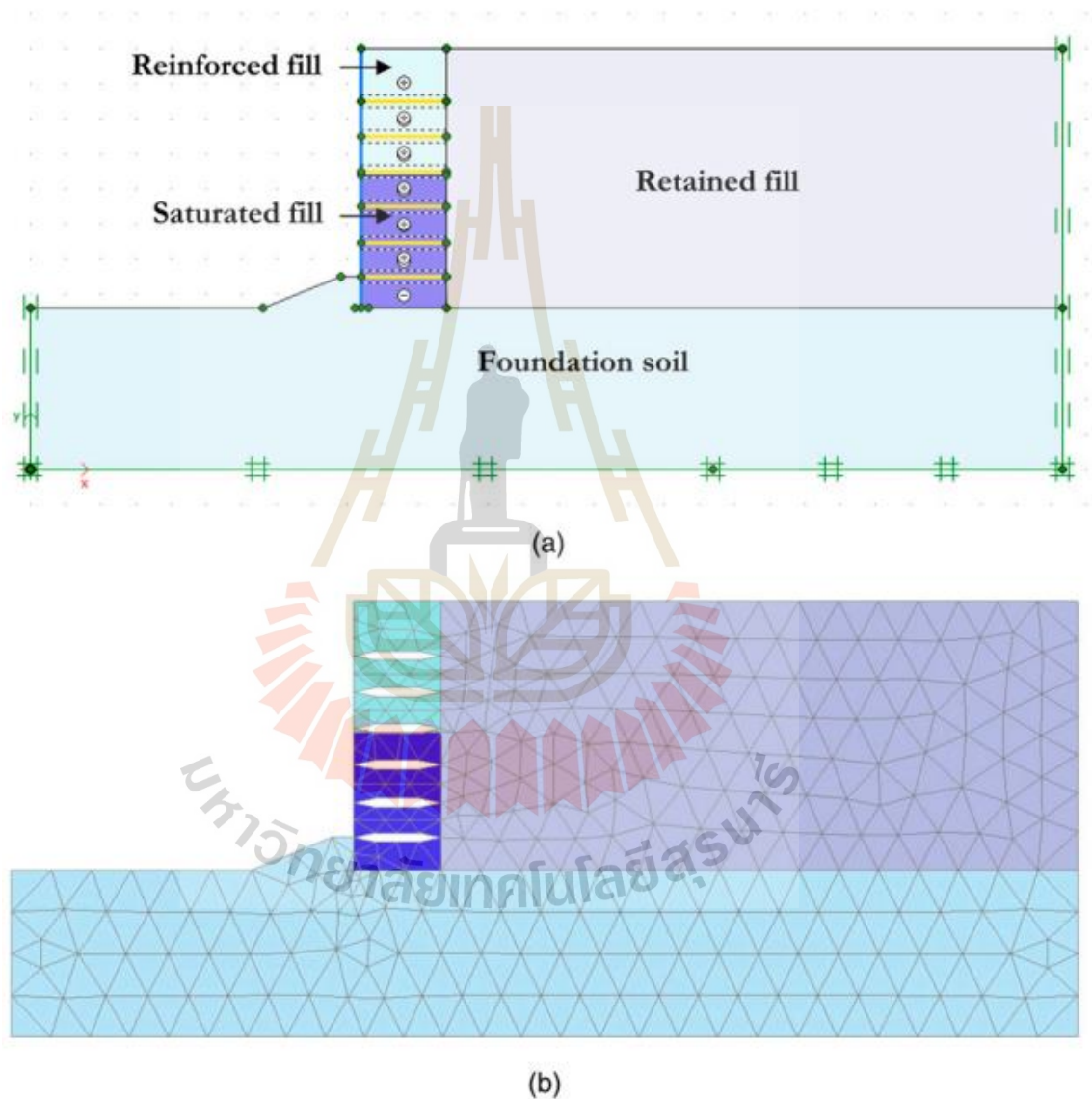


Figure 2.54 (a) Geometry of MSE wall; (b) mesh connectivity (Kibria et al. 2014)

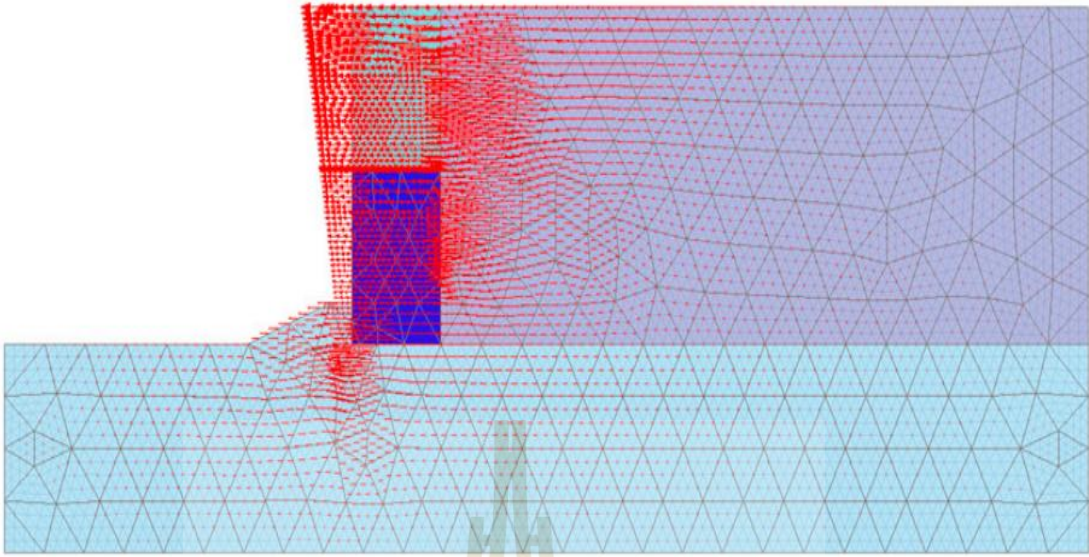


Figure 2.55 Maximum horizontal displacement 287 mm (arrows indicate direction of movement of MSE wall) (Kibria et al. 2014)

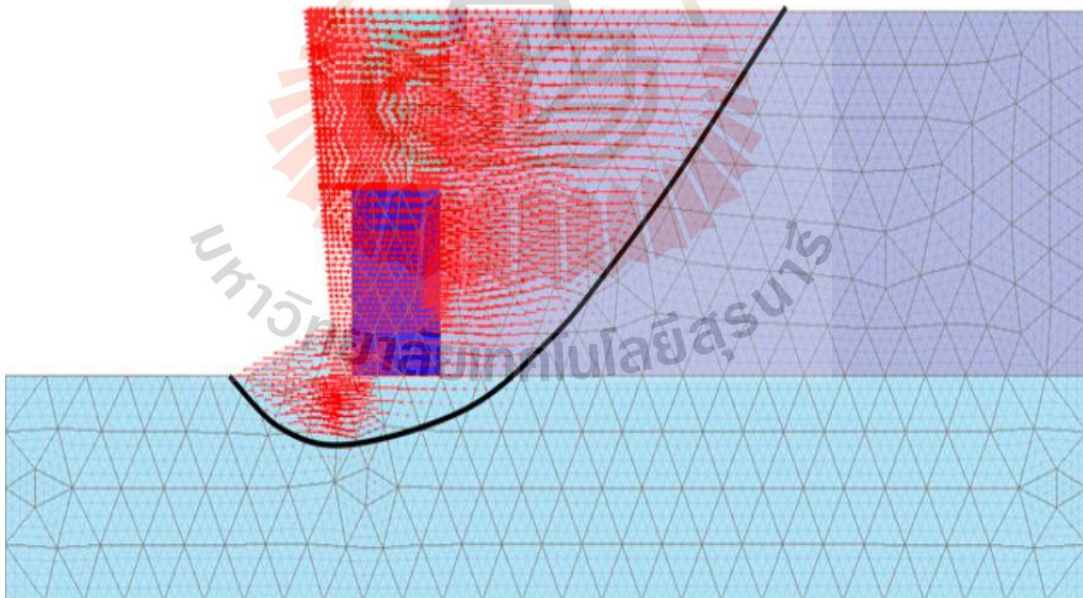


Figure 2.56 Overall factor of safety of 1.2 (arrows indicate direction of movement of MSE wall) (Kibria et al. 2014)

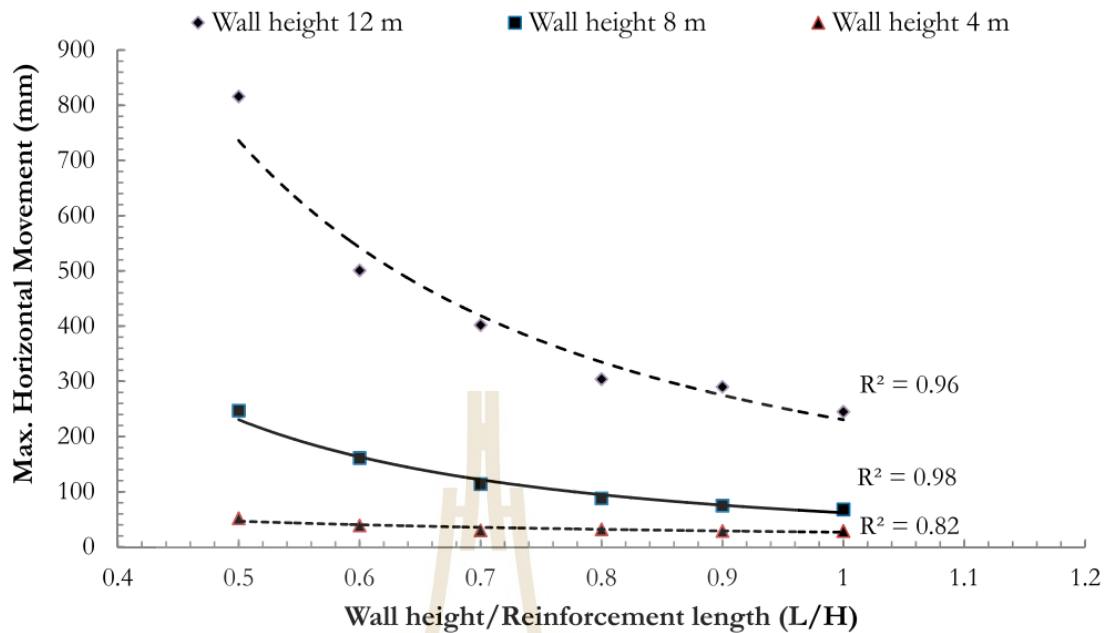


Figure 2.57 Effect of reinforcement length on horizontal displacement of MSE wall (Kibria et al. 2014).

Xu et al. (2014) reported 3D numerical experiments with modelling depiction in **Figure 2.58**, that indicated the downstream water level decreased at greater insertion depth ratios: i.e. a ratio between penetration depth and distance from the tip of the pile to the impervious layer. The wall geometries were focused in this studied for investigating wall performances under their influences. In their literature, the design of a deep retaining wall, it is necessary to consider the blocking effect on groundwater seepage of retaining walls in aquifers. In this study, both laboratory tests and numerical simulation with finite element method (FEM) were adopted to investigate the blocking effect on groundwater seepage under different insertion depths of retaining wall in aquifer. The time duration to reach stable groundwater head remains at around 30 min when insertion depth ratio (J) is less than 70% and then time duration increases with

the increase of J . The difference of groundwater heads between the upper and lower sides of the impervious plate increases with the increase of J when J is greater than 70%.

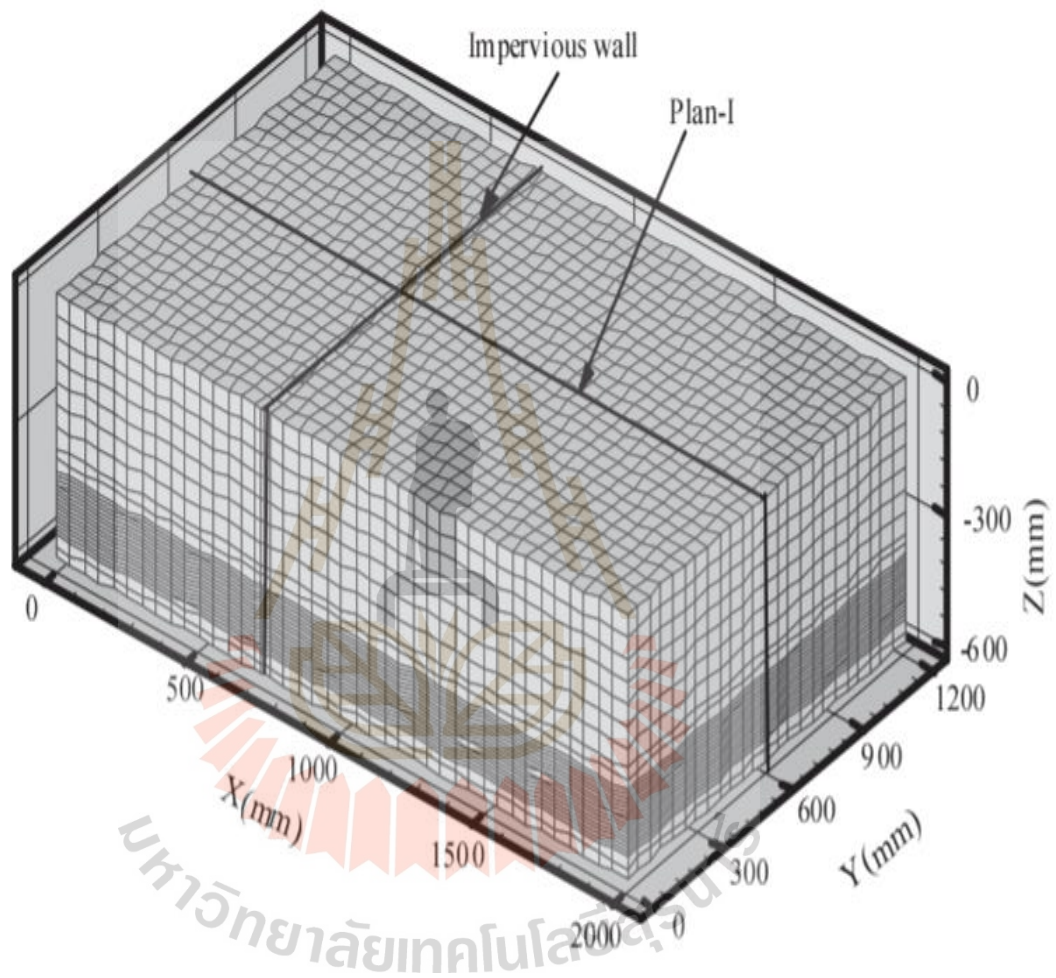


Figure 2.58 Three-dimensional finite element model of laboratory test adapted from Xu et al. (2014).

Finally, through this series of laboratory increment of hydraulic gradient remains constant between the upper and lower sides of the impervious plate. The depth ratio plays as double-wall geometry that caused the change of hydraulic gradient as well

as the drawdown of groundwater in comparison to practical construction. When J is less than 70% (**Figure 2.59**), however, (Δi) increases with the increase of J when J is greater than 70%.

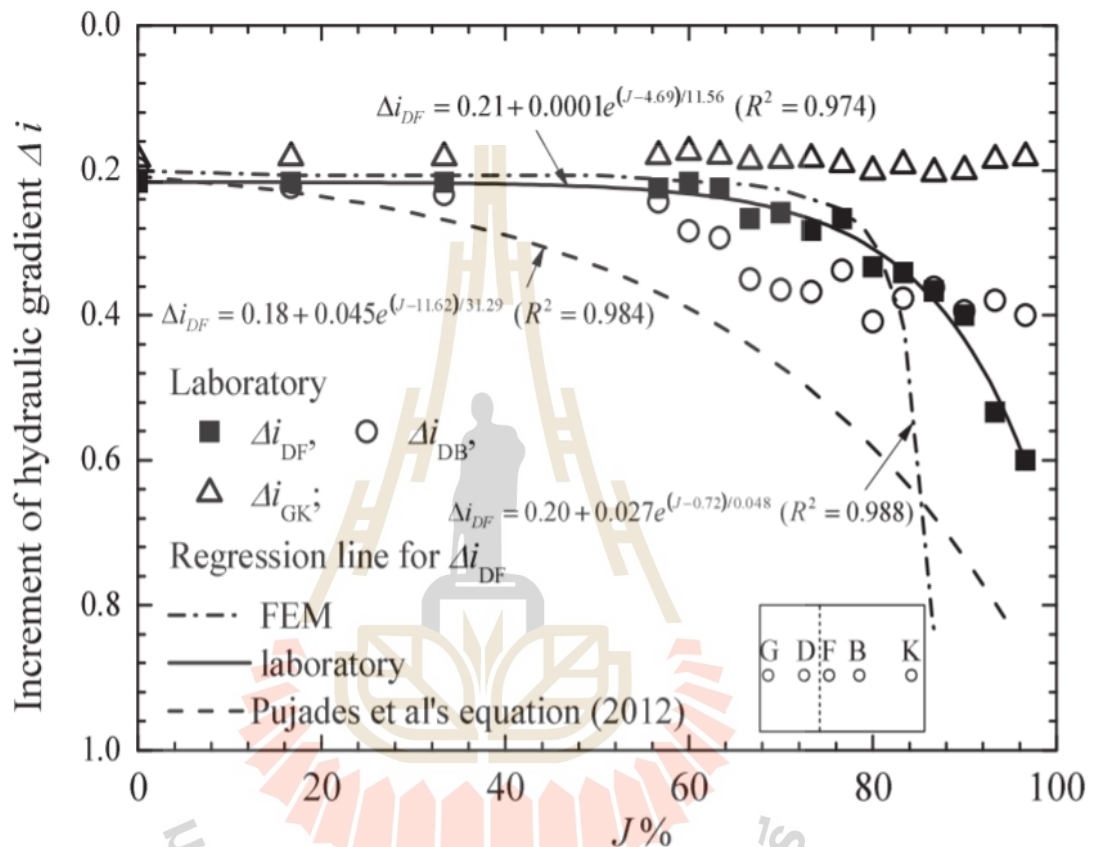


Figure 2.59 Relationship between increment of hydraulic gradient and insertion depth ratio adapted from Xu et al. (2014).

2.6 Linear analysis for maximum water level (h_o) in protected area

Also as given as failures happened in mechanical stabilized earth (MSE) wall with back drainage system during long term rainfall that mention in above section especially in highlight research of Koerner et al. 2015, Koerner et al. 2018, Yoo and Yung et al. 2006. Through the maximum level changes of phreatic surface in the

protected zone of MSE wall, h_o , reflects the effectiveness of the drainage system and also suitability selection of soil backfill and native in practical works. The wide distribution of water content in the protected zone was a major source for many types of failure. To control this water distribution, the backfill soil must consist of least fine particle and the level of phreatic surface inside the protected zone must be minimized.

There are number of literatures reported influence variables that affect the magnitude of h_o such as Chinkulkijniwat et al. 2017, Bui Van et al. 2017, La Duong et al. 2020. However, very few of the previous attempts reported influence of MSE wall dimensions on the variation of phreatic surface in the protected zone. Also, few researches did not integrate and quantify well the rise of h_o with all influenced factors that lead uncomprehensive research for practical wall design.

One of highlight finding from previous reports as La Duong et al. 2020 emphasized that there were many factors influence to the h_o variation such as soil hydrological properties, drainage properties, and the wall dimensions mentioned. Their research drawn a significant correlation existed as linear association between the rate of fall in h_o with geonet transmissivity (T_{net}) and proposed a linear equation with highly coefficient of determination (R^2) greater than 0.96. This value bring reliable estimating of h_o among other relevant influenced factors of MSE wall model.

The mainly results of La Duong et al. 2020 are the main core content of this thesis (refer Chapter III). On the other hand, via their report, permeability coefficient of the soil on the upstream side governs the rate at which h_o falls with increments of T_{net} , and the linear line slope ratio by 36:1 proves not much different from permeability coefficient ratio by 49:1. Nonetheless, their research limited calibrating h_o rise by using wide range of soil permeability for MSE wall backfill and native.

Based on above statements, by numerical simulation, this thesis desires to estimate the linear association rise of h_o comprehensively with geonet transmissivity (T_{net}) in successor from research of La Duong et al. 2020. Moreover, other relevant influenced factors are focused and integrated in final linear analysis especially for proposing mathematic equation. The wide extension of soil permeability range, for representative for each soil type in practical, is successful picked from previous reports (Konukcu et al. 2004, Szymkiewicz et al. 2015, Acharya et al 2012). Selected influenced factors to h_o for linear analysis in this study comprise the geonet transmissivity (T_{net}) in presentative for geocomposite drainage properties; MSE wall dimension as distance from the upstream water level to the drainage face (L); native and backfill soil permeability (k).

The linear model provides an ease for practical via linear equation uses. Good linear estimation of h_o in relevant relationships is, therefore, vital for the best design of MSE wall against failure. Conceptual numerical input data were based on 180 Plaxis-2D experiments conducted.

2.7 References

- Acharya, S., Jawitz, J.W., and Mylavarapu, R.S., 2012. **Analytical expressions for drainable and fillable porosity of phreatic aquifers under vertical fluxes from evapotranspiration and recharge**, *Water Resour. Res.*, 48.
- Albino, U.D.R., Portelinha, F.H.M., Zornberg, J.G., Futai, M.M., 2019. **Numerical simulation of infiltration into the fill of a wall reinforced with nonwoven geotextiles**. *Computers and Geotechnics*. 108, 27-39.

- Bahador, M.,1; Evans, T. M., and Gabr, M. A., 2016. **Modeling effect of geocomposite drainage layers on moisture distribution and plastic deformation of road.** *Journal of Geotechnical and Geoenvironmental Engineering*. 139(9).
- Bourges-Gastaud, S., Blond, E., Touze-Foltz, N., 2013. **Multiscale transmissivity study of drain-tube planar geocomposite: effect of experimental device on test representativeness.** *Geosynthetics International*. 20(3), 119-128.
- Bui Van, D., Chinkulkijniwat, A., Horpibulsuk, S., Yubonchit, S., Limrat, I., Arulrajah, A. and Jothityangkoon, C., 2017. **Steady flow in mechanically stabilised earth walls using marginal soils with geocomposite.** *Geosynthetics International*. 24(6), 590-606.
- Chinkulkijniwat, A., Horpibulsuk, S., Bui Van, D., Udomchai, A., Goodary, R., Arulrajah, A., 2017. **Influential factors affecting drainage design considerations for mechanical stabilised earth walls using geocomposite.** *Geosynthetics International*. 24(3), 224-241.
- Clement, T. P., Wise, W. R., Molz, F. J., & Wen, M., 1996. **A comparison of modeling approaches for steady-state unconfined flow.** *Journal of Hydrology*. 181(1-4), 189-209.
- Dickinson, S., Brachman, R. W. I., & Rowe, R. K., 2010. **Thickness and Hydraulic Performance of Geosynthetic Clay Liners Overlying a Geonet.** *Journal of Geotechnical and Geoenvironmental Engineering*. 136(4), 552-561.
- Giroud, J. P., & Kavazanjian, E., 2014. **Degree of Turbulence of Flow in Geosynthetic and Granular Drains.** *Journal of Geotechnical and Geoenvironmental Engineering*. 140(5), 06014001.

- Iryo, T., Rowe, R., 2005. **Numerical Study of Infiltration Into a Soil–Geotextile Column.** *Geosynthetics International*. 11(5), 377-389.
- Kibria, G., Hossain, M. S., & Khan, M. S. 2014. **Influence of Soil Reinforcement on Horizontal Displacement of MSE Wall.** *International Journal of Geomechanics*, 14(1), 130–141.
- Koerner, R.M., Koerner, G.R., 2011. **The Importance of Drainage Control for Geosynthetic Reinforced Mechanically Stabilized Earth Walls.** *Journal of Geoengineering*. 6(1), 3-13.
- Koerner, R.M., & Koerner, G.R., 2013. **A data base, statistics and recommendations regarding 171 failed geosynthetic reinforced mechanically stabilized earth (MSE) walls.** *Geotextiles and Geomembranes*. 40, 20-27.
- Koerner, R.M., & Koerner, G.R., 2015. **Lessons learned from geotextile filter failures under challenging field conditions.** *Geotextiles and Geomembranes*. 43(3), 272-281.
- Koerner, R.M., & Koerner, G.R., 2018. **An extended data base and recommendations regarding 320 failed geosynthetic reinforced mechanically stabilized earth (MSE) walls.** *Geotextiles and Geomembranes*, 46(6), 904-912.
- Konukcu, F., Istanbuluoglu, A., and Kocaman, I., 2004. **Determination of water content in drying soils: Incorporating transition from liquid phase to vapour phase.** *Australian Journal of Soil Research*. 42(1), 1-8.

- La Duong, H., Chinkulkijniwat, A., Horpibulsuk, S., Do Quang, T., Yaowarat, T., 2020. **Steady state groundwater in mechanical stabilized earth walls of various dimensions with geocomposite back drain installation.** *International Journal of geomechanics.*
- Mualem, Y., 1976. **A new model for predicting the hydraulic conductivity of unsaturated porous media.** *Water Resources Research.* 12(3), 513-522.
- Robinson, J.D., Vahedifard, F., AghaKouchak, A., (2017). **Rainfall-triggered Slope Instabilities under a Changing Climate: Comparative Study using Historical and Projected Precipitation Extremes.** *Canadian Geotechnical Journal.* 54(1), 117-127.
- Roy, D., & Singh, R., 2008. **Mechanically Stabilized Earth Wall Failure at Two Soft and Sensitive Soil Sites.** *Journal of Performance of Constructed Facilities,* 22(6), 373-380.
- Portelinha, F.H.M., and Zornberg, J.G., 2017. **Effect of Infiltration on the Performance of an Unsaturated Geotextile-reinforced Soil Wall.** *Geotextiles and Geomembranes,* 45(3), 211-226.
- Saeedpanah, I., Jabbari, E., & Shayanfar, M. A., 2011. **Numerical simulation of ground water flow via a new approach to the local radial point interpolation meshless method.** *International Journal of Computational Fluid Dynamics.* 25(1), 17-30.
- Stuedlein, A.W., Allen, T.M., Holtz, R.D., & Christopher, B.R., 2012. **Assessment of Reinforcement Strains in Very Tall Mechanically Stabilized Earth Walls.** *Journal of Geotechnical and Geoenvironmental Engineering,* 138(3), 345–356.

- Szymkiewicz, A., Tisler, W., and Burzyński, K., 2015. **Examples of numerical simulations of two-dimensional unsaturated flow with VS2DI code using different interblock conductivity averaging schemes.** *Geologos*. 21(3), 161–167.
- Thuo, J.N., Yang, K.H., Huang, C.C., 2015. **Infiltration into unsaturated reinforced slopes with nonwoven geotextile drains sandwiched in sand layers.** *Geosynthetics International*. 22(6), 457-474.
- Vahedifard, F., Tehrani, F.S., Galavi, V., Ragno, E., AghaKouchak, A., 2017. **Resilience of MSE Walls with Marginal Backfill under a Changing Climate: Quantitative Assessment for Extreme Precipitation Events.** *Geotechnical and Geoenvironmental Engineering*. 143(9), 04017056.
- van-Genuchten, 1980. **A closed-form Equation for Predicting the Hydraulic Conductivity of Unsaturated Soils.** *Soil science society of America journal*. 44(5), 892-898.
- Xu, Y.-S., Shen, S.-L., Ma, L., Sun, W.-J., & Yin, Z.-Y. (2014). **Evaluation of the blocking effect of retaining walls on groundwater seepage in aquifers with different insertion depths.** *Engineering Geology*. 183, 254-264.
- Yarahmadi, N., Gratchev, I., Jeng, D.S., Gibbs, D., 2017. **Effect of Thickness Reduction on Hydraulic Transmissivity of Geonets used in Leachate Collection Systems in Landfills.** *The 19th Southeast Asian Geotechnical Conference and 2nd AGSSEA Conference, Kuala Lumpur, Malaysia*.
- Yoo, C., Jung, H.Y., 2006. **Case history of Geosynthetic Reinforced Segmental Retaining Wall Failure.** *Journal of Geotechnical and Geoenvironmental Engineering*. 132(12), 1538-1548.

Zornberg, J.G., Mitchell, J., 1994. **Reinforced soil structures with poorly draining backfills. Part I: Reinforcement interactions and functions.** *Geosynthetics International*. 1(2), 103-147.



CHAPTER III

STEADY STATE GROUNDWATER IN MECHANICAL STABILIZED EARTH WALLS OF VARIOUS DIMENSIONS WITH GEOCOMPOSITE BACK DRAIN INSTALLATION

3.1 State of problem

Mechanically stabilized earth (MSE) walls have been widely used in cut and fill works for highway construction through mountainous areas. Although MSE walls are very effective for cut and fill works in sloping ground, several MSE wall failures during heavy rainfall have been reported in previous research of Yoo and Jung 2006; Robinson et al. 2017 and Vahedifard et al. 2017. Internal instability is one of the most often reported failure modes in MSE walls (Koerner et al., 2011; Koerner et al., 2013; Thuo et al., 2015; Robinson et al., 2017; Koerner et al., 2018; Valentine. 2013; Thuo et al. 2015; A. Chinkulkijniwat et al. 2017; Bui Van et al. 2017; Robinson et al. 2017. Heavy rainfall might cause an increment of water content and phreatic level in MSE wall, and hence the drop of soil suction. Based on the extended Mohr-Coulomb criterion proposed by Fredlund et al. 1978, cohesive strength is divided to two components: (1) cohesion c' , and (2) apparent cohesion due to suction. Escario and Saez. 1986, among others, reported from their test results a nonlinear drop of the apparent cohesion due to increment of water content, and hence suction drop. Iryo and Rowe 2004 and Thuo et

al. 2015 reported serious reductions in shear strength of the soil in the reinforced zone due to extreme precipitation. Koerner et al. 2018 reported that 41% of all internal failures were caused by the poor performance of the drainage system. Other than internal stability, Zhang et al. 2015 reported the influence of water content on external stability of retaining walls. In order to avoid high water content in MSE wall, drainage system must have a high enough capacity to drain sufficient water in extreme conditions.

To combine high drainage capacity and ease of installation, drainage systems installed in many geostuctures, including MSE walls, have frequently used a geocomposite comprising a geonet core with a large flow channel sandwiched by a nonwoven geotextile (Zornberg et al. 1995, McKean and Inouye 2001, Koerner et al. 2011, Koerner et al., 2015; Koerner et al., 2013). Utilize of geocomposites drain has been conducted as geosynthetics reinforcements with high in-plane transmissivity not only provide mechanical reinforcement to the unsaturated marginal fill, but their drainage properties can prevent destabilizing water flow configurations in reinforced constructions (Mitchell and Zornberg 1995, Christopher et al. 1998). This type of geocomposite system installed as a back drain for an MSE wall is the focus of this study. Although geocomposite drains in MSE walls have been spotlighted in various reports, most of these works focused on aspects of material properties, particularly the influence of factors affecting geonet transmissivity. Dickinson 2010 determined the relationship between geonet transmissivity and geonet thickness. Giroud et al. 2014 and Yarahmadi et al. 2017 studied the reduction of hydraulic transmissivity due to creep deformation. Reports about the influence of geocomposite properties on seepage responses in MSE walls are limited. Chinkulkijniwat et al. 2017 concluded that the

capillary barrier phenomenon plays a role in the distribution of effective saturation at the soil–geotextile interface. Bui Van et al. 2017 proposed that the outer permeability ratio, defined as a ratio of geonet permeability to permeability of upstream soil, affected the phreatic level in the protected zone. No correlation between the phreatic level in the protected zone and the permeability ratio was provided since only 4 simulation cases related to the outer permeability ratio were conducted in their report. This study conducted a series of numerical experiment for further elaborating the finding in Bui Van et al. 2017.

Other than geocomposite properties, the hydrological properties of the relevant soils also play an important role in seepage responses such as the distribution of water content and the location of the phreatic surface in MSE walls. A number of studies reported the effect of hydrological properties of the soil on seepage responses in MSE walls (Zornberg et al. 1994, Christopher 1998, Vahedifard et al. 2017; Albino et al. 2019). Previous significant research reports indicated the build-up of pore water pressure (i.e. The appearance of wide distribution of water content inside protected zone occurred in backfill soil walls due to low permeability and high fine content particle (Santos et al. 2010; Koerner et al. 2013; Valentine. 2013). In mountainous terrain, where heavy rainfall could raise the upstream water level due to huge amounts of rainwater flowing from high ground towards an MSE wall (Bui Van et al., 2017), the seepage responses in the MSE wall were also governed by the relevant shape parameters. These parameters included the level of the upstream water table, the distance from the upstream water to the drainage face, the depth below the wall of the impervious rock interface, and the width and height of the protected zone.

Theoretically, these shape parameters affect groundwater flow geometry and, hence, related seepage responses.

For steady-state unconfined flow in rectangular-flow systems, Clement et al. 1996 investigated the effect of flow domain aspect ratio on the height of the seepage face, which is the difference between the phreatic surface at the exit and the downstream water level. They found that effects on the seepage face were diminished for long, shallow flow domains, while the position of the phreatic surface was relatively insensitive to downstream water level for deep flow domains. Saeedpanah et al. 2011 reported that the length of the groundwater flow path plays a more important role in the flow rate than the upstream water level does. Despite their importance to seepage responses, the relevant shape parameters are yet to be investigated thoroughly enough to comprehensively explain their influence on seepage responses in an MSE wall.

In this thesis, a well-calibrated numerical model, computed in the Plaxis environment and introduced by Chinkulkijiwat et al. 2017, was further elaborated with regard to the effect of scaling. To ensure the validity of the Plaxis-based model on different scales, it was established using identical shape ratios at double the size of the physical model. The calibrated model was further employed to perform a series of parametric studies focusing on the influence of the shape parameters and geonet transmissivity on seepage responses in the modeled MSE wall. Results from this study will reinforce research into the influence of the dimensions of MSE walls and drainage properties on seepage responses.

3.2 Governing equations

Steady-state of unconfined aquifer is considered as flow regime expressed that when the magnitude and direction of flow is constant with time throughout the entire domain. With steady state flow appearance, time is no longer an independent variable and thus the storage term in the groundwater flow equation disappears; Since there is no change in the amount of water stored in the domain (i.e. the hydraulic head and pressure at any points get constant value over time. Steady-state flow condition is also chosen in order to quantify the final state of ground flow which act in homogeneous soil mass against phreatic surface growth in this conceptual numerical simulation. In addition, under the impacts of groundwater level behind the wall rise due to extreme precipitation, the phreatic surface changes and water content distribution at steady-state condition present and determine critical conditions at a particular upper stream state since the increase of water level in research.

The equation governing transient water flow for a two-dimensional homogeneous anisotropic material within an unsaturated porous medium is given as follows:

$$k_x \frac{\partial^2 h}{\partial x^2} + k_y \frac{\partial^2 h}{\partial y^2} = \frac{\partial \theta}{\partial t} \quad (3.1)$$

where θ is volumetric water content which defined as volume of water presents in a unit volume of soil mass, h is the total head, k_x and k_y are the unsaturated coefficients of permeability in the x - and y - directions, and t is time. When the variables describing the water states at a given point do not change in time, the flow is

treated as steady, the time derivatives in the equations of motion are zero and Eq. 1 becomes

$$k_x \frac{\partial^2 h}{\partial x^2} + k_y \frac{\partial^2 h}{\partial y^2} = 0 \quad (3.2)$$

To supplement Eq. 2, constitutive equations are required, relating θ , k_x , and k_y to h . In this study, the van Genuchten model (Eq. 3a) (van Genuchten 1980) and van Genuchten-Mualem model (Eq. 3b), which is an integration of the van Genuchten model with the Mualem hypothesis (Mualem 1976), were employed to approximate the water retention curve (WRC) and permeability functions for every porous media in the MSE wall problem. These models are later named in this paper as VG and VGM model, respectively. The models gave the following equations:

$$S_e = \frac{S - S_{res}}{S_{sat} - S_{res}} = \frac{\theta - \theta_{res}}{\theta_{sat} - \theta_{res}} = \left[1 + (\alpha |h_p|)^n \right]^{-m} \quad (3.3a)$$

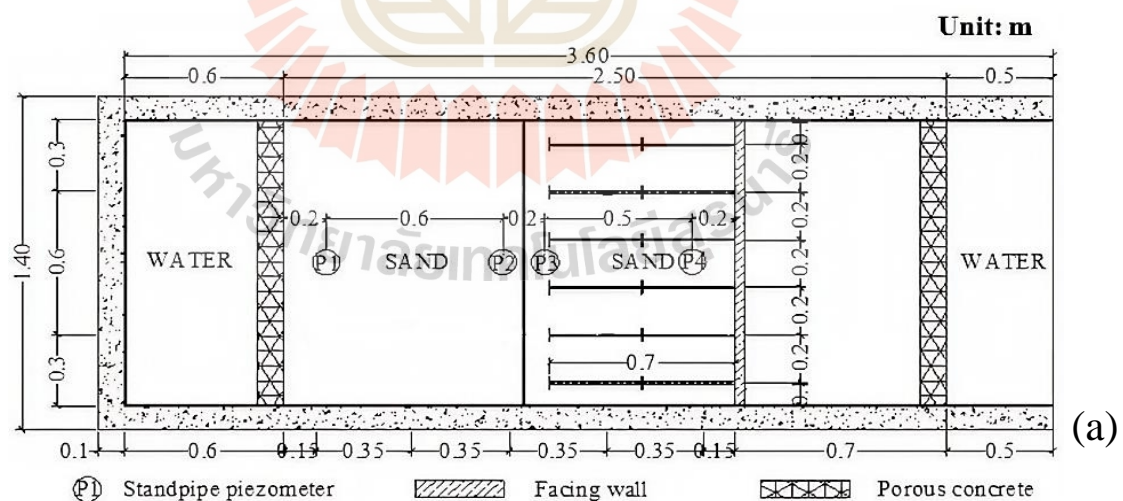
$$k_r(S_e) = S_e^{0.5} [1 - (1 - S_e^{1/m})^m]^2 \quad (3b)$$

In the above equations, S_e is effective degree of saturation, S is degree of saturation, S_{res} is residual saturation at very high values of suction, S_{sat} is the maximum saturation of saturated soil, θ_{res} is residual volumetric water content, θ_{sat} is maximum volumetric water content of saturated soil, h_p is matric suction head, and k_r is the relative permeability coefficient: α [m^{-1}] and n are fitting parameters which represent respectively the air-entry value of the soil and the rate of water extraction from the soil

once the air entry value has been exceeded: m , according to the Mualem hypothesis (Mualem, 1976), is assigned the value $1-1/n$. Steady-state flow conditions were the focus of our study in order to quantify the final state of groundwater flow in the porous media.

3.3 Materials and methods

Figure 3.1 presents a sketch of a physical model designed to investigate responses in an MSE wall with a geocomposite installation as a back drain under high upstream ground water level. This large-scale model was established by Chinkulkijniwat et al. 2017 who also reported the results from tests conducted with this model filled with sandy soil. Basic and hydrological properties of the studied materials; including sandy soil, lateritic soil, geotextile, and geonet, are given in **Figure 3.2** and **Table 3.1**.



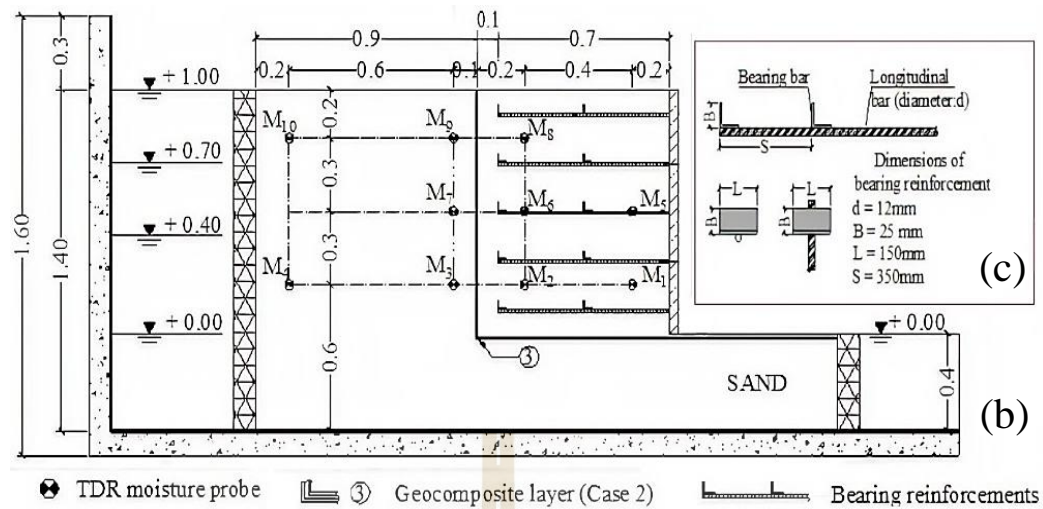


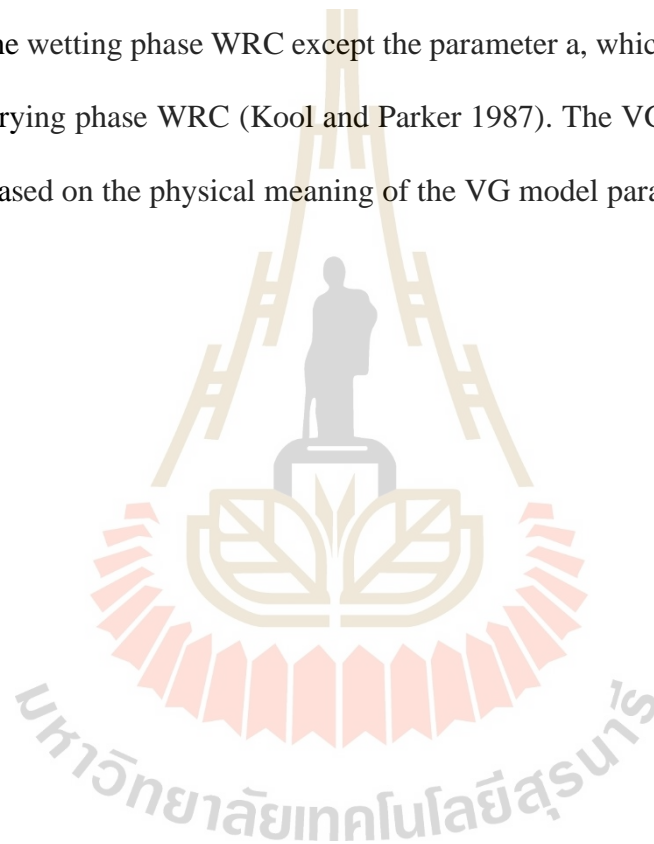
Figure 3.1 Sketch of the physical test model and its instrumentation: (a) plan view of the model, (b) side view of the model, (c) sketch of bearing reinforcement (adapted from Chinkulkijniwat et al. 2017 with permission).

Figure 3.2a presents grain size distribution of the sandy soil and the lateritic soil. Since the problem in this study involves with water flow into the MSE wall, the wetting phase water retention curve (WRC) of the corresponding materials must be obtained. **Figure 3.2b** present the wetting phase WRC of sandy soil, lateritic soil, and geotextile. Nonlinear regression was conducted fit the VG model (Eq.3a) to the measured WRC. The best-fit VG model parameters of the studied materials are also given in **Table 3.1**.

Although we obtained the wetting phase WRC from the previous studies (Chinkulkijniwat et al., 2017 and Bui Van et al., 2017), determinations of WRC are briefly given in the following paragraph for clarification. Different techniques were employed to obtain the curves. The wetting phase WRC of the geotextile was obtained from a capillary rise test (Lafleur et al., 2000).

The wetting phase WRC of the sandy soil was obtained using double-walled triaxial cell. Due to difficulty of direct determination of wetting phase WRC in the lateritic soil, the drying phase WRC of the lateritic soil was obtained using a pressure plate apparatus (ASTM D6836-02).

After getting the best-fit VG model parameters for the drying phase WRC of the lateritic soil, every VG model parameter values for the drying phase WRC were assigned to the wetting phase WRC except the parameter a , which was twice as high as that for the drying phase WRC (Kool and Parker 1987). The VG model parameters of geonet was based on the physical meaning of the VG model parameters.



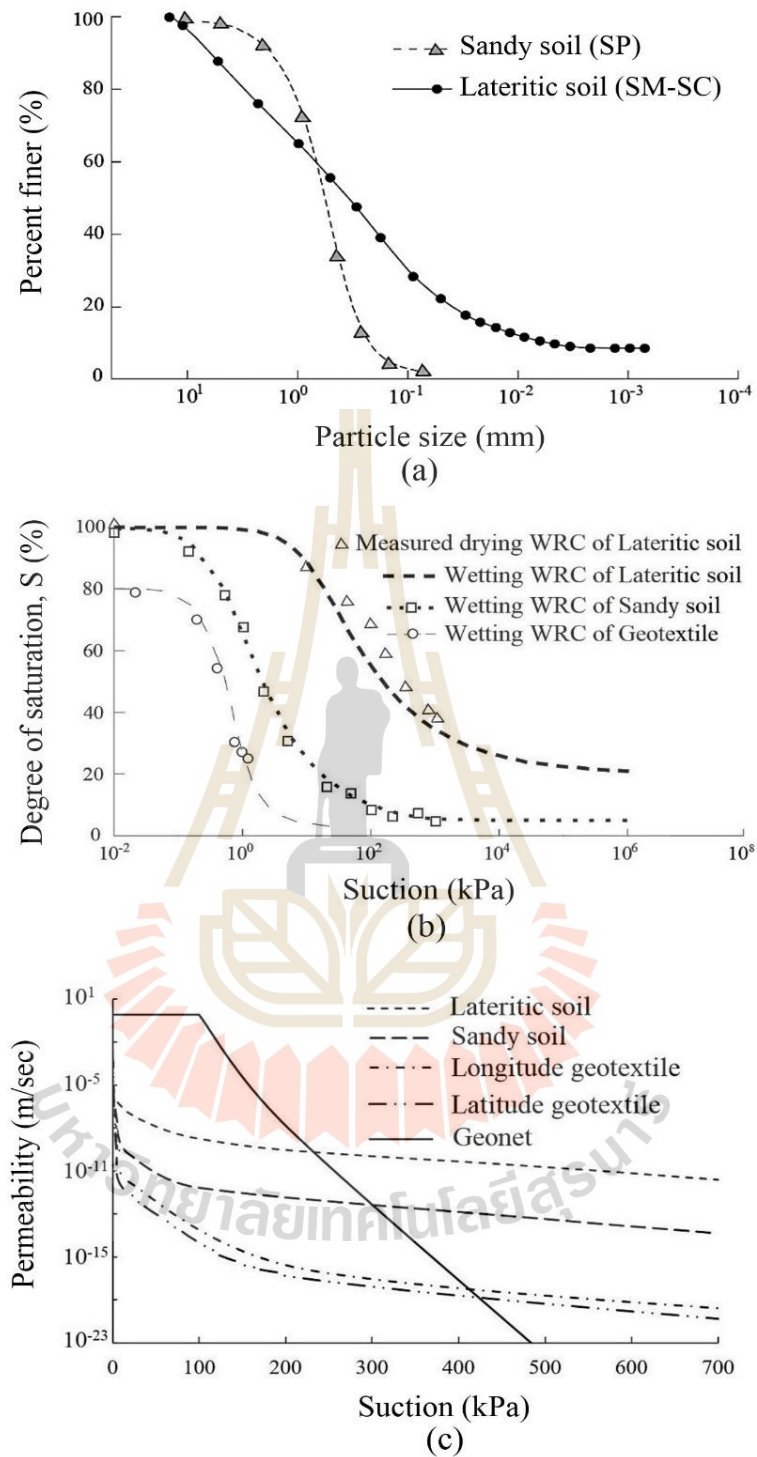


Figure 3.2 (a) Grain size distribution, (b) WRC, and (c) permeability function of studied sandy soil, geotextile, geonet and lateritic soil utilized in this study (adapted from Bui Van et al. 2017 with permission).

The α parameter is related to the largest pore size and the n parameter is related to the pore distribution. As the geonet has a very open structure, VG and VGM models with the following considerations were assigned to the geonet (1) The geonet has a large and single pore size attribution. (2) The geonet can be completely dried ($S_{res} = 0.0$) and completely saturated ($S_{sat} = 1.0$). With respect to the first consideration, high values of α and n reflect a large pore size and a more uniform pore size distribution, respectively. Hence, high α and n values were assigned to the geonet. According to Chinkulkijniwat et al. 2017, the geonet parameters α and n were assigned values of 600 m^{-1} and 40, respectively. These values were summarized after finding that the calculation results were no changed after assigning magnitudes of a greater than 600 m^{-1} and n greater than 40. Since it is easier to measure WRC than to measure the permeability function, estimation of the permeability function can be achieved through the model parameters extracted from WRC of the corresponding material.

Figure 3.2c plots the permeability function of every materials used in this study. At low suction (high saturation) level, the geonet permeability is much higher than the permeability of the other studied materials. In this condition, the geonet accepts water flowing from its adjacent material and collects water to drain away at the downstream side. The geonet permeability, however, drops sharply with suction and becomes notably lower than the permeability of the other materials. At high suction (low saturation) level, the geonet is filled with air, and hence no water flow across the boundary between the geonet and its adjacent material.

Table 3.1 Basic and relevant physical and hydraulic properties of studied sandy soil, geotextile, geonet (adapted from Chinkulkijniwat et al., 2017) and lateritic soil (adapted from Bui Van et al., 2017) utilized in this study.

Soil material	Physical property				Hydraulic property and VG model parameter						
	γ (kN/m ³)	G_s (-)	PL (%)	LL (%)	Permeability (m/sec)			α (m ⁻¹)	n (-)	S_{sat} (-)	S_{res} (-)
Sandy soil	15.0	2.74	-	-	1.97×10 ⁻⁴			20	1.5	1.0	0.03
Lateritic soil	18.27	2.75	26	42	4.0×10 ⁻⁶			0.8	1.4	1.0	0.2
Geosynthetic material	Porosity (-)	Open size (mm)	Weight per area (kg/m ²)	Thickness (mm)	Permeability ×10 ⁻² (m/sec)	Transmissivity ×10 ⁻⁶ (m ² /sec)	Permittivity (sec ⁻¹)	α (m ⁻¹)	n (-)	S_{sat} (-)	S_{res} (-)
Geotextiles	0.9	0.15	0.339	2.5	2.3(0.37) ^a	57.9(9.26) ^b	9.23(1.48) ^c	20	2.5	0.8	0.03
Geonet	-	-	1.0	5.0	80	0.004	160	600	40	1.0	0.0

^a Permeability of geotextile in lateral direction.

^b Transmissivity of geotextile in lateral direction.

^c Permittivity of geotextile in lateral direction.

In the remaining part of this section, model preparation, test procedure and test results reported by Chinkulkijniwat et al. (2017) are briefly mentioned for the sake of clarification. The sandy soil, geocomposite drain, reinforcement of the wall facing and instrumentation were carefully positioned in the model. Groundwater flow during the test was activated by the difference of water levels in upstream and downstream water tanks. The water level in the downstream tank was kept constant at a depth of 0.4 m (+0.0 m) using a control weir. The water level in the upstream tank was increased stepwise from a depth of 0.4 m (+0.0 m), to 0.8 m (+0.4 m), 1.1 m (+0.7 m), and 1.4 m (+1.0 m). Increments in water level in the upstream tank were made when steady state was observed, which was indicated by steady water content values, detected by Time Domain Reflectometry (TDR) probes.

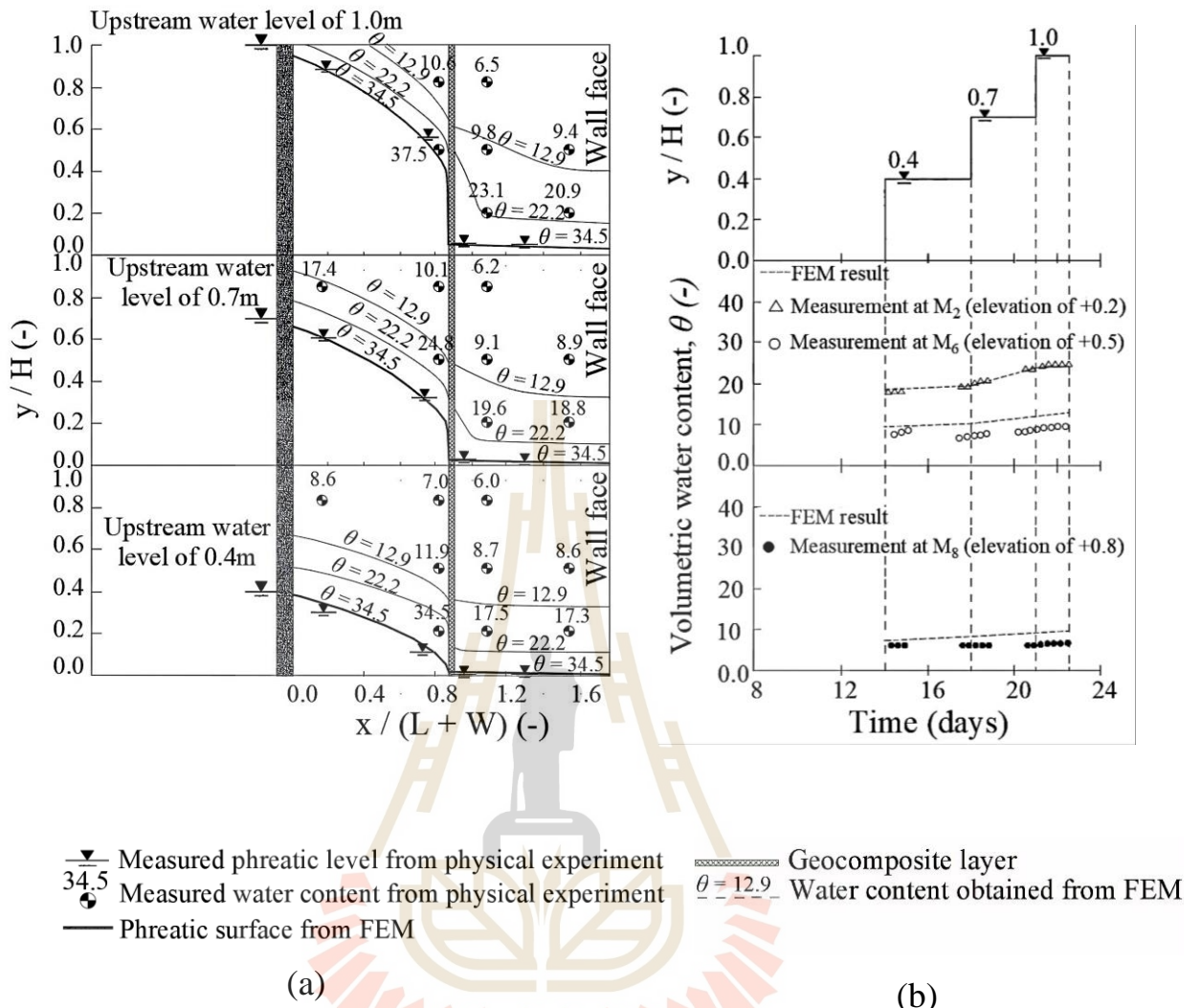


Figure 3.3 (a) Water saturation profiles, phreatic level and (b) time series plot of water content adopted from the physical model test reported in adapted from Chinkulkijniwat et al. (2017) and the corresponding calculations.

Figure 3.3 presents time series plots of water content at M2, M6, and M8 TDR probes and distribution of water content and groundwater levels at steady state in sandy soil for an upstream water level of +0.4 m, +0.7 m, and +1.0 m. At any height of upstream water, the groundwater level decreased through the wall face and dropped drastically in the protected zone (or reinforced zone). The water content values in the

protected zone were also much lower than that outside the zone. These measurements showed that installation of high permeable geocomposite could prevent water flow to the protected zone effectively.

3.4 Numerical simulations

A series of numerical experiment was conducted using the finite element code Plaxis. **Figure 3.4** depicts the discretized finite element mesh for the MSE wall model and the shape parameters investigated in this study. The shape parameters included the height of the wall (H), the width of the protected zone (W), the distance from the upstream water source to the drainage face (L), and the distance from the wall base to the impervious boundary (D). The “groundwater flow only” mode was selected for the Plaxis calculations.

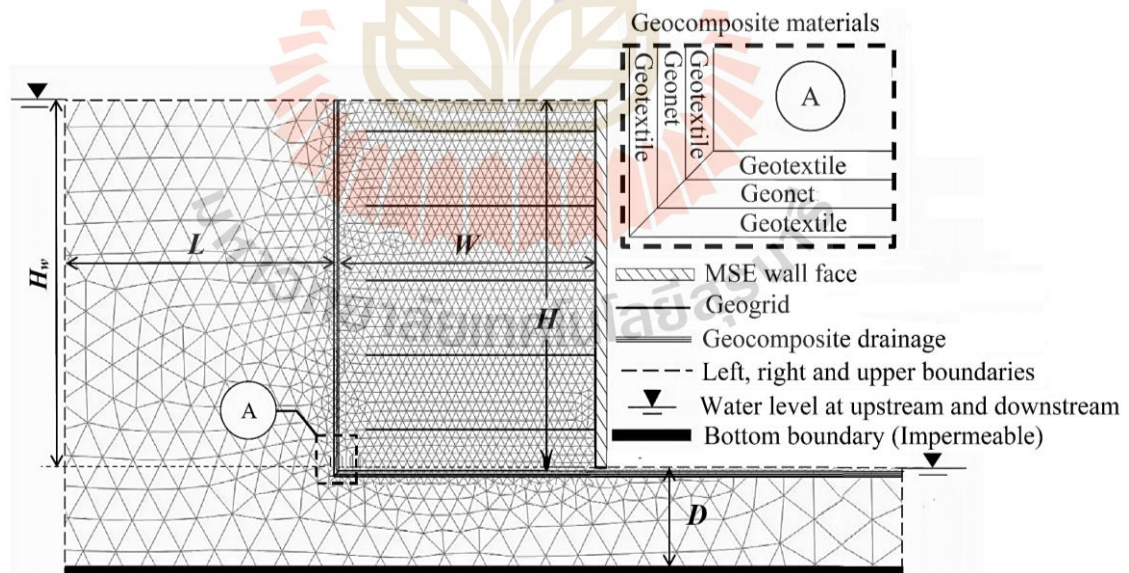


Figure 3.4 Plaxis model of mesh discretization and the relevant shape parameters of MSE wall with back drain using geocomposite.

Fifteen-node triangles were assigned to the generated models, and a very fine mesh with an average element size of 0.05 m was selected. The very fine meshing brings much accuracy in interpolation than others as coarse and medium mesh. On the other hand, very fine mesh with accuracy for small scale interpolation when extracting values of research objects such as h_o and S_{eff} . The mesh size much expansion near the left, right, upper and bottom model boundaries. That is in purpose that avoid the boundary effect in simulation. Since the hydrological related properties; including permeability and VG parameters, had to assigned to the geotextile and geonet, the geotextile and geonet in this study were prescribed as soil materials having own hydrological related properties. Finer meshes of fifteen-node triangle was also assigned to the geotextile and the geonet. Dirichlet boundary conditions with prescribed pressures were imposed on the left, right, and upper boundaries of the model, and the bottom boundary of the model was defined as impermeable. The left and right boundaries were assigned hydrostatic pressure whereas the upper boundary was assigned atmospheric pressure. Interface setting up is not applied for studied materials in this numerical simulation. This is because the model desires the continuous at many materials for indicating the continuous phreatic water level from the upstream to downstream water level, and water saturation profile inside protected area. Groundwater flow was simulated by applying hydrostatic pressure according to the upstream water level equal to any desired height. Time steps were automatically assigned by the software. At each time step, the nonlinear differential equation (Eq. 2) was solved iteratively using a modified Newton-Raphson model. In each iteration, the increment of the groundwater head was calculated from the imbalance in the nodal discharge and added to the active head. This process continued

until the norm of the imbalanced vector – that is, the error in the nodal discharge – was smaller than that of the error tolerance of 0.01 (or 1%).

For calibration purposes, the model was designed to replicate the experimental studies mentioned above. This model incorporated sandy soil, structural components (reinforced bar and acrylic facing), and drainage components (geotextile, and geonet). The seepage characters of the relevant materials were described using Eq. 2 and Eq. 3. To ensure the validity of the Plaxis-based model on different scales, the Plaxis-based model was established to keep identical shape ratios at double the size of the physical model: $H = 2.0$ m, $H_w = 2.0$ m, $W = 1.6$ m, and $D = 0.8$ m. Furthermore, the thickness of geotextile and geonet was also enlarged 2.0 time thicker than that of the physical model, i.e. thickness values of geonet and geotextile were 10 mm and 5 mm, respectively.

The results of the simulations were plotted and are shown in **Figure 3.3**. Since the calculations were extracted from the double-sized model, the dimensions shown in **Figure 3.3** are presented in terms of ratios to the wall height H . Good agreement between the data from the physical tests and the corresponding simulations was obtained from the plots, proving that the relevant seepage responses, including water content and ground water level, were well captured using the established model in the Plaxis environment regardless the size of the model.

The numerical experiment was carried out in two parts. In the first part, a series of numerical simulations was produced to investigate the individual effects of shape parameters W , H , L , and D on seepage responses, including the highest water level in the protected (ho), and the water saturation profile inside the protected zone. During the experiment, all the shape parameters, except the parameter being varied, were kept

constant at $H = 2.0$ m, $W = 1.6$ m, $L = 2.0$ m and $D = 0.8$ m. The simulations were conducted in three scenarios based on the soil types prescribed as native and backfill soils. The numerical simulations conducted in this part are summarized in **Table 3.2**. Noteworthy that the *S-S* scenario, which the native and backfill soils were placed by the sandy soil, rarely exists in field conditions.

This scenario, however, was established for sake of comparison. In total, 66 simulations were made, 22 for each scenario. The height of upstream water level H_w was kept constant at 2.0 m though 66 simulation cases. Constant H_w as 2.0 m even H parameter increases for reflecting unchanged h_o subject to MSE wall height rises (**Figure 3.5**). Other reason for that keeping H_w constant is for ignorance of H_w influences in this parametric research of thesis.

All model parameters imposed for the seepage characters of the sandy soil, lateritic soil, geotextile, and geonet were those reported by Chinkulkijniwat et al. (2017) and Bui Van et al. (2017) and are presented in **Table 3.2**. These model parameters (k , a , n , S_{res} , S_{sat}) including thickness of geotextile and geonet were kept constant throughout the first part of the numerical experiment.

The second part of numerical experiment comprised 27 cases. In this part, a series of numerical simulations was produced to investigate the effects of geonet transmissivity (T_{net}) on seepage responses, including the highest water level in the protected (h_o), and the water saturation profile inside the protected zone. Geonet transmissivity was controlled by geonet thickness (t_{net}) and geonet permeability (k_{net}) through the relationship written in Eq. 4,

Table 3.2 Detail of 66 simulations conducted for shape parameters.

Material	Permeability (m/sec)	Thickness (mm)	α (m^{-1})	n (-)	S_{sat} (-)	S_{res} (-)
Sandy soil	1.97×10^{-4}	-	20	1.5	1.0	0.03
Lateritic soil	4.0×10^{-6}	-	0.8	1.4	1.0	0.2
Geotextile	0.023 (0.0037) ^a	5.0	20	2.5	0.8	0.03
Geonet	0.8	10	600	40	1.0	0.0
Scenario	Native soil			Backfill soil		
<i>S-S</i>	<i>Sandy soil</i>			<i>Sandy soil</i>		
<i>L-L</i>	<i>Lateritic soil</i>			<i>Lateritic soil</i>		
<i>L-S</i>	<i>Lateritic soil</i>			<i>Sandy soil</i>		
Varied parameter	Definition				Studied values	
<i>W</i> (m)	Protected zone width				1.6, 2.0, 2.5	
<i>L</i> (m)	Length from upstream water to the drainage face				0.5, 1.0, 3.0, 4.0, 5.0	
<i>H</i> (m)	MSE wall height				2.5, 3.0, 3.5, 4.0, 4.5, 5.0	
<i>D</i> (m)	Distance from the wall base to the impervious boundary				0.0, 0.2, 0.8, 0.5, 1.0, 2.0, 3.0, 4.0, 5.0	

^a Permeability of geotextile in lateral direction.

Note: The height of upstream water level (H_w) was kept constant at 2.0 m for all 66 simulations.

$$T_{net} = k_{net} \times t_{net} \quad (3.4)$$

where T_{net} is geonet transmissivity (m^2/sec), t_{net} is geonet thickness (m) and k_{net} is geonet permeability (m/sec). In this experimental part, all the shape parameters were kept constant at $H = 2.0$ m, $w = 1.6$ m, $H_w = 2.0$ m, $L = 2.0$ m and $D = 0.8$ m. The t_{net} was varied at 10 mm, 15 mm and 20 mm while the k_{net} was varied at 0.8 m/sec, 0.08 m/sec and 0.008 m/sec. The simulations were also conducted in three scenarios based on the soil types prescribed as native and backfill soils. **Table 3.3** summarizes detail of the second part of the numerical experiment.

Table 3.3 Detail of 27 simulations conducted for T_{net} study

Scenario	Native soil	Backfill soil
<i>S-S</i>	<i>Sandy soil</i>	<i>Sandy soil</i>
<i>L-L</i>	<i>Lateritic soil</i>	<i>Lateritic soil</i>
<i>L-S</i>	<i>Lateritic soil</i>	<i>Sandy soil</i>
Geometry parameters are kept constant at $H(H_w) = 2.0$ m, $L = 2.0$ m, $D = 0.8$ m, $W = 1.6$ m		
Varied parameter	Definition	Studied values
t_{net} (mm)	Geonet thickness	10, 15, 20
k_{net} (m/sec)	Geonet permeability	0.8, 0.08, 0.008

A steady flow mode was selected to calculate the final groundwater states due to elevated upstream water. The groundwater states at steady state, including h_o and water saturation, extracted from the numerical experiment were used to analyze the influence of the studied parameters.

3.5 Influence of shape parameters

This section describes, via the location of the phreatic surface and the distribution of water saturation inside the protected zone, the influence of shape parameters w , H , D , and L . The location of the phreatic surface inside the protected zone was represented by its highest level (h_o) and the distribution of water saturation inside the protected zone was determined from the water saturation profile in the protected zone along a vertical section located at 0.8 m apart from the drainage interface.

3.5.1 The highest water level inside protected zone (h_o)

For the sake of brevity and comparability, the variations of h_o for every shape parameter and every scenario were plotted together (**Figure 3.5**). For the *S-S*

scenario, the native soil was sandy soil which was different from *L-L* and *L-S* scenarios whose native soil was lateritic soil. The calculation results show that h_o in *S-S* scenario was higher than that in *L-L* and *L-S* scenarios. In fact, the phreatic surfaces in every scenario before approaching the geocomposite were not much different (ref. **Figure 3.6**). The significant difference of phreatic surface took place only near the drainage interface.

It is known that flow across a boundary between two materials of different permeabilities might result in a reflection of the flow direction (as shown in the top right of **Figure 3.6**) and the relationship between the reflected angles and the permeability of the materials is written as:

$$\frac{\tan \beta_1}{\tan \beta_2} = \frac{k_1}{k_2} \quad (3.5)$$

where β_1 is incident angle or angle of flow vectors in the native soil, β_2 is reflected angle or angle of flow vectors in the drainage material, k_1 is permeability of the native soil, k_2 is permeability of drainage material.

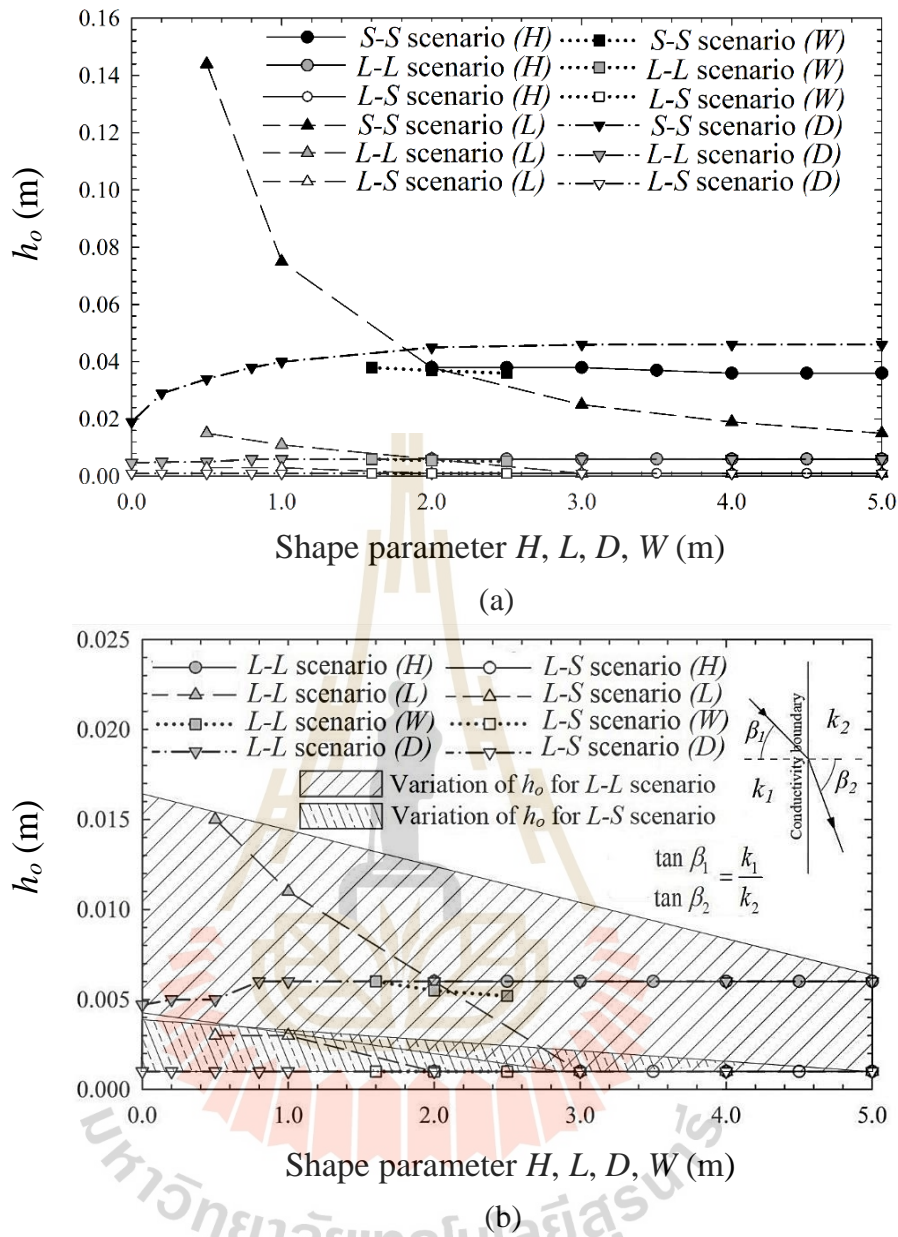


Figure 3.5 Variation of h_o subjected to change in all shape parameters for (a) *S-S*, *L-L* and *L-S*; and (b) *L-L* and *L-S* scenarios.

Since the drainage material possessed very high permeability, the flow vectors in the drainage material directed almost vertical, i.e. β_2 was almost 90° . The flow vectors in the soil before approaching the drainage interface had to direct themselves such that the relationship between the incident angle (β_1) and the reflected angle (β_2)

followed Eq. 5. For a given permeability of drainage material, the high permeability native soil yielded the higher incident angle than the low permeability native soil did. Accordingly, near the drainage interface, the phreatic surface in *L-L* and *L-S* scenarios dropped below the phreatic surface in *S-S* scenario.

Figure 3.5 also shows that the h_o band in *L-L* scenario was higher than the band in *L-S* scenario, indicating a higher mean phreatic surface in *L-L* scenario than that in *L-S* scenario. This finding is similar to that reported in Bui Van et al. (2017). They argued that soil in the protected zone was more permeable in *L-S* scenario than in *L-L* scenario, therefore the flow path reflection resulted in the lower phreatic surface in the protected zone for *L-S* scenario than that for *L-L* scenario.

3.5.1.1 Dimensions of the protected zone

The dimensions of the protected zone comprised the protected zone width (W) and the wall height (H). It is widely accepted that these shape parameters play important roles in the mechanical responses, and hence internal and external stabilities of an MSE wall (Roy and Singh 2008; Stuedlein et al. 2012; Kibria et al. 2014). However, the effect of these shape parameters on the seepage responses in an MSE wall are yet to be investigated. In this study, since the protected zone was encapsulated by the geocomposite, W and H were also the length of geocomposite at the bottom and the back side of the protected zone, respectively. The W was varied from 1.6 to 2.5 m. Based on based H value of 2.0 m, the W/H ratio in this study ranges from 0.8 to 1.25 which is about the practical recommendation of 0.8 to more than 1.1 (Berg et al 2009). Keeping horizontal distance from upstream to downstream water sources constant at 5.0 m, the h_o negligibly drops with W (**Figure 3.5**). As for the influence of

the wall height H on h_o , since this shape parameter has no effect on flow geometry, the value of h_o did not change with H , as indicated in **Figure 3.5**.

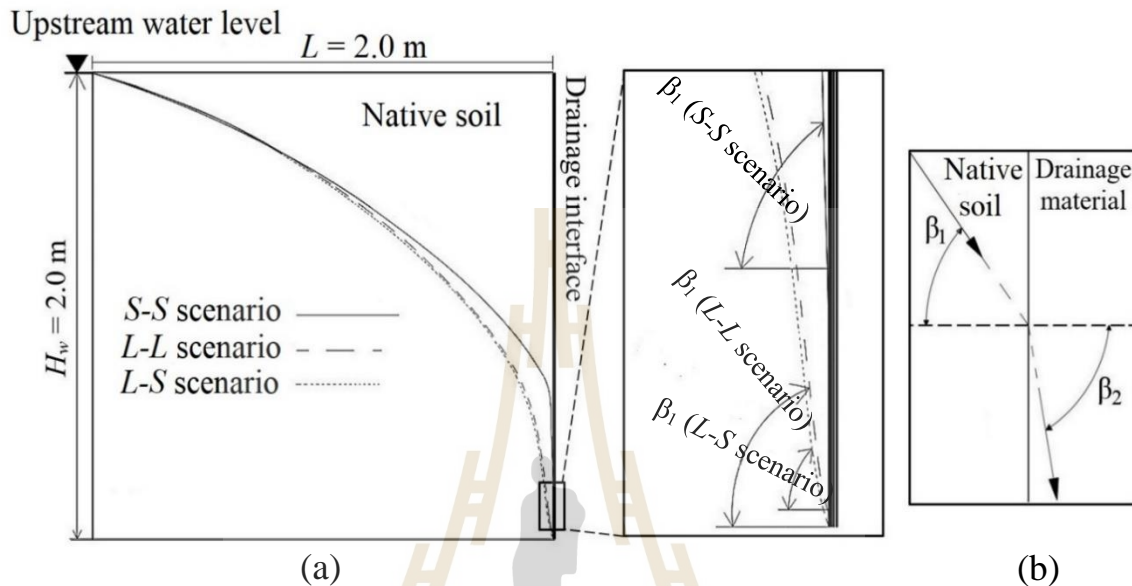


Figure 3.6 (a) Phreatic surface approaching drain interface and (b) reflection of flow directed from native soil to drain material.

3.5.1.2 The distance from the wall base to the impervious boundary (D)

Theoretically the distance from the base of an MSE wall to the impervious layer beneath, identified as the shape parameter D , affects the discharge of water flowing beneath the wall to the downstream side. In a study of groundwater flow through a sheet pile barrier, Xu et al. (2014) reported 3D numerical experiments that indicated the downstream water level decreased at greater insertion depth ratios: i.e. a ratio between penetration depth and distance from the tip of the pile to the impervious layer. In MSE walls without a back drain, an influence of D distance depends on the combination of soil types in the flow domain. **Figure 3.7** presents influence of D

distance in three conditions of MSE wall without back drain installation; including (a) the backfill and the native soils were identical, (b) the backfill soil was sandy soil and the native soil was lateritic soil, and (c) the backfill soil was lateritic soil and the native soil was sandy soil. Noteworthy that the last condition rarely exists in real condition since it is no sense to use lateritic soil as backfill material if sandy is available. However, this study shows three different conditions; including the rarely exist condition (c), for sake of comparison and understanding the flow behavior. For condition (a), whose backfill and the native soils were identical, the greater D distance resulted in a lower phreatic level due to the exist of larger flow channel beneath the protected zone. For conditions (b) and (c), whose backfill and the native soils were different, the type of backfill soil played role to the flow behaviors. In condition (b), whose backfill material was the sandy soil and the native soil was lateritic soil, the water flow tended to direct to the sandy soil as it possessed high permeability.

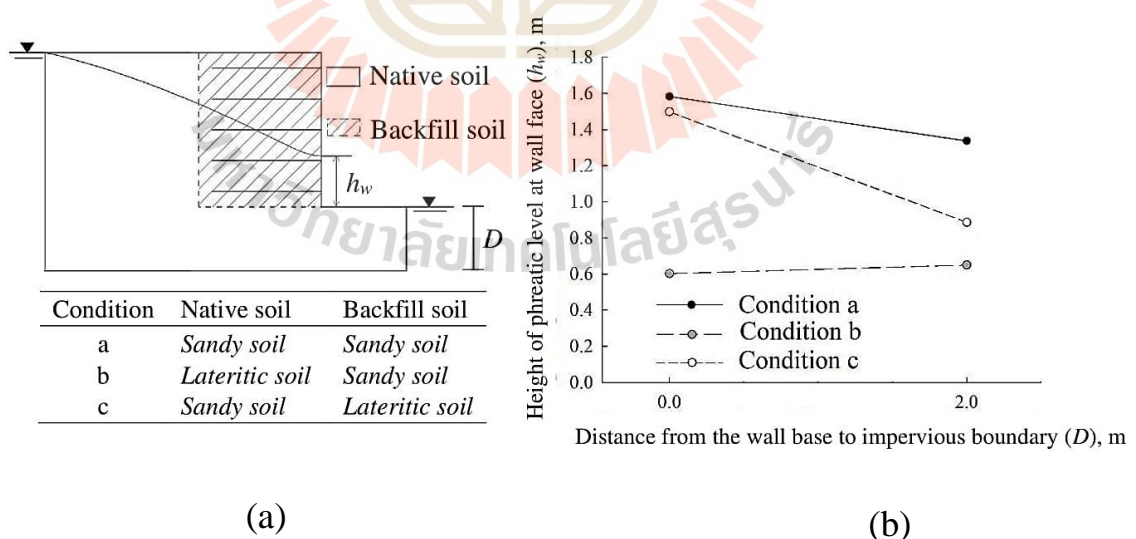


Figure 3.7 (a) Setup of conditions a, b, and c for modeling of MSE wall without back drain installation and (b) variation of h_w with D for conditions a, b, and c.

For the larger D distance, there was the wider area to allow the water flow into the concerned domain. Since the water flow tended to direct to the sandy soil which was placed as backfill soil, enlarging D distance would result in higher phreatic level. In the condition (c), the lateritic soil was placed as backfill soil and the native soil was sandy soil.

Enlarging D distance resulted in the drop of phreatic level since the sandy soil which located below the MSE wall could accept more amount of water flow. For an MSE wall with geocomposite back drain installation, enlarging D distance resulted in little rise of h_o level as shown in **Figure 3.5**. Variation of h_o with D distance was found only within limit range of D from 0.0 to 2.0 m. Increment of D beyond 2.0 m did not change the h_o level. Noteworthy that the cases with D of 0.0 m were conducted to simulate impervious foundation at the wall base. However, it is yet to be clarified whether the contribution to this increment of h_o is due to the thickness of the foundation soil or the area of water contribution on the upstream side.

Extra numerical experiment was conducted in MSE wall with back drain installation model. In this model, vertical impervious boundary of length I was prescribed at the bottom corner of the upstream side as shown in **Figure 3.8**. In this experiment enlarging the distance D was incorporated with extending the length of vertical impervious boundary line (I) such that the entry length of the upstream water (see **Figure 3.8a**) keeps unchanged at 2.0 m. **Figure 3.8b** presents variation of h_o with D distance when the entry length of upstream water was kept constant. The h_o level did not change with D for all scenarios implying that increment of h_o with D found in **Figure 3.5** was solely contributed by the entry length of the upstream water.

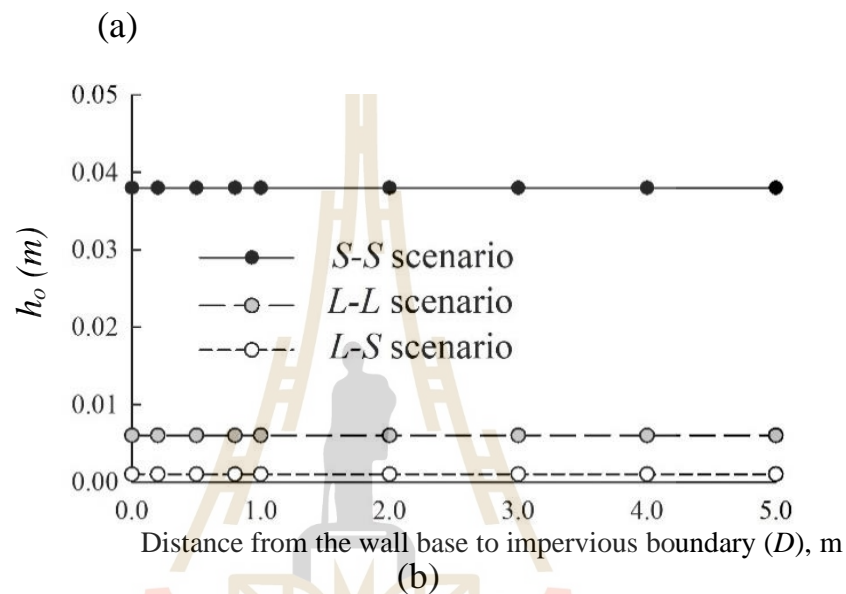
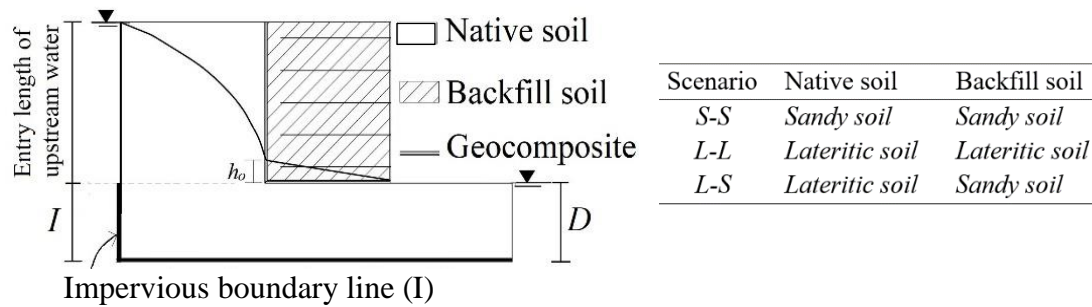


Figure 3.8 (a) Setup of extra numerical experiment to model MSE wall with back drain installation keeping the entry length of upstream water unchanged and (b) variation of h_o with D .

One must be aware that the geonet transmissivity, which is product of geonet permeability ($k_{net} = 0.8$ m/sec) and geonet thickness ($t_{net} = 10$ mm), assigned in this study is very high (0.008 m²/sec). In field condition, reduction of geonet- and geotextile transmissivities might be encountered by various factors; including creep, mineral/biological clogging, geocomposite intrusion, damage on implementation, discontinuity at the connection, etc. Conclusion drawn in this study is valid if the geocomposite does not exceed its drainage capacity.

3.5.1.3 Length from upstream water to the drainage face (L)

There is no doubt that the longer the distance from the upstream water to the drainage face (L), the more the hydraulic head falls and with it the phreatic level h_o at the downstream exit. **Figure 3.5a** shows the variability of h_o with shape parameter L . When L was small, h_o fell very fast with increments of L but the rate of fall decreased when L was greater. In S - S scenario, the magnitude of h_o approached asymptote when the shape parameter L was greater than 4.0 m, i.e. 200% of the wall height. This behavior implies that the influence of shape parameter L was eliminated if L was large enough. On the other hand, the phreatic height in the protected zone could be as high as 10% of the wall height when L was shorter than one fourth of the wall height. When MSE walls are installed in mountainous areas, the distance from the upstream water source to the protected zone can be very short. Accordingly, engineers must pay close attention to the potential phreatic levels in the protected zone of an MSE wall in mountainous terrain.

3.5.2 Water saturation profile in the protected zone

The distribution of water saturation inside the protected zone was determined from the water saturation profile along the vertical line located at 0.8 m apart from the drainage interface. In general, the water saturation profile in a given soil is governed by the shape of the WRC and the phreatic level in the corresponding soil. Consequently, water saturation profiles in the protected zone were plotted according to the type of soil used as backfill material. Water saturation profiles for S - S and L - S scenarios are presented in **Figure 3.9a** and profiles for L - L scenario in **Figure 3.9b**.

The profiles were plotted along a vertical direction and they were plotted from the wall base to the top of the wall. In other word, the saturation profiles were

plotted to equal height of the wall height (H). Since the wall height was kept constant at 2.0 m when modeling the influence of the shape parameters W , L , and D , the profiles for these shape parameters were generated from elevation of 0.0 m at the wall base to elevation of 2.0 m at the top of the wall (**Fig. 9a** and **9b**). For the shape parameter H , the height of wall was varied from 2.0 to 5.0 m. The profiles must be extended equal to the height of the wall and plotted separately in **Figure 3.9c**.

In S - S and L - S scenarios, a high level of water saturation was found only near the wall base. The level dropped very fast with distance from the wall base and water saturation was lower than 50% at a height of 0.2 m from the wall base. The water saturation curve approached asymptote at the middle height of the wall. In L - L scenario, water saturation dropped so slowly that it was greater than 80% over the entire height of the wall. The influences of the studied shape parameters on the water saturation profile are also presented in **Figure 3.9**. This figure combines the plots of all assigned values of every shape parameter and presents the plots as the boundaries of the profiles of each shape parameter.

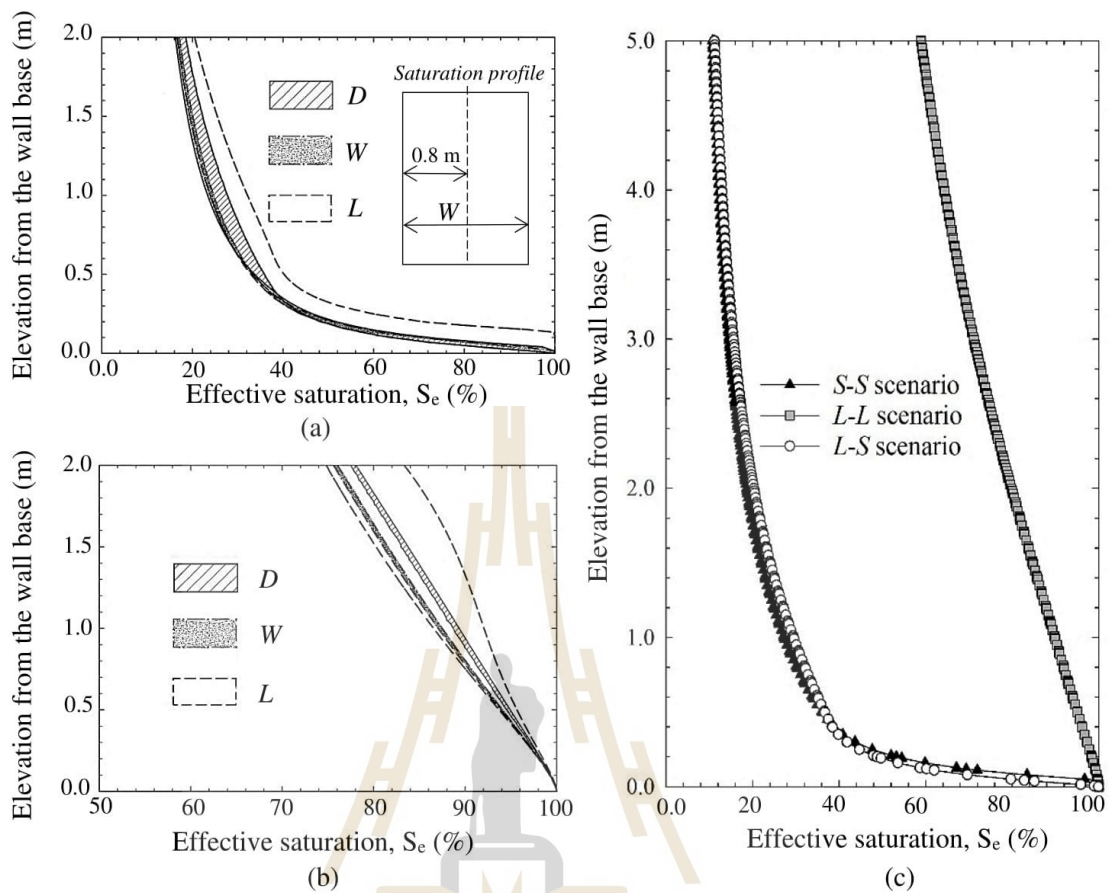


Figure 3.9 Water saturation profile subjected to variation of D , W , L shape parameter in (a) S - S and L - S scenarios, (b) L - L scenario and (c) for H shape parameter in 3 scenarios as S - S , L - L and L - S .

Wider boundaries indicate a greater influence of the corresponding shape parameter on the water saturation profile. As shown by the boundary plots in **Figure 3.9**, the influence of all shape parameters on the water saturation profile is in accordance with the influence on h_o . The boundary width of water saturation profiles for shape parameter L is larger than it is for the other shape parameters. The water saturation profiles for shape parameter H are plotted as three single lines, one line for each scenario. There is little deviation between the water saturation profiles for S - S and L - S

scenarios, in which the backfill soil was identical. This similarity indicates that the water saturation profile was mainly governed by the WRC of the corresponding soil.

3.6 Geocomposite drain properties

The transmissivity of the geonet (T_{net}) is widely accepted as a crucial property for drainage purposes (Gallichand et al. 1992; Clement et al. 1996; Koerner and Soong et al. 2005; Giroud et al. 2000; Bourges-Gastaud et al. 2013; Yarahmadi et al. 2017). In Plaxis, the magnitude of T_{net} must be prescribed through the geonet thickness (t_{net}) and its permeability (k_{net}). A series of numerical simulations was produced to investigate the individual effects of t_{net} and k_{net} on seepage responses, including the highest water level in the protected zone (h_o), and the water saturation profile inside the protected zone. The t_{net} and k_{net} were varied at 10 mm and 20 mm and 0.8 m/sec and 0.008 m/sec, respectively (Table 3.3).

Figure 3.10 presents variation of water saturation profile with t_{net} for three studied scenarios having k_{net} of 0.8 m/sec. The profiles were plotted along a vertical section at 0.8 m apart from the drainage interface inside the protected zone. In general, varying t_{net} had very little effect on the water saturation profile. The water saturation profile in the protected zone mainly depended on the soil type prescribed. Since the soil type in the protected zone in *S-S* and *L-S* scenarios was sandy soil, and in *L-L* scenario, lateritic soil, the water saturation profiles of *S-S* and *L-S* scenarios differed significantly from the profiles of *L-L* scenario.

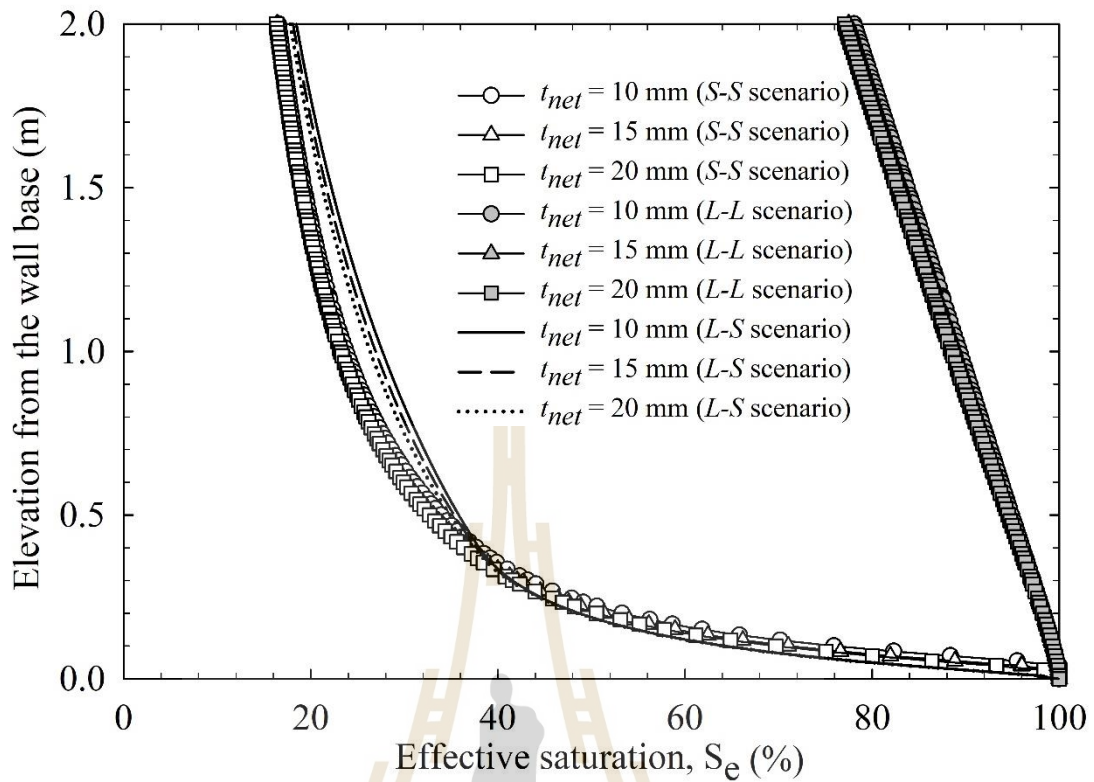


Figure 3.10 Water saturation profile subjected to variation of geonet thickness (t_{net}) in *S-S*, *L-L* and *L-S* scenarios.

Furthermore, **Figure 3.10** also shows little difference in the water saturation profiles of *S-S* and *L-S* scenarios. In *S-S* scenario, water saturation in the lower part of the protected zone was greater than in *L-S* scenario because the phreatic level inside the protected zone in *S-S* scenario was higher than in *L-S* scenario (**Figure 3.5a**). However, in the upper part of the protected zone, water saturation was higher in *L-S* scenario than in *S-S* scenario.

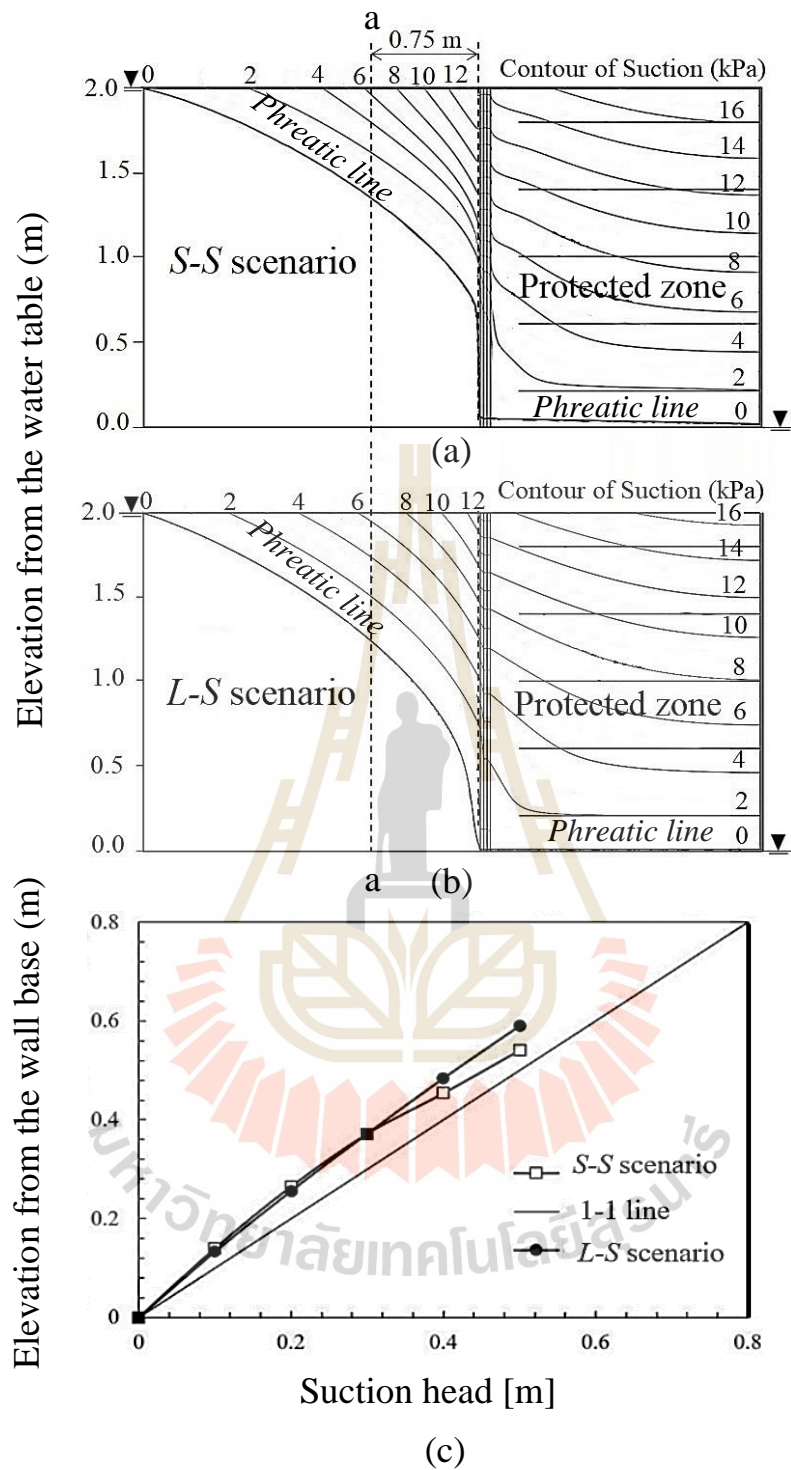


Figure 3.11 Suction profiles for (a) *S-S* scenario, (b) *L-S* scenario, and (c) variation of suction with elevation above water table along vertical section *a-a* located at 0.75 m right apart from the drainage interface.

Figure 3.11a and 3.11b present suction profiles over the domains in question for *S-S* and *L-S* scenarios, respectively. The variation of suction with elevation above water table along a vertical section *a-a* located at 0.75 m right apart from the drainage interface is shown in **Figure 3.11c**. Since the water flow directed inclined downward to the downstream side, the variation of suction with elevation above water table deviated from 1:1 line to the left (Bear 1972). **Figure 3.12** plots the *k*-function curves of the geotextile and the native soil. The suction at the place where water started penetrating the geocomposite in both scenarios was read from the point where plots of *k*-functions intersected. The suction values at the intersection of *k*-functions are about 1 kPa and 3 kPa in *S-S* and *L-S* scenarios, respectively. Water saturation in the upper part of the protected zone was higher in *L-S* scenario than in *S-S* scenario because, in *L-S* scenario, water started to penetrate the geocomposite at a higher elevation (ref. **Fig. 12a and 12b**).

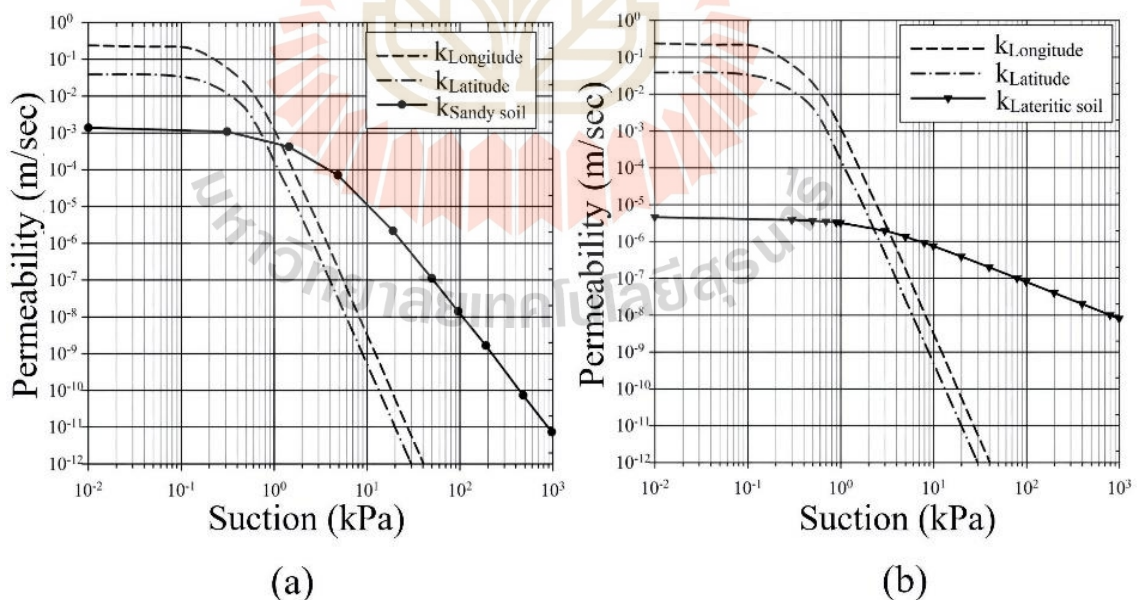


Figure 3.12 *k*-functions of the geotextile and native soil for (a) *S-S* scenario and (b) *L-S* scenario.

Figure 3.13 presents the effects of t_{net} and k_{net} on h_o in the three studied scenarios. Increasing t_{net} and/or k_{net} produced a fall in h_o due to the increased capacity of the drainage channel. The h_o axis was plotted in log scale for sake of ease comparison. For each k_{net} , the ratio of h_o for the lowest t_{net} to h_o for the highest t_{net} value is indicated as number appeared on the corresponding line. The drop of h_o ratio with increasing t_{net} is greater for the higher k_{net} , which means that reduction of h_o by enlarging geonet thickness is more effective in the higher geonet permeability.

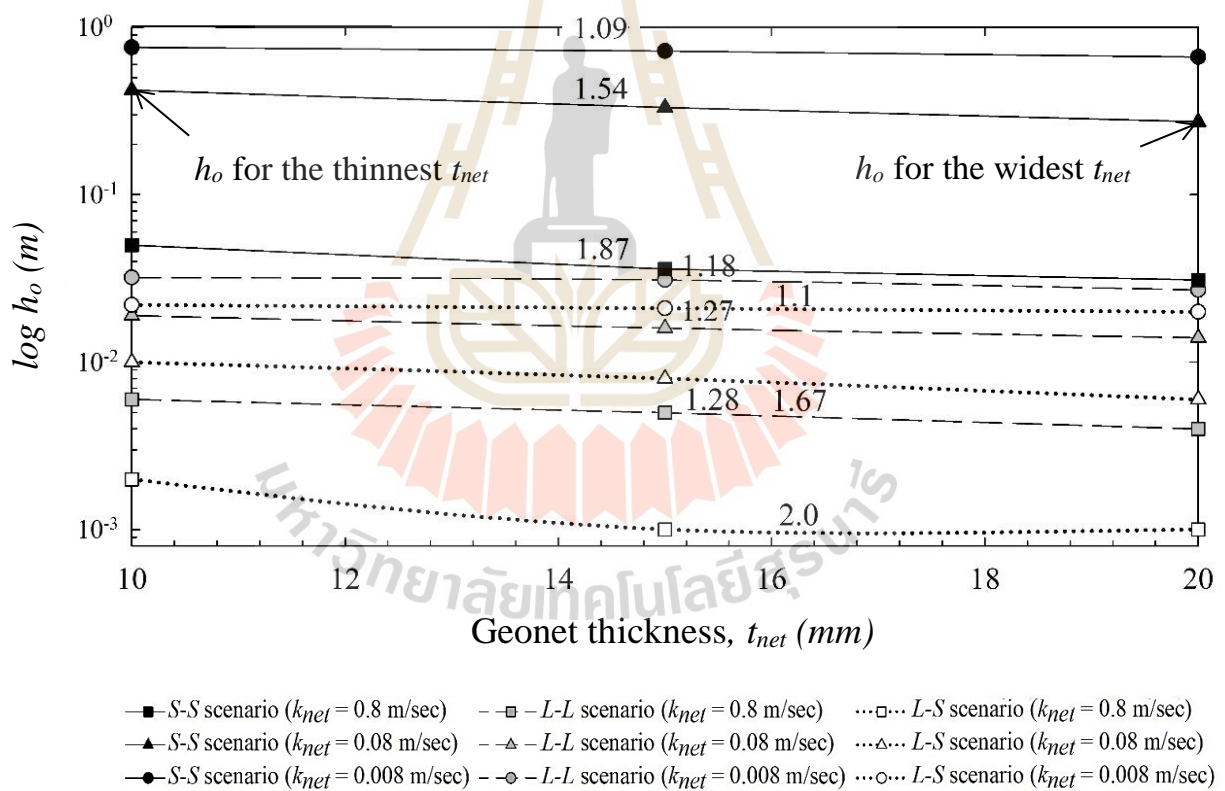


Figure 3.13 Variation of h_o subjected to the effect geonet thickness (t_{net}) and geonet permeability in S-S, L-L, L-S scenarios (The number appeared on the corresponding line is ratio of h_o for the lowest t_{net} to h_o for the highest t_{net}).

3.7 Conclusions

This article investigated the influence of relevant shape parameters on seepage responses, including the highest water level in the protected (h_o) and the water saturation in the protected zone, in an MSE wall with a geocomposite back drain. Other than the relevant shape parameters, the influence of geonet transmissivity, which is a main component of geocomposite drainage systems, was also investigated. The following conclusions were drawn from this study.

- Where distance from the upstream water to the drainage face (L) is short, this shape parameter (L) plays a significant role in the seepage responses in the MSE wall. Accordingly, involved engineers must pay close attention to the phreatic level in the protected zone when dealing with an MSE wall in a mountainous area, where the distance from upstream water to the drainage face might be very short (**Fig. 3.5**).
- The height of the wall (H) and the width of protected zone (W) play no to negligible role to the magnitude of h_o . Whereas, the vertical distance from the wall base to impervious boundary (D) also plays no role to the magnitude of h_o whenever the contribution upstream water source does not change (**Fig. 3.8**). This conclusion is based on an assumption that the geocomposite does not exceed its drainage capacity.
- Water saturation in the protected zone mainly depended on the water retention curve of the soil used as fill material (**Fig. 3.9 and 3.10**).
- Although distribution of water saturation in the protected zone mainly depends on the properties of backfill material, the k-function of the soil at the upstream

side might play little role to the water distribution in the protected zone particularly at the upper elevation. This conclusion is based on k-function plots of upstream soils and geotextile (**Figure 3.10 - 3.12**).

- The permeability of the upstream soil is important properties contributes to the h_o level. The difference between permeability of the drainage material and that of the upstream soil governs the h_o value (**Figure 3.6**). Furthermore, the permeability coefficient of the soil on the upstream side governs the rate at which h_o falls with increments of geonet transmissivity.

3.8 References

- Albino, U.D.R., Portelinha, F.H.M., Zornberg, J.G., Futai, M.M., 2019. **Numerical simulation of infiltration into the fill of a wall reinforced with nonwoven geotextiles.** *Computers and Geotechnics*. 108, 27-39.
- Bear, J., 1972. **Dynamics of fluids in porous media.** Dover, New York.
- Berg, R., Christopher, B.R., Samtani, N., 2009. **Design of Mechanically Stabilized Earth Walls and Reinforced Soil Slopes**, Vol. 1. Report No. FHWA-NHI-10-024, Federal Highway Administration
- Bourges-Gastaud, S., Blond, E., Touze-Foltz, N., 2013. **Multiscale transmissivity study of drain-tube planar geocomposite: effect of experimental device on test representativeness.** *Geosynthetics International*. 20(3), 119-128.
- Bui Van, D., Chinkulkijniwat, A., Horpibulsuk, S., Yubonchit, S., Limrat, I., Arulrajah, A. and Jothityangkoon, C., 2017. **Steady flow in mechanically stabilised earth walls using marginal soils with geocomposite.** *Geosynthetics International*. 24(6), 590-606.

- Chinkulkijniwat, A., Horpibulsuk, S., Bui Van, D., Udomchai, A., Goodary, R., Arulrajah, A., 2017. **Influential factors affecting drainage design considerations for mechanical stabilised earth walls using geocomposite.** *Geosynthetics International*. 24(3), 224-241.
- Christopher, B., Zornberg, J., Mitchell, J., 1998. **Design Guidance for Reinforced Soil Structures with Marginal Soil Backfills.** *Proceedings of the Sixth International Conference on Geosynthetics, Atlanta, Georgia, 2 March*, 797-804.
- Clement, T. P., Wise, W. R., Molz, F. J., & Wen, M., 1996. **A comparison of modeling approaches for steady-state unconfined flow.** *Journal of Hydrology*. 181(1-4), 189-209.
- Dickinson, S., Brachman, R.W.I., & Rowe, R.K., 2010. **Thickness and Hydraulic Performance of Geosynthetic Clay Liners Overlying a Geonet.** *Journal of Geotechnical and Geoenvironmental Engineering*. 136(4), 552-561.
- Escario, V., and Saez, J. 1986. **The shear strength of partly saturated soils.** *Geotechnique*, 36(3), 453-456.
- Fredlund, D. G., Morgenstern, N. R., and Widger, R. A. 1978. **Shear strength of unsaturated soils.** *Canadian Geotechnical Journal*, 15(3), 313–321.
- Gallichand, J., Marcotte, D., & Prasher, S. O., 1992. **Including Uncertainty of Hydraulic Conductivity into Drainage Design.** *Journal of Irrigation and Drainage Engineering*. 118(5), 744-756.
- Giroud, J.P., Zornberg, J.J., Zhao, A., 2000. **Hydraulic Design of Geosynthetic and Granular Liquid Collection Layers.** *Geosynthetics International*. 7(4-6), 285-380.

- Giroud, J. P., & Kavazanjian, E., 2014. **Degree of Turbulence of Flow in Geosynthetic and Granular Drains.** *Journal of Geotechnical and Geoenvironmental Engineering.* 140(5), 06014001.
- Iryo, T., Rowe, R., 2004. **Numerical Study of Infiltration Into a Soil–Geotextile Column.** *Geosynthetics International.* 11(5), 377-389.
- Kibria, G., Hossain, M. S., & Khan, M. S. 2014. **Influence of Soil Reinforcement on Horizontal Displacement of MSE Wall.** *International Journal of Geomechanics,* 14(1), 130–141.
- Koerner, R.M., Soong, Koerner, G.R., 2005. **Back Drainage Design and Geocomposite Drainage Materials.** Proc., *GRI-19 Conference,* 51-86.
- Koerner, R.M., Koerner, G.R., 2011. **The Importance of Drainage Control for Geosynthetic Reinforced Mechanically Stabilized Earth Walls.** *Journal of Geoengineering.* 6(1), 3-13.
- Koerner, R.M., Koerner, G.R., 2013. **A data base, statistics and recommendations regarding 171 failed geosynthetic reinforced mechanically stabilized earth (MSE) walls.** *Geotextiles and Geomembranes.* 40, 20-27.
- Koerner, R. M., & Koerner, G. R. 2015. **Lessons learned from geotextile filter failures under challenging field conditions.** *Geotextiles and Geomembranes.* 43(3), 272-281.
- Koerner, R. M., & Koerner, G. R. 2018. **An extended data base and recommendations regarding 320 failed geosynthetic reinforced mechanically stabilized earth (MSE) walls.** *Geotextiles and Geomembranes,* 46(6), 904-912.

- McKean, J., Inouye, K., 2001. **Field Evaluation of the long-term Performance of Geocomposite Sheet Drains.** *Geotextiles and Geomembranes*. 19(4), 213-234.
- Mitchell, J. and Zornberg, J.G 1995. **Reinforced Soil Structures with Poorly Draining Backfills Part II: Case Histories and Applications.** *Geosynthetics International*. 2(1), 265-307.
- Mualem, Y., 1976. **A new model for predicting the hydraulic conductivity of unsaturated porous media.** *Water Resources Research*. 12(3), 513-522.
- Robinson, J. D., Vahedifard, F., and AghaKouchak, A., 2017. **Rainfall triggered slope instabilities under a changing climate: Comparative study using historical and projected precipitation extremes.** *Canadian Geotechnical Journal*. 54(1), 117-127.
- Roy, D., & Singh, R. 2008. **Mechanically Stabilized Earth Wall Failure at Two Soft and Sensitive Soil Sites.** *Journal of Performance of Constructed Facilities*, 22(6), 373–380.
- Saeedpanah, I., Jabbari, E., & Shayanfar, M. A., 2011. **Numerical simulation of ground water flow via a new approach to the local radial point interpolation meshless method.** *International Journal of Computational Fluid Dynamics*. 25(1), 17-30.
- Santos, E.C.G., Vilar, O.M., Palmeria, E.M., (2010). **The use of recycled construction and demolition waste in geosynthetic reinforced structures: Influence of the re-cycling process.** Proc. 6th International Conference on Environmental Geotechnics - 6ICEG, New Delhi.

- Stuedlein, A. W., Allen, T. M., Holtz, R. D., & Christopher, B. R. (2012). **Assessment of Reinforcement Strains in Very Tall Mechanically Stabilized Earth Walls.** *Journal of Geotechnical and Geoenvironmental Engineering*, 138(3), 345–356.
- Thuo, J.N., Yang, K.H., Huang, C.C., 2015. **Infiltration into unsaturated reinforced slopes with nonwoven geotextile drains sandwiched in sand layers.** *Geosynthetics International*. 22(6), 457-474.
- Vahedifard, F., Tehrani, F.S., Galavi, V., Ragno, E., AghaKouchak, A., 2017. **Resilience of MSE Walls with Marginal Backfill under a Changing Climate: Quantitative Assessment for Extreme Precipitation Events.** *Geotechnical and Geoenvironmental Engineering*. 143(9), 04017056.
- Valentine, R.J., 2013. **An assessment of the factors that contribute to the poor performance of geosynthetics-reinforced earth retaining wall.** Proc., Int. Symp. on Design and Practice of Geosynthetic-reinforced Soil Structures, H. I. Ling, et al. eds., DEStech Publication, Inc., Lancaster, USA, 318-327.
- van-Genuchten, 1980. **A closed-form Equation for Predicting the Hydraulic Conductivity of Unsaturated Soils.** *Soil science society of America journal*. 44(5), 892-898.
- Xu, Y.S., Shen, S.L., Ma, L., Sun, W.J., & Yin, Z.Y., 2014. **Evaluation of the blocking effect of retaining walls on groundwater seepage in aquifers with different insertion depths.** *Engineering Geology*. 183, 254-264.

- Yarahmadi, N., Gratchev, I., Jeng, D.S., Gibbs, D., 2017. **Effect of Thickness Reduction on Hydraulic Transmissivity of Geonets used in Leachate Collection Systems in Landfills.** *The 19th Southeast Asian Geotechnical Conference and 2nd AGSSEA Conference, Kuala Lumpur, Malaysia.*
- Yoo, C., Jung, H.Y., 2006. **Case history of Geosynthetic Reinforced Segmental Retaining Wall Failure.** *Journal of Geotechnical and Geoenvironmental Engineering.* 132(12), 1538-1548.
- Zhang, C., Chen, X, Fan, W., 2015. **Overturning Stability of a Rigid Retaining Wall for Foundation Pits in Unsaturated Soils.** *International Journal of Geomechanics*, doi.org/10.1061/(ASCE)GM.1943-5622.0000613.
- Zornberg, J.G., Mitchell, J., 1994. **Reinforced soil structures with poorly draining backfills. Part I: Reinforcement interactions and functions.** *Geosynthetics International.* 1(2), 103-147.
- Zornberg, J.G., Barrows, R.J., Christopher, B.R., and Mitchell, J.K., 1995. **Constructing a Geotextile-Reinforced Slope.** *Geotechnical Fabrics Report.* 13(7), 26-28.

CHAPTER IV

GROUNDWATER ESTIMATION IN MSE WALL WITH GEOCOMPOSITE BACK DRAINAGE: LINEAR ASSOCIATION ANALYSIS

4.1 State of problem

Nowadays, many kinds of failures happened in mechanical stabilized earth (MSE) wall with back drainage system during long term rainfall. MSE wall failure cases have been mentioned detail in many reports (Koerner et al. 2015, Koerner et al. 2018, Yoo et al. 2006). Through the maximum level changes of phreatic surface in the protected zone of MSE wall, h_o , reflects the effectiveness of the drainage system and also suitability selection of soil backfill and native in practical works. There are number of literatures reported influence variables that affect the magnitude of h_o (Chinkulkijniwat et al. 2017, Bui Van et al. 2017). However, very few of the previous attempts reported influence of MSE wall dimensions on the variation of phreatic surface in the protected zone. Also, few researches did not integrate and quantify well the rise of h_o with all influenced factors that lead uncomprehensive research for practical wall design.

One of highlight finding from previous reports as La Duong et al 2020 emphasized that there were many factors influence to the h_o variation such as soil hydrological properties, drainage properties, and the wall dimensions mentioned. Their research drawn a significant correlation existed as linear association between the rate

of fall in h_o with geonet transmissivity (T_{net}) and proposed a linear equation with highly coefficient of determination (R^2) greater than 0.96. On the other hand, via their report, permeability coefficient of the soil on the upstream side governs the rate at which h_o falls with increments of T_{net} , and the linear line slope ratio by 36:1 proves not much different from permeability coefficient ratio by 49:1. Nonetheless, their research limited calibrating h_o rise by using wide range of soil permeability for MSE wall backfill and native.

Based on above statements, by numerical simulation, this study desires to estimate the linear association rise of h_o comprehensively with geonet transmissivity (T_{net}) in successor from research of La Duong et al 2020. Moreover, other relevant influenced factors are focused and integrated in final linear analysis especially for proposing mathematic equation. The wide extension of soil permeability range, for representative for each soil type in practical, is successful picked from previous reports (Konukcu et al. 2004, Szymkiewicz et al. 2015, Acharya et al 2012). Selected influenced factors to h_o for linear analysis in this study comprise the geonet transmissivity (T_{net}) in presentative for geocomposite drainage properties; MSE wall dimension as distance from the upstream water level to the drainage face (L); native and backfill soil permeability (k).

The linear model provides an ease for practical via linear equation uses. Good linear estimation of h_o in relevant relationships is, therefore, vital for the best design of MSE wall against failure. Conceptual numerical input data were based on 180 Plaxis-2D experiments conducted.

4.2 Methods and materials

4.2.1 Research methodology

Throughout this thesis, a steady flow mode was selected to calculate the final groundwater states due to elevated upstream water. Steady-state flow conditions were focused in this to quantify the final state of ground flow in MSE wall. All values of h_o was extracted from the numerical experiment in PLAXIS-2D in using to analyze linear correlation existed among other relevant influenced factors. A series of 180 numerical simulations was produced to investigate correlation of geonet transmissivity (T_{net}), soil permeability (k) and L shape parameter, to rise of h_o . Geonet transmissivity was controlled by geonet thickness (t_{net}) and geonet permeability (k_{net}) as written in Equation 4.1.

$$T_{net} = k_{net} \times t_{net} \quad (4.1)$$

where T_{net} is geonet transmissivity (m²/sec), t_{net} is geonet thickness (m) and k_{net} is geonet permeability (m/sec).

Soil-water model is based on van Genuchten model (Equation 4.2a) (van Genuchten 1980) and van Genuchten - Mualem model (Equation 4.2b) for all studied materials (Mualem 1976); as following equations:

$$S_e = \frac{S - S_{res}}{S_{sat} - S_{res}} = \frac{\theta - \theta_{res}}{\theta_{sat} - \theta_{res}} = \left[1 + (\alpha |h_p|)^n \right]^{-m} \quad (4.2a)$$

$$k_r(S_e) = S_e^{0.5} [1 - (1 - S_e^{1/m})^m]^2 \quad (4.2b)$$

In which, S_e is effective degree of saturation, S is degree of saturation, S_{res} is residual saturation at very high values of suction, S_{sat} is the degree of saturation at saturated state, h_p is matric suction head, and k_r is the relative permeability coefficient: α [m^{-1}] and n are fitting parameters which represent respectively the air-entry value of the soil and the rate of water extraction from the soil once the air entry value has been exceeded: m

4.2.2 Simulation set up for linear association analysis

This study used successful calibrated MSE wall model in previous research of La Duong et al. 2020 for linear analysis of h_o . The VG parameter of studied materials are shown in **Table 4.1** and scenarios for all numerical simulation cases in **Table 4.2**. Accordingly, influence of the wall geometry variables; including upstream water level H_w , length from upstream water to the drainage face (L), protected zone width (W), distance from the wall base to the impervious boundary (D), on the variation of h_o were investigated through a set of numerical experiment in Plaxis environment (Plaxis-2D 2018) depicted in **Figure 3.4**.

According to reports of Bui Van et al. 2017, Chinkulkijniwat et al. 2017 and La Duong et al. 2020, they emphasized the high effects of soil permeability (k) and geonet transmissivity (T_{net}) to the level of phreatic surface in the protected zone. Therefore, k_{soil} and T_{net} were included in this study among other influence factors. It is noteworthy that this model was well calibrated in Chinkulkijniwat et al 2017. VG parameters of all studied materials prescribed in this model are presented in **Table 4.1**.

Table 4.1 Relevant VG model parameters of studied materials.

Material	Symbol	Permeability (m/sec)	α (m^{-1})	n (-)	S_{sat} (-)	S_{res} (-)
Coarse sand	<i>CS</i>	1.3×10^{-3}	49.36	1.53	1.0	0.002
Sandy soil	<i>S</i>	1.97×10^{-4}	20	1.5	1.0	0.03
Clayey sand	<i>CLS</i>	4.1×10^{-5}	12.4	2.28	1.0	0.14
Lateritic soil	<i>L</i>	4.0×10^{-6}	0.8	1.4	1.0	0.03
Clay	<i>CL</i>	5.56×10^{-7}	0.08	8.0×10^{-5}	0.74	0.12
Geotextile	-	0.023 (0.0037) ^a	20	2.5	0.8	0.03
Geonet	-	0.8	600	40	1.0	0.0

^a Permeability of geotextile in lateral direction.

The set up for soil at native and backfill soil were identical assigned for each specific soils. The foundation soil below MSE wall and geocomposite system was considered as native soil or surrounded soil behind the protected area. Five kinds of soil permeability following as coarse sand (Konukcu et al. 2004), sandy soil (Chinkulkijniwat et al. 2017) and clayey sand (Szymkiewicz et al 2015), lateritic soil (Bui Van et al. 2017) and clay (Acharya et al 2012).

Accordingly, for wall dimension set up in this study, constant values was fixed for wall height (H) was fixed at 2.0 m; distance from the wall base to the impervious boundary (D) at 0.8 m; Protected zone width (W) at 1.6 m for all simulation cases. Due to significant effect for h_o mentioned on previous research of (Chinkulkijniwat et al. 2017, Bui Van et al. 2017, La Duong et al. 2020), this research varied the values of (L) shape parameter in range mentioned in **Table 4.2**. The assigned hydrological properties of

geonet as thickness (t_{net}), permeability (k_{net}) and transmissivity (T_{net}) are shown in **Table**

4.2.

Table 4.2 180 PLAXIS-2D simulation cases set up in this studied.

Scenario	Native soil	Backfill soil
CS-CS	Coarse sand	Coarse sand
S-S	Sandy soil	Sandy soil
CLS-CLS	Clayey sand	Clayey sand
L-L	Lateritic soil	Lateritic soil
CL-CL	Clay	Clay
Varied parameter	Definition	Varied value
W (m)	Protected zone width	1.6
L (m)	Length from upstream water to the drainage face	2.0, 3.0, 4.0, 5.0
H (m)	MSE wall height	2.0
D (m)	Distance from the wall base to impervious boundary	0.8
t_{net} (mm)	Geonet thickness	10, 15, 20
k_{net} (m/sec)	Geonet permeability	0.8, 0.08, 0.008

Upstream water level (H_w) is kept as constant 2.0 for all simulation cases

4.3 Results

4.3.1 Estimating h_o against geonet transmissivity (T_{net})

The drop of h_o ratio with increasing t_{net} is greater for the higher k_{net} , which means that reduction of h_o by enlarging geonet thickness is more effective in the higher geonet permeability. From those numerical data set were further employed to investigate the relationship between h_o and geonet transmissivity (T_{net}) in this chapter

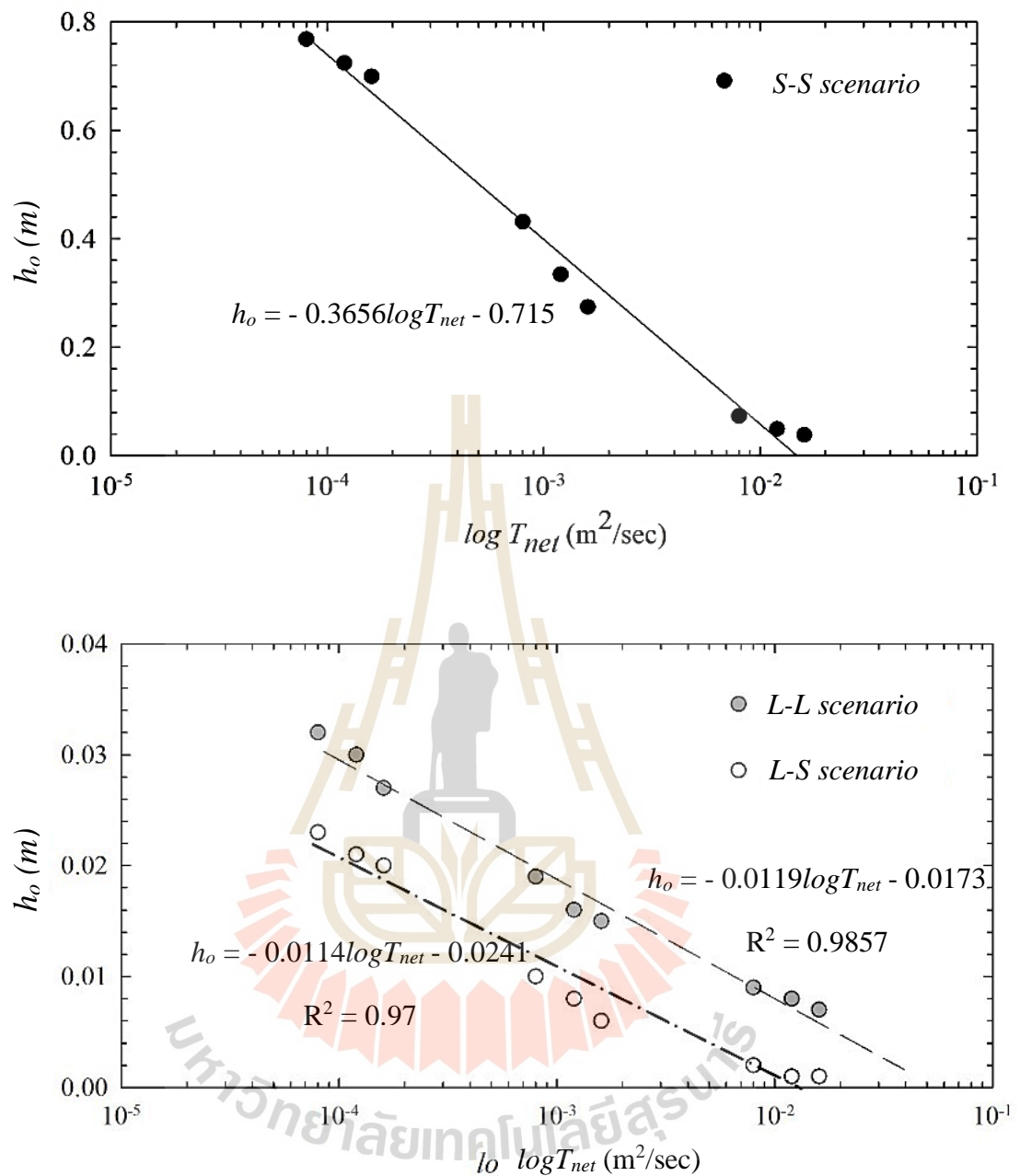


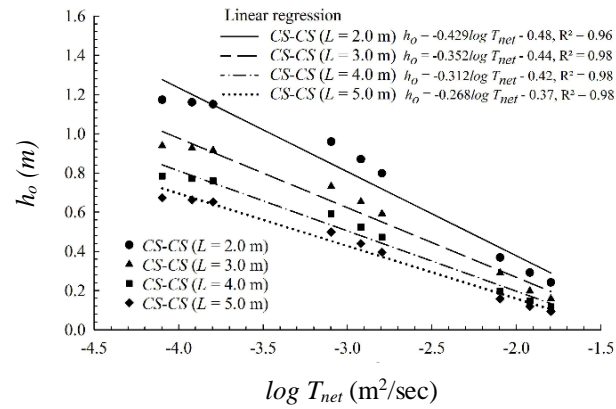
Figure 4.1 Linear relationship between h_o and $\log T_{net}$ for all 27 cases conducted in the second part of the numerical experiment.

as plotted in **Figure 4.1**. **Figure 4.1** shows the variation of h_o against geonet transmissivity (T_{net}) in semi-log scale for the three studied scenarios.

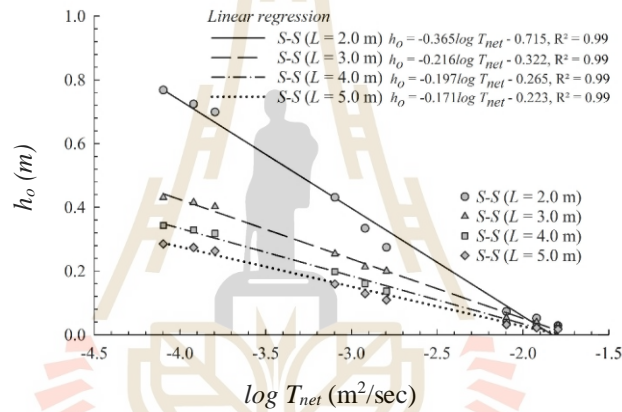
A linear relationship existed between h_o and $\log T_{net}$ that was represented with a coefficient of determination (R^2) greater than 0.96. The gradients of the linear plots were equal to 0.36 in *S-S* scenario and 0.01 in *L-L* and *L-S* scenarios. The identical gradients in *L-L* and *L-S* scenarios indicate that the fall in h_o with increments of $\log T_{net}$ was mainly governed by the soil type on the upstream side.

Since the gradient in *S-S* scenario was 36 times steeper than in *L-L* and *L-S* scenarios and the permeability coefficient of the upstream soil in *S-S* scenario was 49 times the permeability coefficient in *L-L* and *L-S* scenarios, taking into account the very wide range of the permeability coefficients ($1.0 - 10^{-12}$ m/sec), the gradient ratio of 36:1 is not very different from the permeability coefficient ratio of 49:1. The conclusion was drawn that a significant correlation existed between the rate of fall in h_o with $\ln T_{net}$ and the permeability coefficient of the upstream soil.

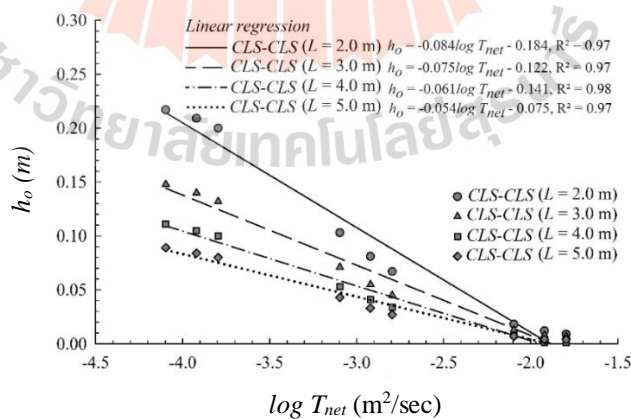
The variables T_{net} was transformed to $\log T_{net}$ for the best sake of linear association analysis. Two parameters comprise gradient or slope (S) and intercept (I) were identified through linear approach for h_o variation for all simulations. Those parameters are presentative for effect of geonet transmissivity (T_{net}), soil permeability as well as L shape parameter in investigating the tendency and approximation for h_o variation in practical. This research conducted total by 180 simulation experiments.



(a)

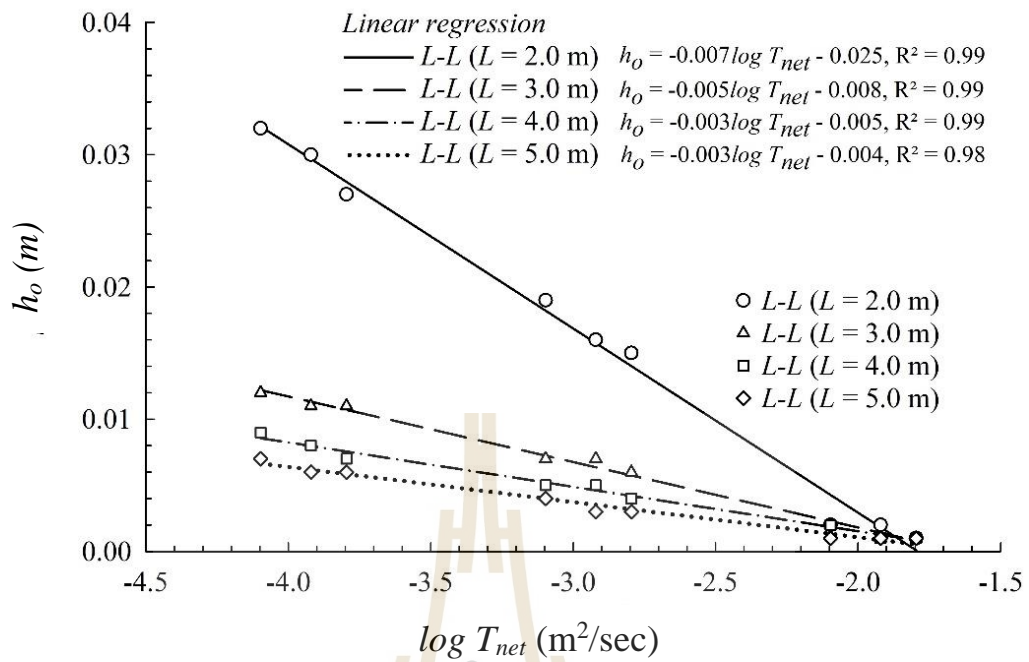


(b)

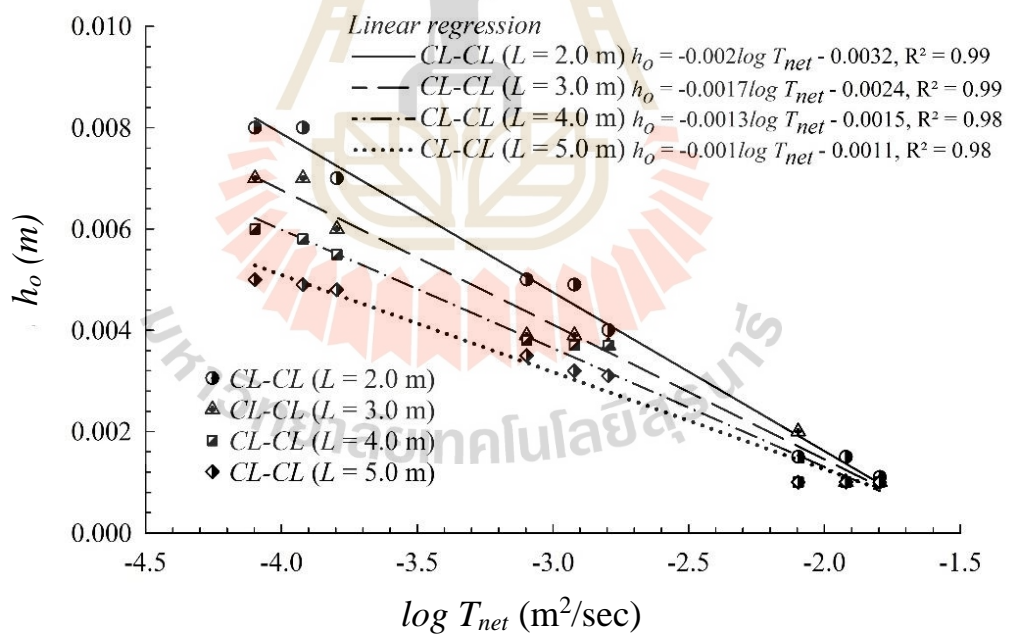


(c)

Figure 4.2 Linear relationship of h_o subject to $\log T_{net}$ and L shape parameter for (a) coarse sand, (b) sandy soil and (c) clayey sand.



(a)



(b)

Figure 4.3 Linear relationship of h_o subject to $\log T_{net}$ and L shape parameter for (a) lateritic soil and (b) clay.

A series of concept Plaxis simulation results for linear approximation of h_o against $\log T_{net}$ subjected to the increase of L shape parameter for coarse sand, sandy soil and clayey sand respectively shown in **Figure 4.2a, 4.2b and 4.2c**; and lateritic soil, clay shown in **Figure 4.3a and 4.3b**.

According linear line and equation for simulation cases, all simulation cases reflect themselves best fit with linear association via high R^2 by more than 0.96. Also, the extension of L shape parameter leads more drops of h_o that consistency with statements in previous research of (La Duong et al. 2020). These drops of h_o are under effected by the increase of $\log T_{net}$ or the increase of geonet transmissivity due to much amount of water is able to penetrate the drainage interface. The obviously change of h_o are easier been seen in case with high permeable soil types ($k = 10^{-3} - 10^{-5}$ m/sec).

4.3.2 Linear slope (S) and intercept (I) for h_o estimation

The slope S and intercept I **Figure 4.4a** and **Figure 4.4b** for each linear line reflects varied magnitude and developed direction of h_o to other relevant parameters. Their changes also indicate, for each soil permeability k , not identical and strongly reduce when extending L shape parameter. Based on behaviors of S and I , this study continues plotting more results for investigating those relations. **Figure 4.4a** and **Figure 4.4b** indicate the linear behavior of S and I in logarithm scale against to variations of L shape parameter. The absolute format of S and I is set absolute value for all cases. Along with increase of L , the changes of $\log |S|$ and $\log |I|$ for each linear line in **Figure 4.2** and **Figure 4.3**, respectively, appears identically downward for each assigned soil type and parallel in comparing all, R^2 value of linear equations greater than 0.98 (**Figure 4.4a and 4.4b**).

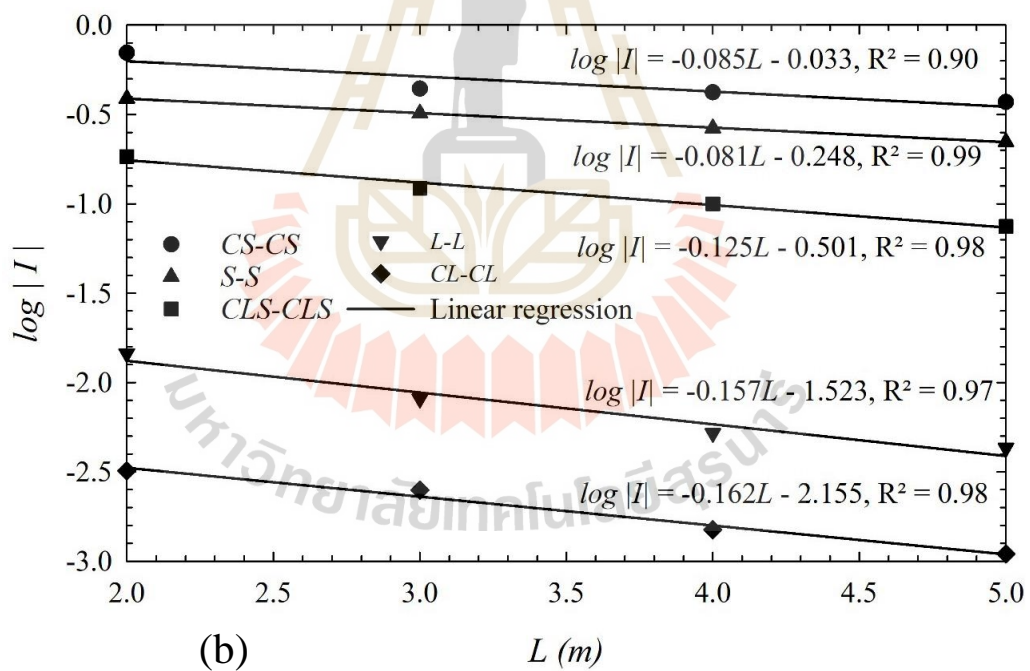
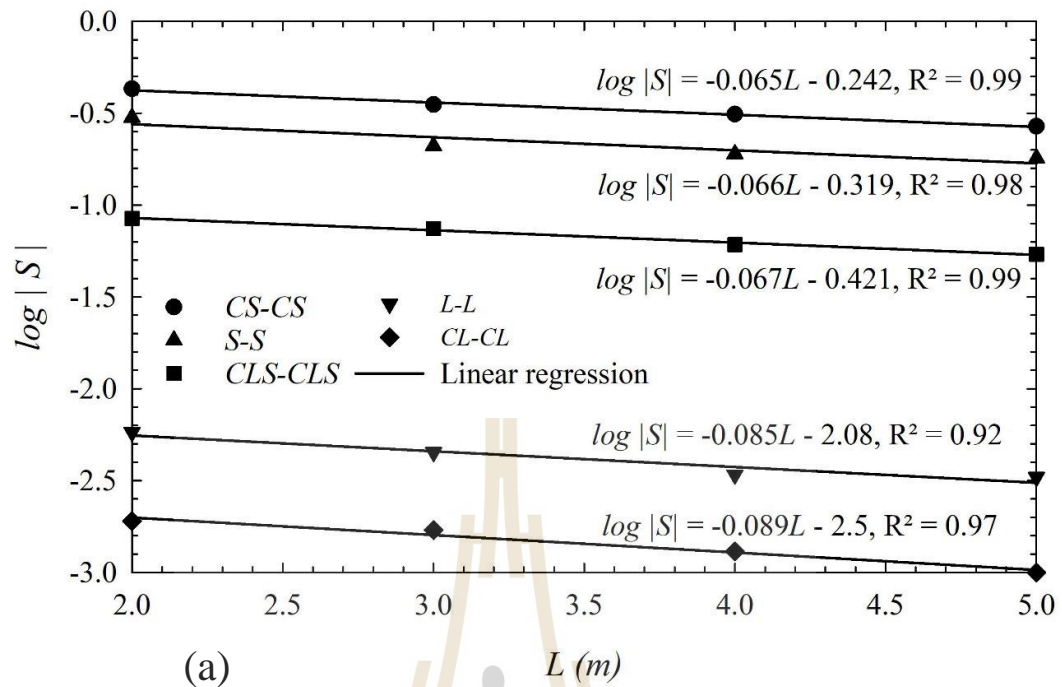


Figure 4.4 Linear relationship of (a) $\log |S|$ and (b) $\log |I|$ subjected to L shape parameter.

In order to expand linear association, normalized results of S and I as with studied soil permeabilities k defined as $\log S/k$ and $\log I/2k$, perspective, was investigated and indicated in **Figure 4.5a and 4.5b** with linear equation (Equation 4.3) and (Equation 4.4). The linear analysis shows little differences among variation of them and highly R^2 by more than 0.9. By appropriate normalized S and I with soil permeability (k) against $\log L$ shape parameter, accuracy for estimating h_o in relationship among other relevant factors strongly fitting to linear association.

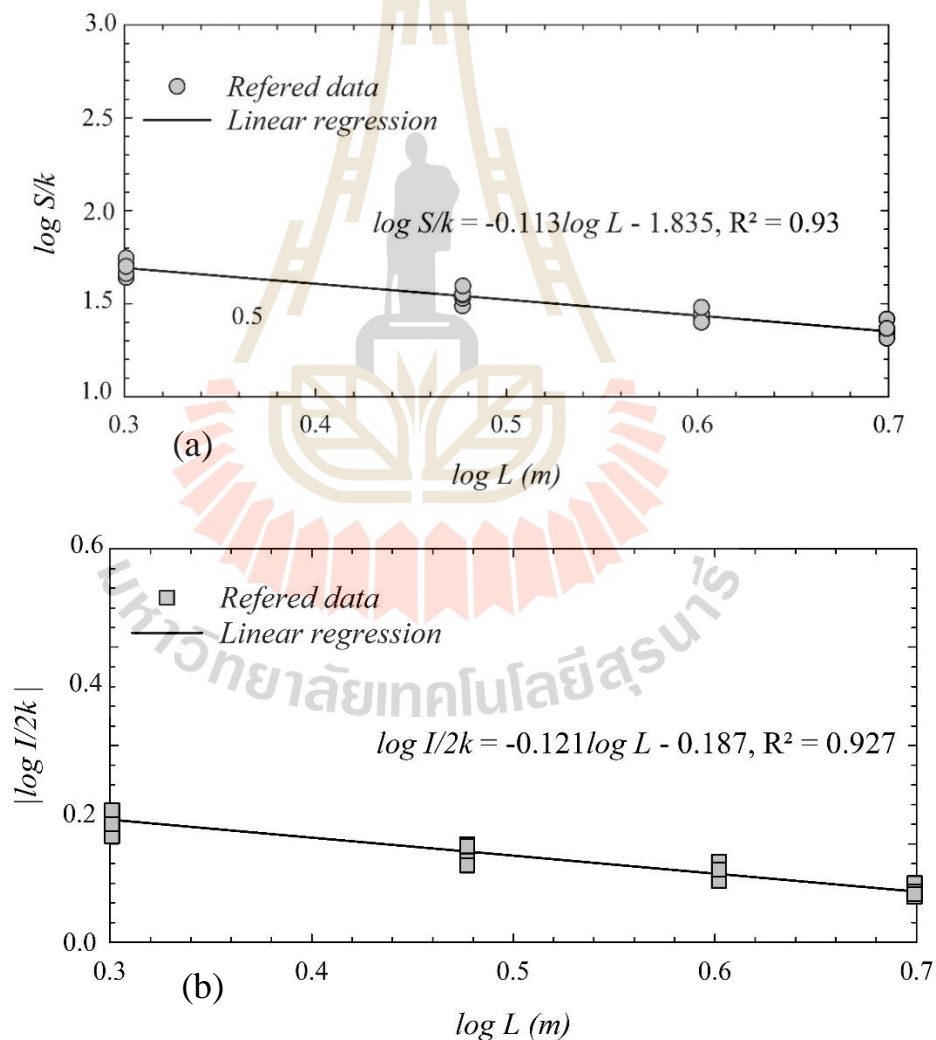


Figure 4.5 Linear relationship of (a) $\log S/k$ and (b) $\log I/2k$ subjected to $\log L$ shape parameter.

The integration of slope S and intercept I in Equation 4.3 and Equation 4.4 to linear equation for h_o rise in relationship with geonet transmissivity (T_{net}) from research of La Duong et al. 2020 (Refer. **Figure 4.1**) as modified linear equation Equation 4.5.

$$\log (S/k) = -0.113 \log L - 1.835 \quad R^2 = 0.93 \quad (4.3)$$

$$\log (I/2k) = -0.121 \log L - 0.187 \quad R^2 = 0.923 \quad (4.4)$$

4.3.3 Linear equation establishing for h_o

The proposed linear equation between h_o and geonet transmissivity (T_{net}) in **Figure 4.1** and also mentioned in their study that the increment of T_{net} lead mainly to the fast drop of h_o . The trendy variation h_o always moves in opposite way of T_{net} varying. This thesis based on above statement and express mathematical format for integrating linear relationship among h_o and more other relevant factors such as soil permeability and MSE wall dimension, as following:

$$h_o = -|S| \log T_{net} - |I| \quad (4.5)$$

where, S is developed gradient of linear line, I is intercept at y – axis of linear line. In term to consistent with Equation 4.5, in order to ensuring the Equation 4.3 as following format linking to the effect of geonet transmissivity to rise of h_o . The conversion of the mathematic form indicated in Equation 4.3 and 4.4, respectively, in to Equation 4.6 and 4.7.

$$|\log (S/k) | = 0.113 \log L + 1.835 \quad R^2 = 0.93 \quad (4.6)$$

$$|\log (I/2k)| = 0.121 \log L + 0.187 \quad R^2 = 0.923 \quad (4.7)$$

The ultimate equation for h_o estimation for groundwater estimation via values of h_o in MSE wall with geocomposite back drainage is created from mathematic deliver component equations as following in Equation 4.8.

$$h_o = -(10^{0.113 \log L + 1.853 + \log k}) \log T_{net} + (10^{0.121 \log L + 0.187 + \log 2k}) \quad (4.8)$$

4.4 Model verification results

Addition 12 simulation cases having the influence variables were randomly assigned to Plaxis model for verifying the proposed equation (Equation 3.8). **Table 4.3** presents variation of influence variables and the corresponding h_o values extracted from every Plaxis simulation and for checking with the linear proposed equation, respectively. The results of h_o variation also examined in **Table 4.3** with randomly selecting series of soil permeability $k = 1.97 \times 10^{-4}$, 2.23×10^{-3} , 3.0×10^{-6} ; MSE wall shape parameter $L = 0.5, 2.1, 2.6, 2.8, 3.0, 3.5, 4.2, 4.5, 5.0, 5.5, 6.5, 7.7$; geonet transmissivity $T_{net} = 1.7 \times 10^{-3}$, 3.0×10^{-3} , 6.0×10^{-3} , 8.0×10^{-3} , 1.2×10^{-2} , 2.7×10^{-2} .

Following points are concluded from this thesis shown that comparison between the Plaxis reads and linear association model calculations is plotted in **Figure 4.6**. The coefficient of determination R^2 along 1:1 line is by 0.9726 which indicates strongly linear correlation between h_o values read from Plaxis and that calculated from the proposed model. Those identification of verification results are present from the distribution of referenced points in plot of **Figure 4.6**.

Table 4.3 Variables assigned in 12 verification cases and the corresponding h_o values from Plaxis calculation and the linear proposed equation (Eq. 4.5).

Soil type and its permeability	L (m)	T_{net} (m²/sec)	h_o (Plaxis)	h_o (Proposed equation)
<i>Soil type 1</i> $k = 1.97 \times 10^{-4}$ (m/sec)	0.5	8.0×10^{-3}	0.0214	0.0255
	3.0	1.7×10^{-3}	0.058	0.0415
	3.5	6.0×10^{-3}	0.013	0.033
	6.5	3.0×10^{-5}	0.025	0.0429
<i>Soil type 2</i> $k = 2.23 \times 10^{-3}$ (m/sec)	2.1	3.0×10^{-3}	0.298	0.413
	5.0	2.7×10^{-2}	0.212	0.274
	5.5	6.0×10^{-3}	0.284	0.402
	7.7	8.0×10^{-3}	0.1465	0.374
<i>Soil type 3</i> $k = 3.0 \times 10^{-6}$ (m/sec)	2.6	3.0×10^{-3}	0.042	0.0566
	2.8	8.0×10^{-3}	0.001	0.003
	4.2	1.2×10^{-2}	0.0198	0.01452
	4.5	6.0×10^{-3}	0.001	0.004

*Note that the VG parameters were assigned to the corresponding soils according to their permeability

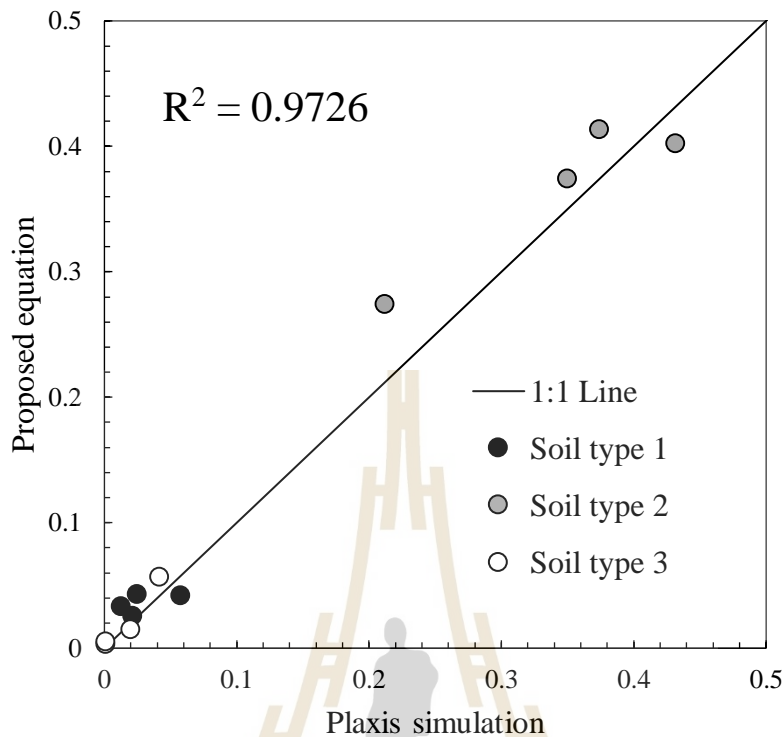


Figure 4.6 Verification results between Plaxis simulation and Proposed equation.

4.5 Conclusions

Following points are concluded from this thesis:

- The greater the permeability coefficient of native and backfill soil, the faster h_o falls with geonet transmissivity.
- Estimating of h_o through linear equation (Equation 4.8) is establishing with wide range of the studied soil assignment in relationship with MSE wall dimension, L , and geonet transmissivity (T_{net}).
- Generally, linear association results reveal that variables as L shape parameter, soil permeability (k) and $\log(T_{net})$ are three variables playing major role to maximum water level in protected zone h_o as according to previous statement.

- Verification results of proposed linear equation for estimation of h_o value indicate high accuracy and identical in comparing with Plaxis simulation, the reliability is shown via coefficient of determination of R^2 greater than 0.95 so that prove the initial selection of input simulation cases were acceptable for this thesis research.
- Practical wall design must be paid attention to obtain correct value of soil permeability (k), geonet transmissivity (T_{net}) as well as distance from the upstream to drainage face (L) for approximation of h_o . This highlight the practical uses for wall design again negative impacts of hydrological factor.

4.6 References

- Acharya, S., Jawitz, J.W., and Mylavarapu, R.S., 2012. **Analytical expressions for drainable and fillable porosity of phreatic aquifers under vertical fluxes from evapotranspiration and recharge**, *Water Resour. Res.*, 48.
- Bui Van, D., Chinkulkijniwat, A., Horpibulsuk, S., Yubonchit, S., Limrat, I., Arulrajah, A. and Jothityangkoon, C., 2017. **Steady flow in mechanically stabilised earth walls using marginal soils with geocomposite**. *Geosynthetics International*. 24(6), 590-606.
- Chinkulkijniwat, A., Horpibulsuk, S., Bui Van, D., Udomchai, A., Goodary, R., Arulrajah, A., 2016. **Influential factors affecting drainage design considerations for mechanical stabilised earth walls using geocomposite**. *Geosynthetics International*. 24(3), 224-241.

- Koerner, R. M., & Koerner, G. R. 2018. **An extended data base and recommendations regarding 320 failed geosynthetic reinforced mechanically stabilized earth (MSE) walls.** *Geotextiles and Geomembranes*, 46(6), 904-912.
- Koerner, R. M., & Koerner, G. R., 2015. **Lessons learned from geotextile filter failures under challenging field conditions.** *Geotextiles and Geomembranes*. 43(3), 272-281.
- Konukcu, F., Istanbuluoglu, A., and Kocaman, I., 2004. **Determination of water content in drying soils: Incorporating transition from liquid phase to vapour phase.** *Australian Journal of Soil Research*. 42(1), 1-8.
- La Duong, H., Chinkulkijniwat, A., Horpibulsuk, S., Do Quang, T., Yaowarat, T., 2020. **Steady state groundwater in mechanical stabilized earth walls of various dimensions with geocomposite back drain installation.** *International Journal of geomechanics*.
- Mualem Y. 1976. **A new model for predicting the hydraulic conductivity of unsaturated porous stone media.** *Water Resource Research*. 12(3), 513-522.
- Plaxis-2D, 2018. Scientific and Reference manual. Plaxis bv, Delft, Netherlands.
- Szymkiewicz, A., Tisler, W., Burzyński, K., 2015. **Examples of numerical simulations of two-dimensional unsaturated flow with VS2DI code using different interblock conductivity averaging schemes.** *Geologos*. 21(3), 161–167.
- Vahedifard, F., Tehrani, F.S., Galavi, V., Ragno, E., AghaKouchak, A., 2017. **Resilience of MSE Walls with Marginal Backfill under a Changing Climate: Quantitative Assessment for Extreme Precipitation Events.** *Geotechnical and Geoenvironmental Engineering*. 143(9), 04017056.

- van-Genuchten, 1980. **A closed-form Equation for Predicting the Hydraulic Conductivity of Unsaturated Soils.** Soil science society of America journal. 44(5), 892-898.
- Yoo, C., Jung, H.Y., (2006). **Case history of Geosynthetic Reinforced Segmental Retaining Wall Failure.** Journal of Geotechnical and Geoenvironmental Engineering 132, No. 12, 1538-1548.
- Zhang, C., Chen, X, Fan, W., 2015. **Overturning Stability of a Rigid Retaining Wall for Foundation Pits in Unsaturated Soils.** *International Journal of Geomechanics.* 16(4), 06015013.



CHAPTER V

CONCLUSION AND RECOMMENDATIONS

5.1 Summarize and conclusions

The thesis comprises 3 key research objectives Recently, considerable risks to the internal instability of mechanically stabilized earth (MSE) walls have been encountered from the inadequate drainage capacity of some backfill under extremely heavy rainfall. Due to its high drainage capacity, geocomposite is regarded as an appropriate material for drainage purposes in many geotechnical structures, including MSE walls. However, the installation of a geocomposite drain produces hydrologically complex boundary conditions, and unsaturated flow through the MSE wall becomes more complicated. This article reports a series of numerical simulations conducted to *investigate* the influences of MSE wall dimensions and drainage capacity on seepage responses inside the protected zone of the wall. The results indicated that the distance from the upstream water source to the drainage face (L) contributes most to the level of the phreatic surface inside the protected (reinforced) zone. Furthermore, a relationship existed between the permeability of the soil on the upstream side and the lowering of the phreatic surface due to increased geonet transmissivity. Results reported in this study might reinforce understanding of complex flow behaviors in MSE wall with back drain installation. Based on the linear relationship among influenced factors to the change of h_o , this thesis were also utilized for linear association analysis for adapting and provide a convenient and simple linear equation for estimation the variation of h_o

following the relationship among many influenced parameters such as native and backfill soil permeability (k), MSE wall dimension (L), geonet transmissivity (T_{net}). The linear model provides an ease for practical via linear equation uses. Good linear estimation of h_o in relevant relationships is, therefore, vital for the best design of MSE wall against failure.

5.1.1 Chapter III: Steady state groundwater in mechanical stabilized earth walls of various dimensions with geocomposite back drain installation.

This article investigated the influence of relevant shape parameters on seepage responses, including the highest water level in the protected (h_o) and the water saturation in the protected zone, in an MSE wall with a geocomposite back drain. Other than the relevant shape parameters, the influence of geonet transmissivity, which is a main component of geocomposite drainage systems, was also investigated. The following conclusions were drawn from this study. Where distance from the upstream water to the drainage face (L) is short, this shape parameter (L) plays a significant role in the seepage responses in the MSE wall. Accordingly, involved engineers must pay close attention to the phreatic level in the protected zone when dealing with an MSE wall in a mountainous area, where the distance from upstream water to the drainage face might be very short. The height of the wall (H) and the width of protected zone (W) play no to negligible role to the magnitude of h_o . Whereas, the vertical distance from the wall base to impervious boundary (D) also plays no role to the magnitude of h_o whenever the contribution upstream water source does not change. This conclusion is based on an assumption that the geocomposite does not exceed its drainage capacity.

Water saturation in the protected zone mainly depended on the water retention curve of the soil used as fill material.

Although distribution of water saturation in the protected zone mainly depends on the properties of backfill material, the k-function of the soil at the upstream side might play little role to the water distribution in the protected zone particularly at the upper elevation. This conclusion is based on k-function plots of upstream soils and geotextile. The permeability of the upstream soil is important properties contributes to the h_o level. The difference between permeability of the drainage material and that of the upstream soil governs the h_o value. Furthermore, the permeability coefficient of the soil on the upstream side governs the rate at which h_o falls with increments of geonet transmissivity.

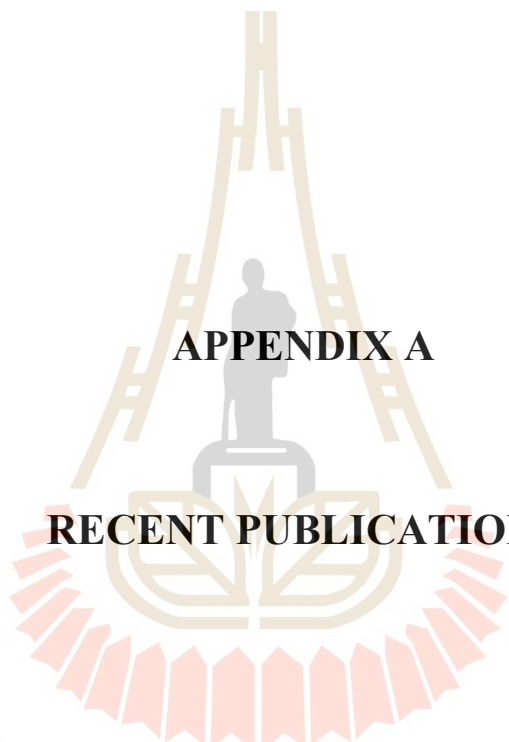
5.1.2 Chapter IV: Groundwater estimation in MSE wall with geocomposite back drainage: linear association analysis

Following points are highlight concluded from this chapter of this thesis: The greater the permeability coefficient of native and backfill soil, the faster h_o falls with geonet transmissivity. Estimating of h_o through linear equation is establishing with wide range of the studied soil assignment in relationship with MSE wall dimension, L , and geonet transmissivity (T_{net}). Generally, linear association results reveal that variables as L shape parameter, soil permeability (k) and $\log(T_{net})$ are three variables playing major role to maximum water level in protected zone h_o as according to statement in La Duong et al. 2020. Verification results of proposed linear equation for estimation of h_o value indicate high accuracy and identical in comparing with Plaxis simulation, the reliability is shown via coefficient of determination of R^2 greater than 0.95 so that prove the initial selection of input simulation cases were acceptable for this

thesis research. Practical wall design must be paid attention to obtain correct value of soil permeability (k), geonet transmissivity (T_{net}) as well as distance from the upstream to drainage face (L) for approximation of h_o . This highlight the practical uses for wall design again negative impacts of hydrological factor.

5.2 Recommendations for future works

- This study investigated the influences of MSE wall dimension, geonet transmissivity as well as soil permeability only used steady state flow conditions. The addition for transient flow model is recommended for the future works in more comparisons of this current results.
- The research works on soil type variation at the MSE wall base as soil foundation is suggested for further research in order to provide much and more detail on h_o values variation.
- The linear equation is needed for addition of more influences factors that related to time factors for transient flow.

The logo of Sakon Nakhon Rajabhat University is centered on the page. It features a stylized golden structure resembling a traditional Thai roof or a tiered stupa. Inside this structure is a grey silhouette of a person standing on a pedestal. Below the person is a circular emblem with a leaf-like design. The entire logo is surrounded by a decorative border of red and orange segments.

APPENDIX A

RECENT PUBLICATIONS

มหาวิทยาลัยเทคโนโลยีสุรนารี

List of Publications

INTERNATIONAL JOURNAL PAPERS

La Duong, H., Chinkulkijniwat, A., Horpibulsuk, S., Do Quang, T., Yaowarat, T.,
2020. **Steady state groundwater in mechanical stabilized earth walls of various dimensions with geocomposite back drain installation.** *International Journal of geomechanics.* (Accepted)

INTERNATIONAL CONFERENCE PAPERS

Do Q.T., ChinkulkijniwatA., Horpibulsuk, S., Hoang N.T.D., and La, D.H, (2020)
Geodynamic Activities at Estuaries in Ha Tinh Province of Vietnam, SUT
International Virtual Conference on Science and Technology, August 28th, at
Suranaree University of Technology, Thailand.

มหาวิทยาลัยเทคโนโลยีสุรนารี

24/11/2020

Gmail - Decision on Manuscript MS GMENG-5372R3 - [EMID:17152a9d85053c6c]



La Duong Hai <hailaduong9@gmail.com>

Decision on Manuscript MS GMENG-5372R3 - [EMID:17152a9d85053c6c]

1 thu

International Journal of Geomechanics <em@editorialmanager.com>

03:31 15 tháng 10, 2020

Trà lời-Tời: International Journal of Geomechanics <editorial.coordinator@asce.kwfco.com>

Tời: Hai La Duong <hailaduong9@gmail.com>

You are being carbon copied ("cc:'d") on an e-mail "To" "Avirut Chinkulkijniwat" avirut@sut.ac.th
 CC: "Hai La Duong" hailaduong9@gmail.com, "Suksun Horpibulsuk" suksun@g.sut.ac.th, "Thien Do Quang" dqthien@hueuni.edu.vn, "Teerasak Yaowarat" teerasakyaowarat@gmail.com

Ref.: Ms. No. GMENG-5372R3
 STEADY STATE GROUNDWATER IN MECHANICAL STABILIZED EARTH WALLS OF VARIOUS DIMENSIONS
 WITH GEOCOMPOSITE BACK DRAIN INSTALLATION
 Hai La Duong; Avirut Chinkulkijniwat; Suksun Horpibulsuk; Thien Do Quang; Teerasak Yaowarat, Ph.D.

Dear Dr. Avirut Chinkulkijniwat,

Congratulations! Your Technical Paper has been accepted for publication in ASCE's International Journal of Geomechanics. Your manuscript will now be forwarded to a Production Editor who will prepare it for publication and you will be notified of a publication date once your Technical Paper has been scheduled for an issue.

Our editors have requested that all accepted authors serve as reviewers for the International Journal of Geomechanics. If you are not already a reviewer for the journal and are willing to serve as one, please reply to this email and let me know.

Your accepted paper is fully citable using its DOI. The DOI for your accepted paper can be found in the "Submissions in Production" folder in your Editorial Manager account. Note that this DOI will not be activated until the paper is published online in the ASCE Library. The paper may be cited before publication as:
 [Authors]. Forthcoming. "[Article title]." [Journal Name]. [DOI].

Your paper is now being transferred to ASCE's Production department. Production staff will perform a quality check upon receipt of your paper, and may contact you to resolve queries or address any issues with files or format before copyediting and page composition begins. Please be aware that your paper will be withdrawn if production queries are not addressed and page proofs are not reviewed and returned in a timely manner.

Following your article: Please note that registered users to the ASCE Library (<https://ascelibrary.org/>) can sign up for a citation alert for any paper. This alert will send you an email anytime your manuscript is cited by another journal in the CrossRef indexed publications. These citations will also appear on the abstract page for your article.

Thank you so much for submitting your work to ASCE's International Journal of Geomechanics and please let us know if you have any further questions.

Sincerely,

Monica Leigh
 Editorial Coordinator

In compliance with data protection regulations, you may request that we remove your personal registration details at any time. (Use the following URL: <https://www.editorialmanager.com/jrnmeng/login.asp?a=r>). Please contact the publication office if you have any questions.

EAT0023 (Invited Paper)

Geodynamic Activities at Estuaries in Ha Tinh Province of Vietnam

Thien Do Quang¹, Avirut Chinkulkijniwat², Suksun Horpibulsuk²,
Do Hoang Ngo Tu¹ and Hai La Duong²

¹ Hydrogeology and Engineering Geological Department, Faculty of Geography and Geology, Hue University of Sciences, Nguyen Hue St, Hue City, Thua Thien Hue, 49000, Vietnam, Tel. +84-0234-38-23-837

² School of Civil Engineering, Suranaree University of Technology, 111 University Avenue, Muang District, Nakhon Ratchasima, 30000, Thailand. Tel-66+ .44-22-4353; and -66+9-767-5759

* Corresponding Author: hailaduong9@gmail.com

Abstract. The main target of paper is applying field investigated method and measuring for 20 cross-sections in dry and flood season, in combination with remote sensing analysis and GIS in period from the years 2000 to 2016 in order to assess erosion and accumulation activities of main 4 sections at estuary of Ha Tinh province with their names as Hoi estuary, Sot estuary, Nhuong estuary and Khau estuary that their distribution almost is uniformed about 137 km with direction from North to South. Study results indicate that in conceptual period from year 2000 to 2016, the erosion activities took advantage with eroded rate 2 - 5 m/year and eroded intensity tend to southern direction and this erosion process mainly occurred in northern part of riverbank. The river channel accumulation and the formatting of sandbar and alluvial delta (accumulated rate > 10m/year) happened extremely, destructed several protected dikes and river embankments and damage civil and economic constructions, and massively damages to domestic water routes at mentioned estuaries in research area.

Keywords: Erosion, accumulation, estuary, remote sensing analysis, Ha Tinh

1. Introduction

Nowadays, the erosion and accumulation activities at estuary are considered as a dangerous geological hazard cause serious damages to civilization, waterway and natural environment becoming most concern in Vietnam. This geodynamic research topic has been implemented almost frequently, especially in the adaptation to unpredictable climate change recently. Via applying remote sensing image analysis and GIS combine with field investigation in order to assess the erosion and accumulation activities in coastal zone that are implemented frequently in many nations in the world [11-13] and Vietnam [1, 9]. Those authors have conducted many researches on this scientific topic in different territories around Vietnam [3, 11-13].

The coastal area in Ha Tinh province with total distance by 137 km from the North to South includes 4 main estuaries: Hoi estuary (Nghì Loc District), Sot estuary (Loc Ha District),

Nhuong estuary (Cam Xuyen District) and Khau estuary (Ky Anh District) (Figure 1), this area concentrates various civil – economic constructions (harbors, tourism, monuments,..) in comparative with other provinces in the Central part of Vietnam. This region got impacted annually 5 or 6 storms coming per year with the highest wind speed reaches higher 40 m/second, that lead to the erosion and accumulation occurred frequently at estuaries with larger scale and higher intensity. These impacts caused serious damages for civilized environment, socio-economic activities and national security and defense in research area. Therefore, this topic of research project on geodynamic activities brings comprehensive supplement of scientific theoretical basic for river - marine dynamic study but also be urgent and high practical for prevented solutions, mitigating damages of erosion and accumulation.



Figure 1. Main 4 estuaries of Ha Tinh province.

2. Documents and research method

The document collections related to research topic and research area are listed in the references, main documentation basis of this paper as below:

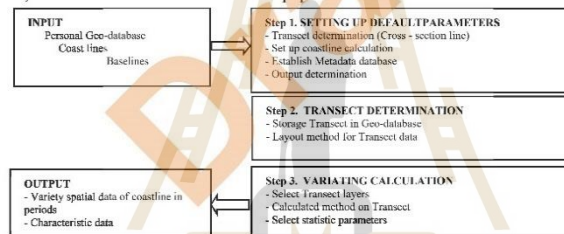


Figure 2. Block diagram of coastline variation analysis steps.

- Remote sensing data are Landsat image TM and LC (OLI) collected from website: <http://glovis.usgs.gov> in the year 2000, 2005, 2010, 2016 (Landsat 7 image – June 6th, 2000; Landsat 5 image – July 14th, 2005; Landsat 5 image - July 12th, 2010; Landsat 8 – May 9th, 2016). These satellite image were taken at different period in the past under the WGS-84 UTM 48-range, 30-meters resolution, collected time from May to July in order to eliminate the temporary coastline variations and locally in stormy season, these images are also adjusted geometry before implement isolation of seashore to compare with initial coastline variation.
- Landsat images got processed and interpreted by ERDAS IMAGINE software, with changes into Vector format to carry out variation analysis. The DSAS (Digital Shoreline Analysis System) tool was integrated into the Environmental Systems Research Institute (ESRI) software, version 4.3 was integrated for ArcGIS 10.x developed in 2012 by the

US. Geological Survey [3, 7, 13, 15]. The block diagram of the shoreline analysis steps is illustrated in Figure 2.

3. Results of geodynamic activities

Field investigation results for erosion and accumulation activities at estuaries in Ha Tinh province conducted by authors in 2 investigated stages in dry and rainy season, simultaneously combine with cross-section measuring by 20 for 4 estuaries (Stage 1, December 13th - 17th 2016; Stage 2, July 9th - 12th 2017; Stage 3 - After tropical storm No.10 on September 23th 2017), other results come from Provincial research project entitle "Research state and propose mitigated solutions for damages cause by erosion and accumulation hazard in coastal area and Ha Tinh estuary".

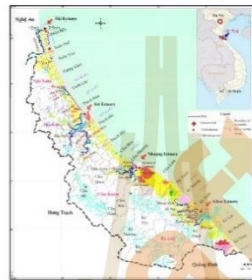


Figure 3. State map of erosion and accumulation at estuaries in Ha Tinh coastal province.

The studied result collecting is clearly presented in state map of erosion and accumulation at studied estuaries (Figure 3) with statistic table of significant erosion and accumulation in research area (Table 1), by Remote sensing analysis and GIS in period 2000 - 2016. An overview of erosion and accumulation in coastal area of Ha Tinh province as following:

Hoi estuary: with the width about from 500 to 900 m, the average depth from 6 to 7 m, tidal flats have 25 - 28 meters wide and formed by medium - fine grained soil) with origin from wind - marine Holocene ($m_{vQ_{2-3}}$). In which, the North of Hoi estuary, there are several independent san barriers which elongate from direction North to South, with 700 m long, 50 - 60 m wide; Since the South estuary is crossed by sand dunes with 50 meters long and 80 - 100 meters wide; And low deltas with small slope degree, wide and elongate to the estuary. In 2013, the government carried out the project of dredging Cua Hoi - Ben Thuy channel (Nghe An province) to ensure waterway transport (Figure 4, 5) [4]. The sand dunes are often unstable and constantly changing in space and time, the dry season extends the area, the flood season is croded to the dunes with an area of 2 - 3 m², 0.7 - 1.5 m high. River dykes have been built in combination with mangrove planting. However, submarine sand bar and embankments in river and coastal estuaries fluctuate continuously over time. In Xuan Pho district, the erosion activities are weak on the small sand layer at the rate lees than 2 m/year, 70 m long. Continuously, controlled and prevented constructions include embankment with 11 dyke embankments in Hoi Thai commune, Hoi Thank commune along 2 kilometers, the length of dyke from 100 to 150 meters, and at present they only have 50 - 70 meters remaining. In the years from 1990 to 2004, ships and boats were difficult to enter the harbor because sand bars lay in front of this estuary (Figure 6). The results of remote sensing analysis for the period of 2000 - 2016 show that the Cua Hoi coastline has an average range of 175 m.

The results of remote sensing analysis for the period of 2000 - 2016 show that the Cua Hoi coastline has an average range of 175 m. In particular, strong variations occur on sand bars in the

South of the estuary > 400 meters and apart of the banks of the river mouth in the north. Sedimentation is prevalent and occurs at a rate of 1.5 m/year.

Table 1. Significant erosion and accumulation area at estuaries in Ha Tinh coastal province

No.	Location	Length (m)		Rate (m/year)		Feature of formed material
		Erosion	Accumulation	Erosion	Accumulation	
1	South of Hoi estuary	-	1500	-	30	Sand barrier cross estuary
2	Xuan Hoi	400	-	2-5	-	Fine sand
3	Xuan Pho	250	-	-	-	-
4	Cuong Giang, Thinh Loc	70	-	<2	-	Fine sand
5	Thinh Loc	250	-	-	-	Fine sand
6	Thach Kim	120	-	-	-	Provincial route 22/12
7	Sot estuary	80	-	-	-	Protected embankments
8	North of Nhuong estuary	-	500	-	>10	Northern sand barriers
9	Nhuong estuary	-	-	-	-	Local erosions of embankment
10	Bridge closes to Nhuong estuary	-	400	-	-	Sand barriers cross estuary
11	Cam Nhuong	-	280	-	-	River delta (50 -100m wide)
12	Cam Linh	-	2200	-	-	River delta with width 35-100m
13	Rock mountain	-	1800	-	-	River delta (50 -100m wide)
14	Khau estuary	-	-	-	-	Bedrock erosion
15	Khau estuary (rivermouth)	700	-	-	2-5	Estuary erosion
16	Ky Ninh beach	50	-	-	2-5	Erosion destructs at casuarina forest

Southern sand bars are heavily eroded on the length of 1.5 km and the further southward the erosion rate decreases and turn to accumulation. Locations inside the estuary have erosion and accumulation rotate to each section with amplitude less than ± 10 m. From the coastline section of Hoi estuary to Sot estuary, coastline at Ken channel where the border between Cuong Gian commune, Nghi Xuan district and Thinh Loc commune, Loc Ha district have average movement is 52 m/year to the South that cause the lost about 20,000 hectares for aqua cultural. In the tropical storm No.10 in 2017, the erosion eliminated many sections of coastline and provincial route 22/12 (Figure 7).

Sot estuary: Within 150 – 450 m wide, depth from 2 to 4 m, tidal flats have from 22 to 138 m wide. Northern side is formed by granular sediments (small sand) with wind marine origin Holocene (mvQ₂₋₃), southern part is granite – biotite bedrock from complex of Phia Bioc (GTsn pb). For flood season in 1989, the coastline in section of Thach Kim commune was eroded hardly lead the massive destruction. By 1994, erosion activities have taken advantaged with rate 2 – 5 m/year after constructing of local Li Bi dyke with tidal flat is about 70 – 100 m (Figure 8).

Nowadays, the government is implementing the project with title "Dredging and channel regulation for anchorage and storm cover" [9] in order to mitigate the accumulation at wharf, harbor and storm shelter from tidal currents for ships and boats at Sot estuary. In which, that also control the disadvantages of coastal dynamic activities, the left flow direction increased the flow rate by 25% of the total initial flow and reduced 50% of the sediment deposited at Sot estuary, also decline the periodic dredging volume (5 years) up to 60% with the dike at Sot estuary is under construction.

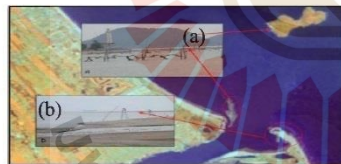


Figure 4. (a) Hon Ngu island acts as breakwater; (b) sand barrier in the South of Hoi estuary.

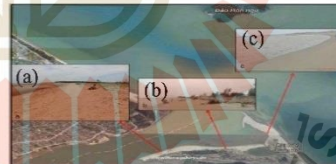


Figure 5. Sand bar along the South of Nam estuary with 1-1.5 meters long in section near estuary (a); Section of estuary bank with 0.5-1 meters long (b); Sand dune crosses estuary (c).



Figure 6. Column - shaped reinforced dyke for embankment protection (Xuan Hoi - Xuan Pho) and anti - accumulation at Hoi estuary.

Nhuong estuary: With 550 – 900 m wide, creeks under southern by 2.5 - 3.0 m deep, tidalflats is from 35 to 150 m wide. The North side is formed from small sand with origin by marine – wind Holocene (mvQ₂₋₃), as for southern side being from granite biotite bedrock which belong to Phia Bioc complex (GT_{3n} pb₁), crossing the mentioned estuary is mainly granite biotite rock and granodiorite which elongate 400 - 500 m in parallel to the coast. The erosion and accumulation of the estuary seem so complicated. In period 1995 -1997, with narrow 150 - 200 m, the erosion expanded the estuary and the area inside the estuary continuously until building a dyke and embankment system of 2 km long from the year 2012 to reduce erosion and protect residential areas of Cam Nhuong commune. The length of each embankment is approximate 20 m under the highly impacts of sea waves the roof embankments are still damages (Figure 9) [2, 5, 7].

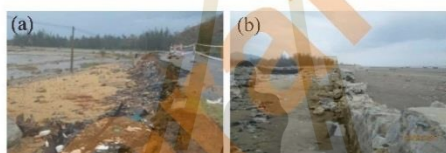


Figure 7. (a) Erosion at provincial route 22/12; and (b) protected embankment of Thach Kim commune after tropical storm No.10, 2017.

In dry season (July 11th, 2017), sand bar extending about 400 m from 200 – 250 m in 1995 from the north shore to the southern side and sand flats along the river and in the middle stream. Under Cua Nhuong bridge also appeared river delta with 280 m long and 50 -100 m wide along the bridge.



Figure 8. (a) Erosion damages in the North estuary; and (b) extremely accumulation at Sot estuary.

According to remote sensing data for the period 2000 - 2016, the coastline varied average about 150 meters long. The erosion of the northern estuaries is at an average rate of 3.8 m/year. In the North of the estuary, the sediments are filled with a speed > 10 m/year, forming sand dunes with a length of about 500 meters. Coastline of Sot estuary to the Nhuong estuary is relatively flat (3-10 slope degree). The current embankment system in northern riverside (Cam Nhuong commune) and southern river bank (Cam Linh commune) combine with mangrove forest and breakwater embankment (3 km),

more effective mitigate flood damages in rainy season and forming various scales of mudflats (35 – 40 meters wide to 100 - 150 meters wide) along the two banks of the river mouth.



Figure 9. System of embankment at the North of Nhuong estuary.

Before the year 2007, under foothill of Rock mountain (Nam estuary, Cam Linh commune) occurred a wide mudflat with 250 - 350 m wide that also concentrate many residents and got the deep estuary. In the section of Cam Linh beach (near estuary), the activities of high weathering granodiorite bedrock erosion happen extremely that cause rock fall at the edge with average dimension of rock masses from 0.5 m to several meters create the rock beds under the foothill. The period results of from 2000 - 2016 via remote sensing image analysis show that the shoreline varied below 100 m. The strongest change at estuary in the north and inside southern estuary area with the average rate of advantaged erosion is 3 m/year.

Khau estuary: This estuary gets 125 – 450 m wide with southern creek depth (< 0.5 – 3.5 m), the tidal flats have width from 90 to 110 m. The northern side of estuary is formed by small sand with wind – marine origin Holocene (mvQ₂₋₃), the southern side is structured Jurassic terrigenous sediments consist of conglomerate, sandstone of Muong Hinh formation (J_{1 mh}). The erosion – accumulation of estuaries and coasts are causing a great impact on the socio-economic activities. In comparison with above ones, this estuary is smaller, but accumulation activities occur strongly in estuaries and also creates mudflats of up to 100 – 150 m wide with accumulation rate 2 - 5 m/year. As for flood season in April of the year 2016, sea waves eroded Casuarina forest about 10 -15 meters, at 100 meters from the Border Gate at Khau estuary (Bac estuary). The eroded edge is 700 m long, 0.5 - 2.0 m of height, extending from the estuary to the coast (Figure 10).



Figure 10. The erosion of Border Gate Station of Khau estuary (Northern side).

4. Conclusions

From above research results, we can conclude that the erosion and accumulation of estuarine and coastal areas of Ha Tinh province as follows:

- The distance among estuaries are relatively equal and 30 - 40 km apart. In the north side, the estuaries are created from medium - small sand and as for the south side are mainly the bedrock. Especially for Hoi estuary, two sides of river are formed by fined sand and considered a natural sea wave prevent.

- Estuaries have the funnel shape specific as inside of the estuary is 500 - 700 m wide and high accumulating in dry season. Average depth of estuaries is from 1 m to 3 - 4 m, especially for Hoi estuary is 6 to 7 m deep, the deep channel is often direct to the south, the shallow part

is on the North side of estuary and also there are also sub-sandbars or floated sandbars under season changes, especially for Hoi estuary has deep channels near the North.

- The erosion and accumulation activity are still occurring complicated. In the period 2000-2016, erosion activities took advantage with the rate of 2 - 5 m and mainly erosion happened in the North side. Accumulation of sandbars and riverside > 10 m/year occurred very extremely, causing high damages to various embankments and many civil construction and waterway transportation at research estuary.

References

- [1] Nga N T 2000 Study on changes in the estuary of the Central part of Vietnam for flood drainage system (Vietnam)
- [2] Que V H 2005 and 2006 *Seminar technical construction design for upgrading sea embankment at Cam Linh estuary in stage 1 and 2, Ha Tinh Irrigation and Construction Consultancy Company (Vietnam)*
- [3] Thien D Q 2013 Research on erosion and sedimentation of river banks and propose appropriate solutions in the Mid – centralpart of Vietnam, *Ministry scientific research project, B2011-DHH02 (Vietnam)*
- [4] North Safety Assurance Corporation 2013 *Report on the dredging of Hoi estuary - Ben Thuy channel, Nghe An province (Vietnam)*
- [5] Dyke Technical Consultancy Center 2001 *Feasibility research report of investment project for rehabilitation of sea dyke, river dyke for sea erosion at Cam Nhung estuary, Department of Dyke Management and Flood Storm Revenge (Hanoi, Vietnam)*
- [6] Dyke Technical Consultancy Center (2008), *Report on upgrading Phuc Long – Nhung dyke system, Cam Xuyen district, Ha Tinh province, Department of Dyke Management and Flood Storm Revenge, Hanoi (Vietnam).*
- [7] Tuan N Q 2012 Investigation and assessment the current state of stability of Quang Nam coastline and propose adaptive solutions to climate change. *Project report on the programme of climate change in Quang Nam (Vietnam)*
- [8] Institute of Irrigation and Drainage - Institute of Water Resources Sciences of Vietnam 2015 *Report on dredging and adjustment of access channel for Sot estuary storm shelter (Vietnam)*
- [9] Niya A K, Alesheikh A A, et al. 2013 Shoreline Change Mapping Using Remote Sensing and GIS: Case Study: Bushehr Province. *International Journal of Remote Sensing Applications*. 3 L3
- [10] Das D D, Mithun D, Kanti K K 2013 River Change Detection and Bankline Erosion Recognition using Remote Sensing and GIS *Forum geografic*. 13 L1, p 12-17
- [11] Pan S 2013 Application of Remote Sensing and GIS in studying changing river course in Bankura District, West Bengal *International Journal of Geomatics and Geosciences*. 4 L1
- [12] Thien D Q 2016, Assessing the Motive of Erosion Process along Main River Channels in the Mid-Central Part of Vietnam, *The 2nd National Conference on Transport Infrastructure with Sustainable Development*, Construction House. p 317-326
- [13] Thien D Q and Do H N T 2016 Assessing and predicting the erosion process riverbank in Quang Binh: Apply for Gianh and Nhat Le river *Proceedings of the 3rd international, Conference Vietgeo 2016, Ha Long City (Vietnam), Geological and Geotechnical Engineering in Response to Climate Change and Sustainable Development of Infrastructure*. p 294-303
- [14] Thien D Q, Do H N T, Nhan T T, Hanh H.V, et al. 2017 Assessing the Lateral Erosion of Main Meandering Rivers in the Mid-Central Part of Vietnam *Journal of Hydrogeology & Hydrologic Engineering*. DOI: 10.4172/2325-96
- [15] Thieler E R., Himmelstoss, et al. 2009 DSAS 4.0 Installation Instructions and User Guide in Digital Shoreline Analysis System (DSAS) Version 4.0 - an ArcGIS extension for calculating shoreline change, *U.S Geological Survey Open-File Report*. 2008-1278

BIOGRAPHY

Mr. La Duong Hai was born on February 9th, 1992 in Thua Thien Hue province, Vietnam. He obtained his Bachelor's degree in Geological Engineering and Hydrology from Faculty of Geography and Geology, Hue University of Sciences in the year 2014. Then, he has been joined the Master program of Geology also from Faculty of Geography and Geology, Hue University of Sciences from the year 2014-2016. After finishing and gained Master degree in 2016, he passed the PhD scholarship candidate from Suranaree University of Technology in Nakhon Ratchashima, Thailand. His doctoral program was in time period 3 academic years from 2017 to 2020. During his Ph.D. study, he also has worked as a teaching assistant for Statistics Class and Geomechanics Laboratory. He has published 1 international journal papers from in Q1 ranking International Journal of Geomechanics.

มหาวิทยาลัยเทคโนโลยีสุรนารี